Oscillations

with Malcolm John

These lectures explore how the weak force gives rise to flavour oscillations and *CP* violation. Flavour oscillation means a reversible transmutation from one flavour to another. This phenomenon is observed within all neutral meson systems ($K^0\overline{K}^0$, $D^0\overline{D}^0$, $B^0\overline{B}^0$, $B_s\overline{B}_s$) and amongst the three neutrino species (ν_e, ν_μ, ν_τ). *CP*-violation is mathematical terminology for a difference between matter and antimatter. It is observed only in a handful of rare kaon and *B*-meson decays. The search for *CP*-violation in neutrinos is a major topic for the next generation of neutrino experiments.

1 Neutral kaon mixing

Fig. 1 show early proof of neutral kaon mixing from a bubble chamber image. The strangeness of the neutral meson appears to change during the flight between creation and decay. This statement is under the [correct] assumption that the creation of the neutral kaon is via the strong force, which is flavour conserving. The transition,

$$K^+ + p^+ \to K^0 + p^+ + \pi^+, \qquad |K^+\rangle = |\bar{s}u\rangle, \;\; |K^0\rangle = |\bar{s}d\rangle,$$

conserves *antistrangeness*. Conversely, the baryon-number-conserving transition,

$$\overline{K}^0 + p^+ \to \Lambda^0 + \pi^+ + \pi^0, \qquad |\overline{K}^0\rangle = |s\bar{d}\rangle, \;\; |\Lambda^0\rangle = |sud\rangle,$$

conserves *strangeness*. The neutral kaon has transmuted from $|\bar{s}d\rangle$ to $|s\bar{d}\rangle$ in a few centimetres. For this to occur, the K^0 and $\overline{K}^0$, cannot be the "mass eigenstates" of the Hamiltonian, those that propagate in time. The mass eigenstates (i.e. the *K*-short, K^0_S and *K*-long, K^0_L as we know them today) are linear superpositions of the flavour eigenstates (states of definite flavour) $\overline{K}^0$ and K^0 and hence have access to both in interactions.

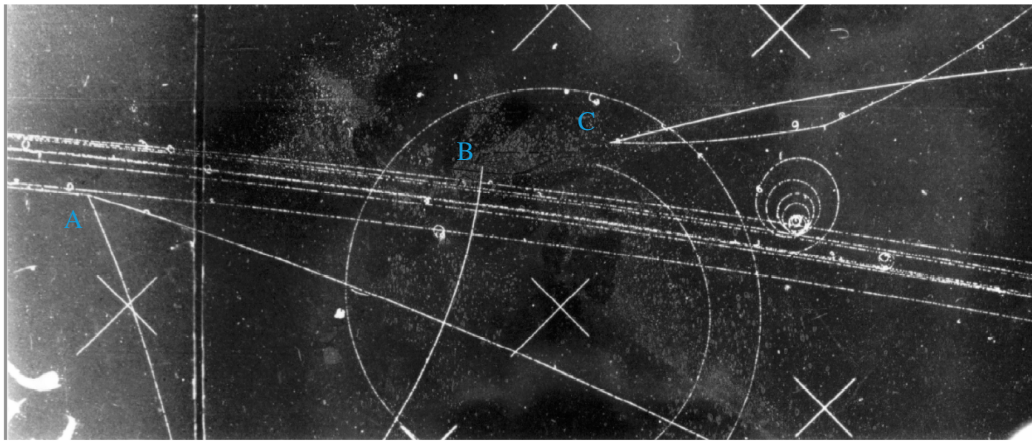


Figure 1: a K^+ beam enters the left edge of a bubble chamber and scatters off a proton at A. A pion and a neutral kaon is formed. The kaon flies to the right without leaving an trace and the recoiling proton and pion move to the bottom of the image. At B, the neutral kaon scatters off another proton to form a Λ^0 baryon with an associated π^+, as well as an untraced π^0. At C, the Λ^0 baryon decays into a proton and a π^- in a characteristic "V" decay.

1.1 Formalism

The time evolution of one neutral meson, in its rest frame, may be written as[1],

$$|K^0(t)\rangle = e^{-iMt}e^{-\Gamma t/2}|K^0\rangle$$

where the first exponential is a plane-wave solution, $\exp(\frac{i}{\hbar}(\mathbf{p}.\mathbf{x} - Et))$ for a state with energy $E = M$ in its rest frame, $|\mathbf{p}| = 0$, with $\hbar = 1$. The second term describes the exponential decay for a state with proper lifetime τ (i.e. width $\Gamma = \hbar/\tau$, again with $\hbar = 1$) such that,

$$|\langle K^0|K^0(t)\rangle|^2 \propto e^{-t/\tau}$$

Generalise to a two state system with 2×2 matrices, $\mathbf{M}$ and $\mathbf{\Gamma}$ encoding the time evolution,

$$\begin{pmatrix} |K^0(t)\rangle \\ |\overline{K}^0(t)\rangle \end{pmatrix} = \Sigma \begin{pmatrix} |K^0\rangle \\ |\overline{K}^0\rangle \end{pmatrix} \quad \text{where } \Sigma = e^{-i\mathbf{M}t - \mathbf{\Gamma}t/2}, \tag{1}$$

where the presence (absence) of the bar above the $K(t)$ shows the flavour of the state at $t = 0$: pure $|\overline{K}^0\rangle$ $\left(\text{or pure } |K^0\rangle\right)$. The states $|K^0\rangle$ and $|\overline{K}^0\rangle$ are of well defined flavour so it is in this basis that it is appropriate to discuss their interaction by the weak force. Thus they are the *weak* eigenstates, as opposed to the *mass* eigenstates of the Hamiltonian. Apply Schrödinger's equation, $i\,d\psi/dt = \mathrm{H}\psi$, identifies the Hamiltonian.

$$\frac{d}{dt}\begin{pmatrix} |K^0\rangle \\ |\overline{K}^0\rangle \end{pmatrix} = \mathbf{H} \begin{pmatrix} |K^0\rangle \\ |\overline{K}^0\rangle \end{pmatrix} \quad \text{with} \quad \mathbf{H} = \mathbf{M} - \frac{i}{2}\mathbf{\Gamma}. \tag{2}$$

Any matrix, $\mathbf{A}$ can be decomposed in the form $\mathbf{B} + i\,\mathbf{C}$ where $\mathbf{B}$ and $\mathbf{C}$ are hermitian because,

$$\begin{aligned} \mathbf{A} &= \frac{\mathbf{A}}{2} + \frac{\mathbf{A}}{2} + \frac{\mathbf{A}^\dagger}{2} - \frac{\mathbf{A}^\dagger}{2} \\ &= \underbrace{\frac{1}{2}\left(\mathbf{A} + \mathbf{A}^\dagger\right)}_{= \mathbf{B}\ (= \mathbf{B}^\dagger)} + \underbrace{\frac{1}{2}\left(\mathbf{A} - \mathbf{A}^\dagger\right)}_{= i\mathbf{C}\ (= -i\mathbf{C}^\dagger)} \quad \text{by inspection.} \end{aligned}$$

So $\mathbf{M}$ and $\mathbf{\Gamma}$ are hermitian matrices: $M_{21} = M_{12}^*, \Gamma_{21} = \Gamma_{12}^*$. This also implies observable quantities because the eigenvalues of hermitian matrices are real. Last, we impose CPT-invariance (identical mass and lifetimes of the K^0 and $\overline{K}^0$), $M_{11} = M_{22} = M, \Gamma_{11} = \Gamma_{22} = \Gamma$. So the hamiltonian of the meson-antimeson system becomes,

$$\mathbf{H} = \begin{pmatrix} M & M_{12} \\ M_{12}^* & M \end{pmatrix} - \frac{i}{2}\begin{pmatrix} \Gamma & \Gamma_{12} \\ \Gamma_{12}^* & \Gamma \end{pmatrix} \tag{3}$$

The off-diagonal terms describe the transitions [mixing] between the meson and antimeson.

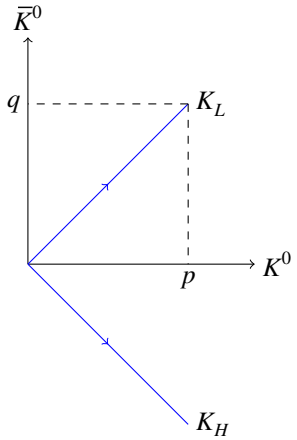
Returning to the wavefunctions, the eigenstates of the hamiltonian propagate in time with defined mass and lifetimes. We label the two mass eigenstates *Heavy*, *Light* and describe them as a combination of the flavour eigenstates,

$$\begin{aligned} |K_H\rangle &= p\,|K^0\rangle - q\,|\overline{K}^0\rangle \\ |K_L\rangle &= p\,|K^0\rangle + q\,|\overline{K}^0\rangle\,, \end{aligned} \tag{4}$$

where $p^2 + q^2 = 1$. The "$p + q,\ p - q$" form is required by orthogonality. Inverting this transformation, gives

$$|K^0\rangle = \tfrac{1}{2p}\left(|K_L\rangle + |K_H\rangle\right) \tag{5}$$

$$|\overline{K}^0\rangle = \tfrac{1}{2q}\left(|K_L\rangle - |K_H\rangle\right)\,. \tag{6}$$



[1] This simplification of time-dependent perturbation theory is known as the *Wigner-Weisskopf* approximation.

Eq. 1 describes the time evolution of the flavour eigenstates and is related to the time evolution of the mass eigenstates by the similarity transformation, $\Sigma = PDP^{-1}$, noting that the the time evolution in the mass basis is diagonal because mass eigenstates propagate in time with definite energy and lifetime.

$$\begin{aligned}\begin{pmatrix}|K(t)\rangle\\ |\overline{K}(t)\rangle\end{pmatrix} &= \begin{pmatrix}\frac{1}{2p} & \frac{1}{2p}\\ \frac{1}{2q} & \frac{-1}{2q}\end{pmatrix}\begin{pmatrix}|K_L(t)\rangle\\ |K_H(t)\rangle\end{pmatrix}\\ &= \quad '' \quad \begin{pmatrix}e^{-i\,M_L t-\Gamma_L t/2} & 0\\ 0 & e^{-i\,M_H t-\Gamma_H t/2}\end{pmatrix}\begin{pmatrix}|K_L\rangle\\ |K_H\rangle\end{pmatrix}\\ &= \quad '' \quad\quad '' \quad\quad \begin{pmatrix}p & q\\ p & -q\end{pmatrix}\begin{pmatrix}|K^0\rangle\\ |\overline{K}^0\rangle\end{pmatrix}\end{aligned}$$

In passing, it is noted that from linear algebra, the columns of P are eigenvectors of Σ. Multiplying out,

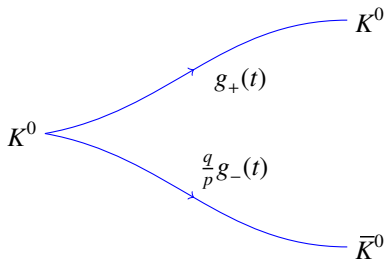
$$\Sigma = \begin{pmatrix}\frac{1}{2p} & \frac{1}{2p}\\ \frac{1}{2q} & \frac{-1}{2q}\end{pmatrix}\begin{pmatrix}e^{-i\,M_L t-\Gamma_L t/2} & 0\\ 0 & e^{-i\,M_H t-\Gamma_H t/2}\end{pmatrix}\begin{pmatrix}p & q\\ p & -q\end{pmatrix} \tag{7}$$

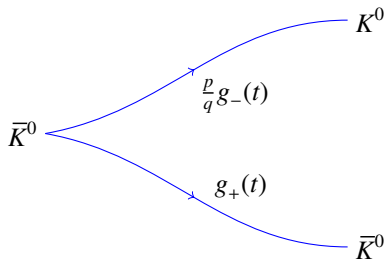
$$= \begin{pmatrix}g_+ & \frac{q}{p}g_-\\ \frac{p}{q}g_- & g_+\end{pmatrix} \quad \text{where} \quad g_\pm = \tfrac{1}{2}\left[e^{-i\,M_L t-\Gamma_L t/2} \pm e^{-i\,M_H t-\Gamma_H t/2}\right] \tag{8}$$

Hence the time evolution of the decaying state is,

$$\begin{aligned}|K(t)\rangle &= \quad g_+\,|K^0\rangle + \frac{q}{p}g_-\,|\overline{K}^0\rangle\\ |\overline{K}(t)\rangle &= \frac{p}{q}g_-\,|K^0\rangle + \quad g_+\,|\overline{K}^0\rangle\end{aligned} \tag{9}$$

Or illustratively,





From which we note, as a precursor to the discussion on *CP* violation, that a difference in the temporal evolution of neutral-meson mixing can arise if q and p are different,

$$\frac{q}{p} \neq \frac{p}{q} \quad , \quad \left(\frac{q}{p}\right)^2 \neq 1.$$

Applying Schrödinger's equation to the off diagonal part of Eq. 8, and equating to Eq. 3 noting that the time dependance is all contained within the $g_\pm$ factors,

$$\begin{aligned}i\frac{d}{dt}\left(\frac{q}{p}g_-(t)\right) &= i\frac{q}{p}\left[M_L - M_H - \frac{i}{2}\left(\Gamma_L - \Gamma_H\right)\right] = M_{12} - \frac{i}{2}\Gamma_{12}\\ i\frac{d}{dt}\left(\frac{p}{q}g_-(t)\right) &= i\frac{p}{q}\left[M_L - M_H - \frac{i}{2}\left(\Gamma_L - \Gamma_H\right)\right] = M^*_{12} - \frac{i}{2}\Gamma^*_{12}\\ \left(\frac{q}{p}\right)^2 &= \frac{M_{12} - \frac{i}{2}\Gamma_{12}}{M^*_{12} - \frac{i}{2}\Gamma^*_{12}}\end{aligned} \tag{10}$$

Where we remind ourselves that M_{12} and Γ_{12} are the elements of the hamiltonian $\mathbf{H}$ that describe the action of $|\overline{K}^0\rangle$ appearing in the initially $|K^0\rangle_{t=0}$ wavefunction.

1.2 Measuring K^0-$\bar{K}^0$ oscillations

For now, we concentrate on kaon oscillations and ignore *CP* violation, i.e. $p = q$. Neutral kaons can be produced in a state of definite antistrangeness by a strong interaction of negatively-charged pions on a proton target, see Fig. 2(a). By strangeness conservation (strong interaction) and baryon number conservation, it is impossible to make a $\bar{\Lambda}^0$.

In the semileptonic decay, the charge of the muon must be that of the strange quark, see Fig. 2 (b) and (c). Hence by counting the number of $\mu^+\pi^-$ decays versus the number of $\mu^-\pi^+$ decays as a function of decay time, this decay can pick out the proportion of K^0 and $\bar{K}^0$ in the propagating neutral kaon wavefunction.

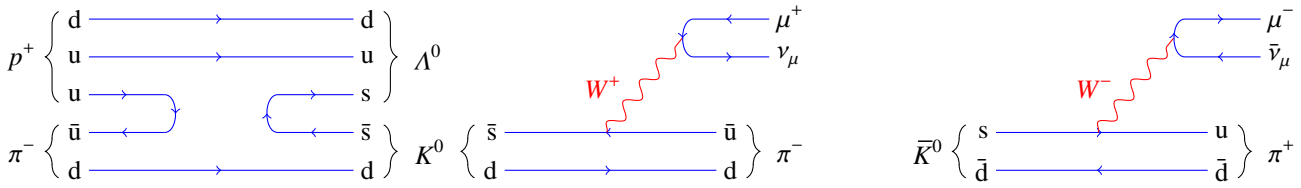


Figure 2: Quark flow diagrams for (a) K^0 production from pion-nucleon scattering (b) semileptonic decay of a K^0 and (c) semleptonic decay of a $\bar{K}^0$. The charge of the muon unabiguously identifies the kaon flavour.

As the system starts with a pure $|K^0\rangle$, Eq. 9 with $p = q$ is appropriate. Writing out completely,

$$\begin{aligned} |K(t)\rangle &= \underbrace{\qquad}_{g_+}|K^0\rangle + \underbrace{\qquad}_{g_-}|\bar{K}^0\rangle \\ &= \tfrac{1}{2}\Big(\underbrace{e^{-iM_Lt-\Gamma_Lt/2}}_{a} + \underbrace{e^{-iM_Ht-\Gamma_Ht/2}}_{b}\Big)|K^0\rangle + \tfrac{1}{2}\Big(\underbrace{e^{-iM_Lt-\Gamma_Lt/2}}_{a} - \underbrace{e^{-iM_Ht-\Gamma_Ht/2}}_{b}\Big)|\bar{K}^0\rangle \end{aligned} \tag{11}$$

The K^0 ($\bar{K}^0$) intensity is found from the probability of finding a K^0 ($\bar{K}^0$) at time t from this combined wavefunction,

$$\begin{aligned} |\langle K^0|K(t)\rangle|^2 &= \frac{1}{4}(a+b)(a+b)^* \\ &= \frac{1}{4}(aa^* + bb^*) + \frac{1}{4}(ba^* + ab^*) \\ |\langle \bar{K}^0|K(t)\rangle|^2 &= \frac{1}{4}(a-b)(a-b)^* \\ &= \frac{1}{4}(aa^* + bb^*) - \frac{1}{4}(ba^* + ab^*) \end{aligned}$$

Taking first the direct "amplitude-squared" term in each line,

$$\begin{aligned} aa^* + bb^* &= e^{(-iM_L-\frac{\Gamma_L}{2})t}e^{(+iM_L-\frac{\Gamma_L}{2})t} + e^{(-iM_H-\frac{\Gamma_H}{2})t}e^{(+iM_H-\frac{\Gamma_H}{2})t} \\ &= \qquad e^{-\Gamma_Lt} \qquad + \qquad e^{-\Gamma_Ht} \end{aligned}$$

The interference term reveals a sinusoidal dependence,

$$\begin{aligned} ba^* + ab^* &= e^{(-iM_H-\frac{\Gamma_H}{2})t}e^{(+iM_L-\frac{\Gamma_L}{2})t} + e^{(-iM_L-\frac{\Gamma_L}{2})t}e^{(+iM_H-\frac{\Gamma_H}{2})t} \\ &= e^{-\frac{\Gamma_L+\Gamma_H}{2}t}e^{-i(M_H-M_L)t} + e^{-\frac{\Gamma_L+\Gamma_H}{2}t}e^{i(M_H-M_L)t} \\ &= e^{-\frac{\Gamma_L+\Gamma_H}{2}t}\cdot 2\cos(\Delta Mt) \end{aligned}$$

So,

$$\begin{aligned} \mathcal{P}_{K^0}(t) = |\langle K^0|K(t)\rangle|^2 &= \frac{1}{4}\left(e^{-\Gamma_Lt} + e^{-\Gamma_Ht}\right) + \frac{1}{2}e^{-\frac{\Gamma_L+\Gamma_H}{2}t}\cos(\Delta Mt) \\ \mathcal{P}_{\bar{K}^0}(t) = |\langle \bar{K}^0|K(t)\rangle|^2 &= \frac{1}{4}\left(e^{-\Gamma_Lt} + e^{-\Gamma_Ht}\right) - \frac{1}{2}e^{-\frac{\Gamma_L+\Gamma_H}{2}t}\cos(\Delta Mt) \end{aligned} \tag{12}$$

which depends on the K_L and K_H lifetimes and their mass difference[2] in the interference term.

The two kaon mass eigenstates have remarkably different lifetimes and are thus always labelled with reference to that property: the K-short $K^0_{\rm S}$ and the K-long, $K^0_{\rm L}$. The $K^0_{\rm S}$ has lifetime of 89.5 ps whereas the $K^0_{\rm L}$ lives 571 times longer. Experiment determines the $K^0_{\rm S}$ is the lighter-mass eigenstate though there is no fundamental reason why this should be the case.

The distributions of $\mathcal{P}_{K^0}(t)$ and $\mathcal{P}_{\bar{K}^0}(t)$ are shown over 1ns in Fig. 3. As expected for the initially well-defined $|K^0\rangle$, $\mathcal{P}_{K^0}(0) = 1$ and $\mathcal{P}_{\bar{K}^0}(0) = 0$. One nanosecond is over 11 $K^0_{\rm S}$ lifetimes so this component will have fallen to $e^{-\Gamma_L t} \sim 0$, leaving

$$\mathcal{P}_{K^0}(1\text{ ns}) \approx \mathcal{P}_{\bar{K}^0}(1\text{ ns}) \approx \frac{1}{4} e^{-\Gamma_H t}\,.$$

1 ns is about one fiftieth the $K^0_{\rm L}$ lifetime, $\frac{1}{4}\exp^{-\frac{1}{50}} = 0.245$.

Considering the oscillatory term note that $\mathcal{P}_{K^0} = \mathcal{P}_{\bar{K}^0}$ when $\cos(\Delta M t) = 0$. This occurs at $t = \frac{\pi}{2}(\Delta M)^{-1}$, $\frac{3\pi}{2}(\Delta M)^{-1}$ ...
The sketch shown this occurring at 300 ps and 900 ps,

$$\Delta M = \tfrac{\pi}{2}(300)^{-1} = 5.24 \times 10^{-3}\,\text{ps}^{-1}\,.$$

Or in eV,

$$\frac{5.24 \times 10^{-3}}{10^{-12}}[\text{s}^{-1}] \times \frac{\hbar}{e} = 3.45 \times 10^{-6}[\text{eV}]\,.$$

Incredibly, this is fourteen orders of magnitude smaller than the mean kaon mass, 492 MeV, yet it readily measurable due of the sensitivity of interference phenomena.

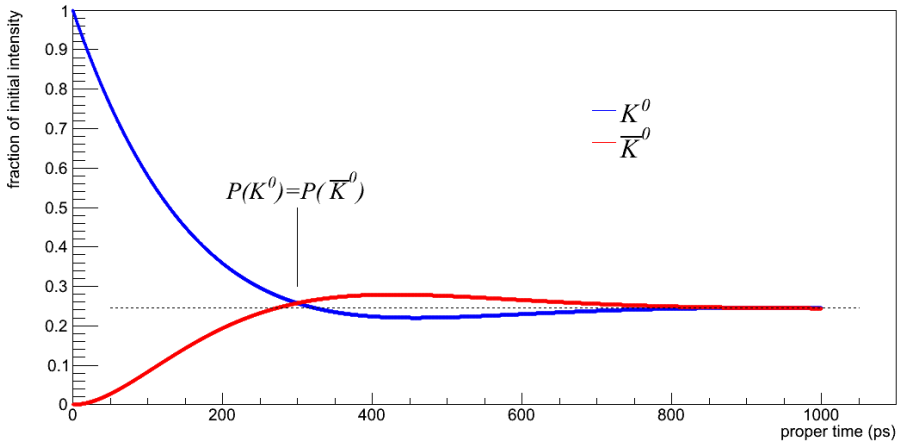


Figure 3: Probabilities of finding each kaon *flavour* eigenstates from from an initially K^0 source.

[2]To reiterate, K_L and K_H are **not** each other's antiparticle. CPT theorem does not apply so they can, and do, have different masses and lifetimes.

2 *CP* violation in kaons

Kaon oscillation occurs because the flavour eigenstates (states of definite flavour) mix into orthogonal superpositions,

$$\begin{aligned} |K^0_{\rm S}\rangle &= p\,|K^0\rangle + q\,|\overline{K}^0\rangle \quad &\equiv \quad & p\,|d\bar{s}\rangle + q\,|s\bar{d}\rangle \\ |K^0_{\rm L}\rangle &= p\,|K^0\rangle - q\,|\overline{K}^0\rangle \quad &\equiv \quad & p\,|d\bar{s}\rangle - q\,|s\bar{d}\rangle\,. \end{aligned} \tag{13}$$

If $p^2 = q^2$ ($=\frac{1}{2}$ when normalised), these eigenstates of the Hamiltonian are *CP* eigenstates, in that they map onto themselves under application of the *CP* operator, with eigenvalue ± 1,

$$CP\,|d\bar{s}\rangle = |s\bar{d}\rangle\,, \quad CP\,|s\bar{d}\rangle = |d\bar{s}\rangle \quad \Rightarrow \quad CP\,|K^0_{\rm S}\rangle = +|K^0_{\rm S}\rangle \text{ and } CP\,|K^0_{\rm L}\rangle = -|K^0_{\rm L}\rangle \text{ if } p^2 = q^2\,.$$

Consider the decay of a neutral kaon to pions ($\to \pi^+\pi^-$, $\to \pi^0\pi^0$, $\to \pi^+\pi^-\pi^0$, $\to \pi^0\pi^0\pi^0$). An ensemble of two $J^P = 0^-$ pions from a ground-state kaon decay must have parity $(-1)^2(-1)^L = +1$ because L is 0 (verified by observing spherical symmetric decay distributions of the pion pair). The particle↔antiparticle transformation is symmetric so this is a *CP*+ final state.

For the same reason, the three-pion state is *CP*− because it has parity $(-1)^3(-1)^{L_{12}}(-1)^{L_3} = -1$. This conclusion assumes $L_{12} = L_3 = 0$ which is verified by inspecting the Dalitz plot of the three-pion decay. Thus if *CP* symmetry is a conserved quantity, one expects only $K^0_{\rm S} \to \pi\pi$ and only $K^0_{\rm L} \to \pi\pi\pi$. To a good approximation, this expectation is correct and indeed, the reduced phase-space for the three-pion final state is the reason why the $K^0_{\rm L}$ has a much-longer lifetime than the $K^0_{\rm S}$.

The large difference of lifetime is experimentally useful for separating the two mass eigenstates. Imagine a neutral kaon beam of average energy 10 GeV ($\gamma \approx 20$) passed into a long tube. The average distance it will travel before decay is,

$$\gamma \cdot c \cdot \tau_{K^0_{\rm S}} \approx 20 \cdot 3 \times 10^8 {\rm ms}^{-1} \cdot 89{\rm ps} \approx 0.5{\rm m}\,.$$

After ~5 metres all $K^0_{\rm S}$ will decay and $K^0_{\rm L}$, whose lifetime is ~ 570× longer, can be studied in isolation.

2.1 Regeneration

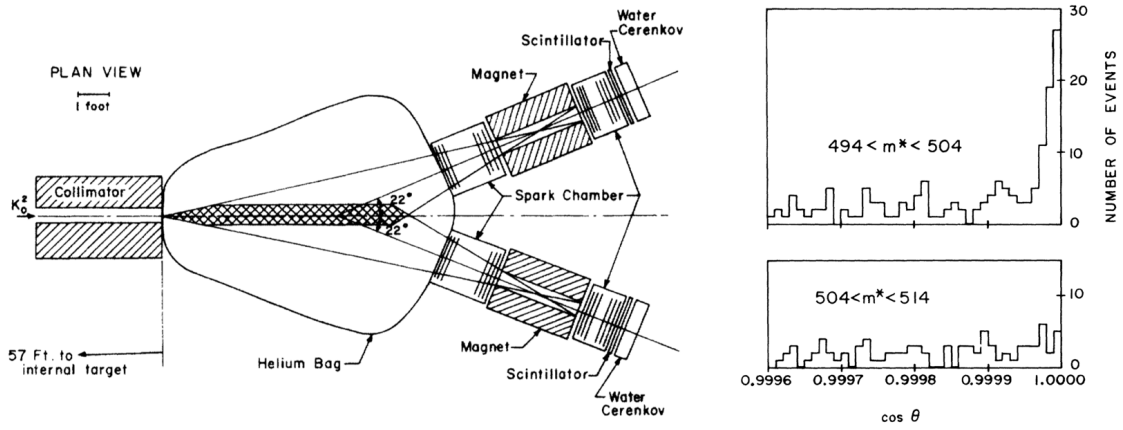
Evacuating the decay tube is vital because it is possible to regenerate a $K^0_{\rm S}$ component in a pure $K^0_{\rm L}$ beam by interaction with matter (Pais & Piccioni, 1955, Muller, 1960). The strange neutral meson, $\overline{K}^0$, interacts with nucleons to produce hyperons, $\overline{K}^0 + N \to \Lambda^0 + \pi$; there is no such process for the anti-strange meson, K^0. Neglecting *CP* violation ($p^2 = q^2 = \frac{1}{2}$), the $K^0_{\rm L}$ wavefunction can be written in terms of proportions f and $\bar{f}$,

$$\begin{aligned} |K^0_{\rm L}\rangle &= \tfrac{1}{\sqrt{2}}\left(f \quad |K^0\rangle \quad - \; \bar{f} \quad |\overline{K}^0\rangle \quad \right), \;\; f = \bar{f} = 1. \\ &= \tfrac{1}{\sqrt{2}}\left(f\tfrac{1}{\sqrt{2}}(|K^0_{\rm S}\rangle + |K^0_{\rm L}\rangle) - \; \bar{f}\tfrac{1}{\sqrt{2}}(|K^0_{\rm S}\rangle - |K^0_{\rm L}\rangle)\right) \\ &= \frac{1}{2}(f - \bar{f})|K^0_{\rm S}\rangle + \frac{1}{2}(f + \bar{f})|K^0_{\rm L}\rangle \end{aligned}$$

Due to the differing interaction lengths in matter, it can evolve that $f \neq \bar{f}$ and a $K^0_{\rm S}$ component appears in the beam. This means two-pion events are observed whereas only three-pion events would be expected for a pure $K^0_{\rm L}$ *CP*− wavefunction.

2.2 Discovery of CP violation

In 1963 Blair *et. al.* reported and excess of $K^0_{\rm S}$ regeneration. A year later, Cronin & Fitch confirmed that observation but concluded that the excess could not be attributed to regeneration alone: the $K^0_{\rm L}$ meson was itself decaying into $\pi^+\pi^-$ and hence violating the supposed invariance of *CP* symmetry. Their experiment, shown below, was setup to count the number



of $\pi^+\pi^-$ decays from a pure K^0_L beam passing through a volume of well controlled density. They reported an excess of decays consistent with two-pion decays along the beam line of 45 ± 10 events, with 10 attributable to K^0_S regeneration. The 35 anomolous decays from around 7 million K^0_L particles estimated to pass through the experiment suggests the *CP* symmetry is violated at a rate of

$$5 \times 10^{-6} \approx (2.3 \times 10^{-3})^2 = \epsilon^2 \,. \tag{14}$$

This result implies that the K^0_L mass eigenstate is not a *CP* eigenstate. Relabelling the *CP* eigenstates K_1 and K_2, we write,

$$|K_1\rangle = \tfrac{1}{\sqrt{2}}\left(|K^0\rangle + |\overline{K}^0\rangle\right) \qquad |K_2\rangle = \tfrac{1}{\sqrt{2}}\left(|K^0\rangle - |\overline{K}^0\rangle\right).$$
$$|K^0_S\rangle = |K_1\rangle + \epsilon|K_2\rangle \qquad |K^0_L\rangle = \epsilon|K_1\rangle + |K_2\rangle \,,$$

which is Eq. 13 with $p = (1+\epsilon)$ and $q = (1-\epsilon)$,

$$|K^0_S\rangle = \frac{1}{\sqrt{2(1+|\epsilon|^2)}}\left((1+\epsilon)|K^0\rangle + (1-\epsilon)|\overline{K}^0\rangle\right) \qquad |K^0_L\rangle = \frac{1}{\sqrt{2(1+|\epsilon|^2)}}\left((1+\epsilon)|K^0\rangle - (1-\epsilon)|\overline{K}^0\rangle\right). \tag{15}$$

Note that Eq. 13, and hence Eq. 15, attributes the *CP*-violation to the mixing parameters p and q such that some amount of $|K_1\rangle$ is present in the $|K^0_L\rangle$ wavefunction. Most generally, one should consider including *direct CP*-violation in the decay $K_2 \to \pi\pi$; but as we shall see later, this makes a very small contribution to the $K^0_L \to \pi\pi$ rate.

2.3 Categories of *CP* violation

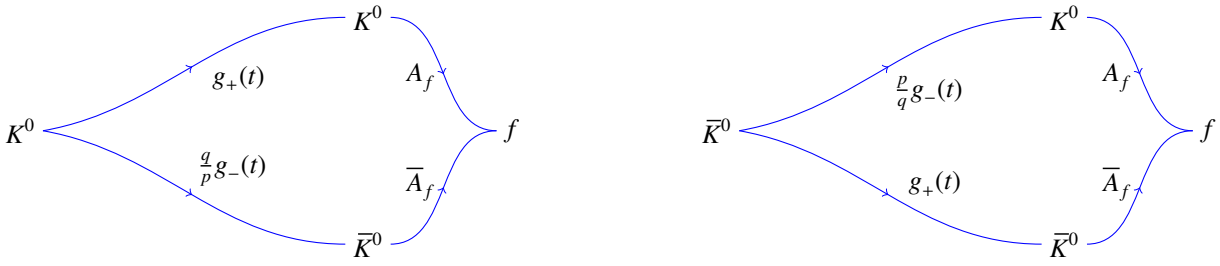
Let us define the amplitude of each flavour eigenstates decaying to a *CP* eigenstate, f (e.g. $\pi\pi$),

$$A_f = \langle f|\mathcal{H}_{\text{weak}}|K^0\rangle \qquad \overline{A}_f = \langle f|\mathcal{H}_{\text{weak}}|\overline{K}^0\rangle \,.$$

We wish to know the probability of observing f at time t from a particle that was of known strangeness (K^0 or $\overline{K}^0$) at $t = 0$.

$$\mathcal{A}_{K^0 \text{ at } t=0}(t) = A_f g_+(t) + \overline{A}_f \frac{q}{p} g_-(t) \qquad \overline{\mathcal{A}}_{\overline{K}^0 \text{ at } t=0}(t) = \overline{A}_f g_+(t) + A_f \frac{p}{q} g_-(t)$$
$$= A_f\left(g_+(t) + \lambda\ g_-(t)\right) \qquad = \overline{A}_f\left(g_+(t) + \lambda^{-1} g_-(t)\right)$$

$$\text{where } \lambda = \frac{q\overline{A}_f}{pA_f} \,.$$



$$\Gamma(K^0_{t=0} \to f) = |A_f|^2 \, |g_+(t) + \lambda \, g_-(t)|^2$$
$$= |A_f|^2 \, \left[|g_+(t)|^2 + |\lambda|^2 | \, g_-(t)|^2 + \;\; 2 \;\; \Re \left(\, \lambda^* \, g_+(t) \, g_-^*(t) \, \right) \right] \tag{16}$$
$$\Gamma(\overline{K}^0_{t=0} \to f) = |\overline{A}_f|^2 \, |g_+(t) + \lambda^{-1} g_-(t)|^2$$
$$= |\overline{A}_f|^2 \, \left[|g_+(t)|^2 + \frac{1}{|\lambda|^2} |g_-(t)|^2 + \frac{2}{|\lambda|^2} \Re \left(\lambda \, g_+(t) \, g_-^*(t) \, \right) \right] \tag{17}$$

Differences between Eqs. 16 and 17 give rise to *CP* violation. This can be of three distinct types:

1. $|\overline{A}_f| \neq |A_f|$: direct *CP* violation in the decay amplitude;
2. $\left| \frac{q}{p} \right| \neq 1$: *CP* violation in mixing amplitudes so $|\lambda|^2 \neq 1$;
3. $\lambda \neq \lambda^*$: $\Im(\lambda) \neq 0$ is *CP* violation in the interference of mixing and decay.

Extension to consider CP-conjugate decays

Eqs. 16 and 17 have been formed considering a common *CP*-eigenstate final state (e.g. $\pi^+\pi^-$) in which the K^0 or $\overline{K}^0$ is reconstructed. More generally, one can consider the case of two final states, f and its *CP* conjugate $\bar{f}$ by taking the *CP* conjugates of Eqs. 16 and 17,

$$\Gamma(\overline{K}^0_{t=0} \to \bar{f}) = |\overline{A}_{\bar{f}}|^2 \, \left[|g_+(t)|^2 + |\overline{\lambda}|^2 | \, g_-(t)|^2 + \;\; 2 \;\; \Re \left(\, \overline{\lambda}^* \, g_+(t) \, g_-^*(t) \, \right) \right] \tag{18}$$
$$\Gamma(K^0_{t=0} \to \bar{f}) = |A_{\bar{f}}|^2 \, \left[|g_+(t)|^2 + \frac{1}{|\overline{\lambda}|^2} |g_-(t)|^2 + \frac{2}{|\overline{\lambda}|^2} \Re \left(\overline{\lambda} \, g_+(t) \, g_-^*(t) \, \right) \right] \tag{19}$$

where we introduce an almost-reciprocal *CP* violating parameter for the *CP*-conjugate final state ($\bar{f}$),

$$\overline{\lambda} = \frac{p A_{\bar{f}}}{q \overline{A}_{\bar{f}}}$$

Comparing $\overline{\lambda}$ to λ, the p and q have swapped places, as have A and $\overline{A}$. Notice that $\overline{\lambda} = \lambda^{-1}$ in the case that f is a *CP* eigenstate. In this case Eqs. 18 and 19 are redundant copies of Eqs. 16 and 17.

Semileptonic final states are a special case of this extension. As f can only come from K^0, and $\bar{f}$ only from $\overline{K}^0$, $\overline{A}_f = A_{\bar{f}} = 0$. Furthermore, only one type of decay amplitude is possible for semileptonic weak decays so not *CP* violation in the decay amplitude is possible, $A_f = \bar{A}_{\bar{f}} = A$. This means Eqs. 16-19 become,

$$\Gamma(K^0_{t=0} \to f_{sl}) = |A|^2 \qquad |g_+(t)|^2$$
$$\Gamma(\overline{K}^0_{t=0} \to f_{sl}) = |A|^2 \, \left(\frac{p}{q} \right)^2 \, |g_-(t)|^2$$
$$\Gamma(\overline{K}^0_{t=0} \to \bar{f}_{sl}) = |A|^2 \qquad |g_+(t)|^2$$
$$\Gamma(K^0_{t=0} \to \bar{f}_{sl}) = |A|^2 \, \left(\frac{q}{p} \right)^2 \, |g_-(t)|^2$$

Thus semileptonic decays probe the *CP* violation in mixing only (i.e. that which is encoded in $p \neq q$).

2.4 Semileptonic asymmetry

Unlike $K \to \pi\pi$ decays, semileptonic decay amplitudes are unambiguous about which flavour eigenstate they have decayed from: $\pi^- l^+ \nu$ must come from a $K^0\,|\bar{s}d\rangle$, $\pi^+ l^- \nu$ from a $\overline{K}^0\,|s\bar{d}\rangle$. By comparing the number of K^0 and $\overline{K}^0$ decays, an asymmetry can be formed: $A = (N_{K^0} - N_{\overline{K}^0})/(N_{K^0} + N_{\overline{K}^0})$. This asymmetry, plotted in Fig. 4, is dominated by the oscillation of the mixing, but the oscillation is not about zero! At $t > 10^{-9}$ seconds (more than ten K^0_S lifetimes) one sees the bias: there are more K^0 than $\overline{K}^0$. If *CP* were conserved, i.e. if the K^0_L were a *CP* eigenstate, an equal amount of K^0 and $\overline{K}^0$ should be seen.

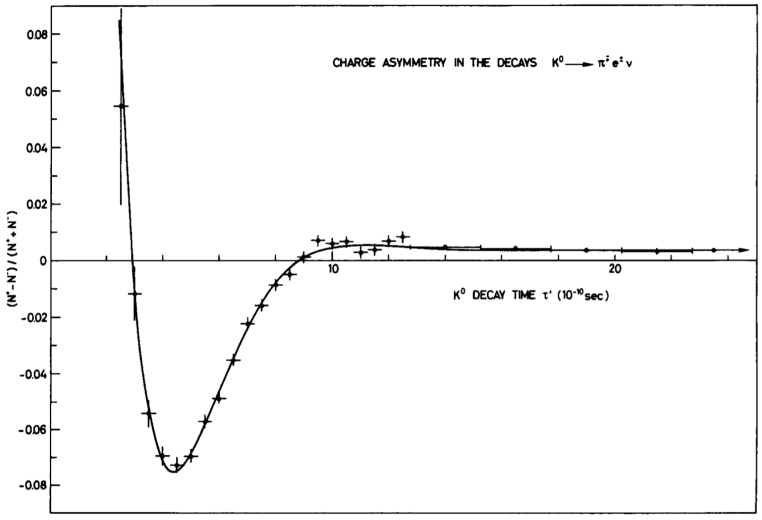


Fig. 1. The charge asymmetry as a function of the reconstructed decay time τ' for the K_{e3} decays. The experimental data are compared to the best fit as indicated by the solid line.

Figure 4: Charge asymmetry in semileptonic kaon decays. Gjesdal *et. al.*, Phys. Lett. **52B** 113 (1974).

Using the definition of the K^0_L including the *CP*-violating parameter, ϵ from Eq. 15, one derives the time-independent asymmetry in semileptonic K^0_L decays,

$$\begin{aligned}
\delta_{sl} &= \frac{\Gamma(K^0_L \to \pi^- l^+ \nu) - \Gamma(K^0_L \to \pi^+ l^- \nu)}{\Gamma(K^0_L \to \pi^- l^+ \nu) + \Gamma(K^0_L \to \pi^+ l^- \nu)} \\
&= \frac{|1+\epsilon|^2 - |1-\epsilon|^2}{|1+\epsilon|^2 + |1-\epsilon|^2} \\
&= \frac{2\Re(\epsilon)}{1+|\epsilon|^2} \\
&= \frac{|p|^2 - |q|^2}{|p|^2 + |q|^2} \quad \text{or} \quad \frac{1-|q/p|^2}{1+|q/p|^2}
\end{aligned} \tag{20}$$

as $p = 1 + \epsilon$ and $q = 1 - \epsilon$. From this (and other) data the semileptonic asymmetry is measured as,

$$\delta_{sl} = (3.32 \pm 0.06) \times 10^{-3}\,.$$

Neglecting the relatively small $|\epsilon|^2$ term in the denominator of Eq. 20, one concludes that $\Re(\epsilon) \approx 1.65 \times 10^{-3}$. Comparing this with the Eq. 14 result, $|\epsilon| \approx 2.3 \times 10^{-3}$, one can conclude that the phase of ϵ is $\cos^{-1}\left(\frac{\Re(\epsilon)}{|\epsilon|}\right) \approx 44°$.

The similarity of the size of δ_{sl} (which is sensitive to type 2) and the effect in $K^0_L \to \pi^+\pi^-$ (sensitive to types 1,2,3) suggests the pionic *CP*-violation is dominated by mixing. To fully explore this, a time-dependent measurement is needed.

2.5 Time-dependent *CP* violation: CPLear

A time dependent study of $K \to \pi^+\pi^-$ decays require the initial flavour of the neutral kaon to be tagged. The CPLear experiment (CERN 1990-1996) used antiprotons incident on, and annihilating with, target protons to produce neutral kaons. The charges of the associated $\pi^\pm$ and $K^\pm$ tag the neutral kaon's flavour: $p\bar{p} \to \pi^+K^-K^0$ or $p\bar{p} \to \pi^-K^+\overline{K}^0$. The decay time is measured from the flight distance on the neutral kaon with its relativistic γ-factor calculated from the fourvector sum of the π^+ and π^-. Fig. 5 shows the time-dependent decay rate data of initially-tagged K^0 and $\overline{K}^0$ mesons to two-pions. By taking the difference of these two curves, an asymmetry is plotted below. The *CP*-violation is expressed in

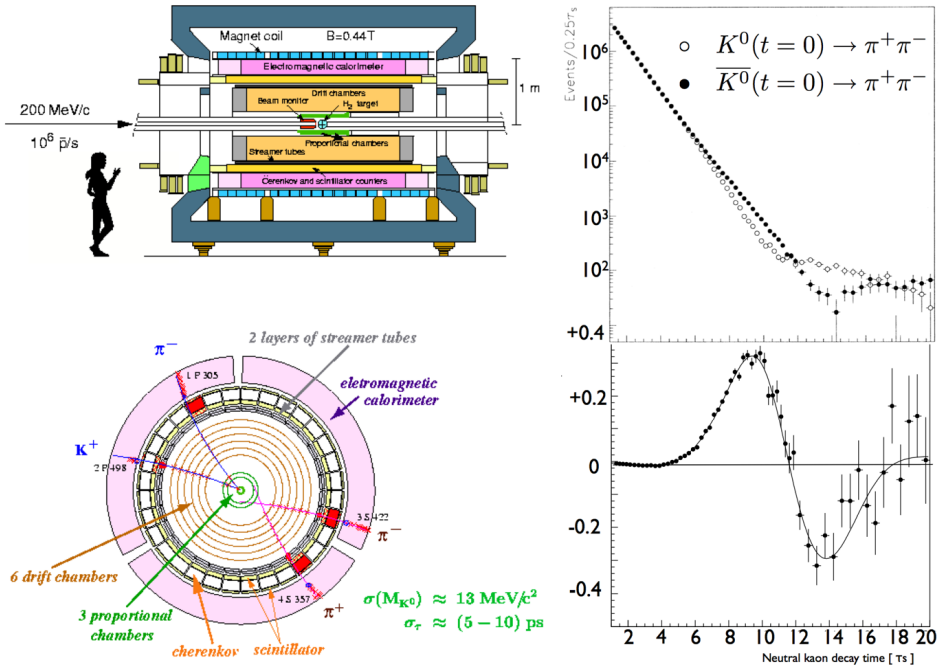


Figure 5: Clockwise from top left: a schematic of the CPLear detector, the decay distribution of initially-tagged K^0 and $\overline{K}^0$ mesons, the normalised asymmetry in % and an event display showing the cleanliness of the tagging.

terms of the observables by multiplying out the time-dependent $g_\pm$ factors labelling the light and heavy mass eigenstates according to their lifetime properties, K^0_S and K^0_L,

$$g_\pm = \tfrac{1}{2}[\underbrace{e^{-iM_St-\Gamma_St/2}}_{a} \pm \underbrace{e^{-iM_Lt-\Gamma_Lt/2}}_{b}] \qquad a^2 = e^{-\Gamma_St} \qquad b^2 = e^{-\Gamma_Lt}$$

From Eq. 16, using the a and b labels to clarify the algebra:

$$\begin{aligned}
\Gamma(K^0_{t=0} \to \pi\pi) &= |A_{\pi\pi}|^2\ \tfrac{1}{4}|(a+b)+\lambda(a-b)|^2 \\
&= |A_{\pi\pi}|^2\ \tfrac{1}{4}|a(1+\lambda)+b(1-\lambda)|^2 \\
&= |A_{\pi\pi}|^2\ \tfrac{1}{4}|1+\lambda|^2\ |\,a+\eta b\,|^2 && \eta = \frac{1-\lambda}{1+\lambda} \\
&= |A_{\pi\pi}|^2\ \tfrac{1}{4}|1+\lambda|^2\left(a^2+|\eta|^2b^2+2\Re[a\,\eta^*b^*]\right) \\
&= |A_{\pi\pi}|^2\ \tfrac{1}{4}|1+\lambda|^2\left(e^{-\Gamma_St}+|\eta|^2e^{-\Gamma_Lt}+2\Re\left[\eta^*\,e^{-iM_St-\Gamma_St/2}\,e^{iM_Lt-\Gamma_Lt/2}\right]\right) \\
&= |A_{\pi\pi}|^2\ \tfrac{1}{4}|1+\lambda|^2\left(e^{-\Gamma_St}+|\eta|^2e^{-\Gamma_Lt}+2|\eta|\Re\left[e^{-i\phi}\,e^{i(M_L-M_S)t}\right]e^{-(\Gamma_L+\Gamma_S)t/2}\right) && \eta = |\eta|e^{i\phi} \\
&= |A_{\pi\pi}|^2\ \tfrac{1}{4}|1+\lambda|^2\left(e^{-\Gamma_St}+|\eta|^2e^{-\Gamma_Lt}+2|\eta|\cos(\Delta Mt-\phi)\,e^{-(\Gamma_L+\Gamma_S)t/2}\right) && \Delta M = M_L - M_S \quad (21)
\end{aligned}$$

Similarly,

$$\Gamma(\overline{K}^0_{t=0} \to \pi\pi) = |\bar{A}_{\pi\pi}|^2 \ \tfrac{1}{4}\left|1+\tfrac{1}{\lambda}\right|^2 \left(e^{-\Gamma_S t} + |\eta|^2 e^{-\Gamma_L t} - 2|\eta|\cos(\Delta M t - \phi)\ e^{-(\Gamma_L+\Gamma_S)t/2}\right)$$
$$= |A_{\pi\pi}|^2 \left|\tfrac{p}{q}\right|^2 \tfrac{1}{4}|1+\lambda|^2 \left(e^{-\Gamma_S t} + |\eta|^2 e^{-\Gamma_L t} - 2|\eta|\cos(\Delta M t - \phi)\ e^{-(\Gamma_L+\Gamma_S)t/2}\right) \qquad \lambda = \frac{q\bar{A}_f}{pA_f} \tag{22}$$

The factor $\left|\frac{p}{q}\right|^2 \approx 1 - 4\Re[\epsilon] \approx 0.993$ from $p = (1+\epsilon)$ and $q = (1-\epsilon)$ and $\Re[\epsilon] \approx 1.65 \times 10^{-3}$. It is thus neglected (= 1) here to form the asymmetry,

$$\begin{aligned} a_{\pi^+\pi^-}(t) &= \frac{\Gamma(\overline{K}^0_{t=0} \to \pi^+\pi^-) - \Gamma(K^0_{t=0} \to \pi^+\pi^-)}{\Gamma(\overline{K}^0_{t=0} \to \pi^+\pi^-) + \Gamma(K^0_{t=0} \to \pi^+\pi^-)} \\ &= \frac{-4|\eta_{+-}|\cos(\Delta M t - \phi_{+-})\ e^{-(\Gamma_L+\Gamma_S)t/2}}{2\left(e^{-\Gamma_S t} + |\eta_{+-}|^2 e^{-\Gamma_L t}\right)} \\ &= \frac{-2|\eta_{+-}|e^{(\Gamma_S-\Gamma_L)t/2}\cos(\Delta M t - \phi_{+-})}{1 + |\eta_{+-}|^2 e^{(\Gamma_S-\Gamma_L)t}} \end{aligned} \tag{23}$$

Which is the form of the time-dependent asymmetry plotted in Fig. 5. A fit to these CPLear data finds,

$$|\eta_{+-}| = (2.26 \pm 0.03) \times 10^{-3} \qquad \arg(\eta_{+-}) = (43.2 \pm 0.7)^\circ .$$

The similarity of this result to that seen in semileptonic decays is evidence that the *CP* violation is dominated by a mixing effect and there is very little, or no, direct *CP* violation in the decay amplitudes.

In this derivation, we introduce an alternative *CP*-violation parameter, η that approaches zero in the limit of *CP* conservation ($\lambda \to 1$) and relate it to the amplitude for $K^0_L \to \pi^+\pi^-$ compared to that of K^0_S,

$$\eta_{+-} = \frac{1-\lambda}{1+\lambda} = \frac{pA_{+-} - q\bar{A}_{+-}}{pA_{+-} + q\bar{A}_{+-}} = \frac{\langle\pi^+\pi^-|K^0_L\rangle}{\langle\pi^+\pi^-|K^0_S\rangle} \ = \ \epsilon + \epsilon' .$$

The ϵ' is introduced to parametrise the additional effect due to direct *CP* violation in the decay amplitudes. In the [very good] approximation implied so far, there is no direct *CP* violation in $K \to \pi\pi$ decays, $\eta_{+-} = \epsilon$.

Finally, we note the advantage measuring *CP* violation in the interference between mixing and decay: the time-integrated effect in K^0_L decays detected by Cronin&Fitch is dependent on $|\eta|^2$ where the oscillatory interference term is proportional to $|\eta|$.

2.6 Direct *CP* violation: NA48

By the 1990s, *CP* violation was well studied but the underlying mechanism was still debated. The CKM mechanism predicted direct *CP* violation but there was not experimental evidence for it. The NA48 experiment (CERN 1997-2001) using a simultaneous K^0_L,K^0_S beam to search for direct *CP* violation. The experiment reported a measurement of the double ratio of the *CP* violation in two different final states, i.e. with differing A_f, $\bar{A}_f$.

$$\frac{|\eta_{00}|^2}{|\eta_{+-}|^2} = \frac{\Gamma(K^0_L \to \pi^0\pi^0)}{\Gamma(K^0_S \to \pi^0\pi^0)} \Big/ \frac{\Gamma(K^0_L \to \pi^+\pi^-)}{\Gamma(K^0_S \to \pi^+\pi^-)} \approx 1 - 6\mathrm{Re}\left(\frac{\epsilon'}{\epsilon}\right), \tag{24}$$

$$\text{because,} \qquad \eta_{+-} \approx \epsilon + \epsilon' \qquad \eta_{00} \approx \epsilon - 2\epsilon' \qquad \text{from isospin.} \tag{25}$$

The world average from NA48 and competitor experiments is $\mathrm{Re}(\epsilon'/\epsilon) = (1.65 \pm 0.26) \times 10^{-3}$ from the analysiss of over a trillion K^0_L on target. This result established that direct *CP* violation was possible, thus giving strong weight to the CKM mechanism of the Standard Model, but that it is a tiny effect in kaon decays.

The derivation of Eq. 25 follows from a isospin decomposition of the two pion state. As pions are bosons, the total final state wavefunction, $\Psi = \psi_{space}\psi_{flavour}$, must be symmetric. Decay from the spin-0 kaon, $L = 0$ so the spatial wavefunction is symmetric. The isospin (flavour) wavefunction must also be symmetric with total isospin $I = 0$ or 2, not 1. The total I_3 of the $\pi\pi$ combination must be 0 by charge conservation, so the Clebsch-Gordan coefficients are,

$$|0,0\rangle = \sqrt{\tfrac{1}{3}}\,|1,+1\rangle|1,-1\rangle - \sqrt{\tfrac{1}{3}}\,|1,0\rangle|1,0\rangle + \sqrt{\tfrac{1}{3}}\,|1,-1\rangle|1,+1\rangle \;\; = \sqrt{\tfrac{2}{3}}\,|\pi^+\pi^-\rangle - \sqrt{\tfrac{1}{3}}\,|\pi^0\pi^0\rangle\,,$$
$$|2,0\rangle = \sqrt{\tfrac{1}{6}}\,|1,+1\rangle|1,-1\rangle + \sqrt{\tfrac{2}{3}}\,|1,0\rangle|1,0\rangle + \sqrt{\tfrac{1}{6}}\,|1,-1\rangle|1,+1\rangle \;\; = \sqrt{\tfrac{1}{3}}\,|\pi^+\pi^-\rangle + \sqrt{\tfrac{2}{3}}\,|\pi^0\pi^0\rangle\,.$$

We decompose η_{+-} into the two isospin amplitudes,

$$\eta_{+-} = \frac{\langle\pi^+\pi^-|K^0_{\rm L}\rangle}{\langle\pi^+\pi^-|K^0_{\rm S}\rangle} = \frac{\sqrt{\frac{2}{3}}\langle\pi\pi_{I=0}|K^0_{\rm L}\rangle + \sqrt{\frac{1}{3}}\langle\pi\pi_{I=2}|K^0_{\rm L}\rangle}{\sqrt{\frac{2}{3}}\langle(\pi\pi_{I=0}|K^0_{\rm S}\rangle + \sqrt{\frac{1}{3}}\langle(\pi\pi_{I=2}|K^0_{\rm S}\rangle}$$
$$\eta_{00} = \frac{\langle\pi^0\pi^0|K^0_{\rm L}\rangle}{\langle\pi^0\pi^0|K^0_{\rm S}\rangle} = \frac{-\sqrt{\frac{1}{3}}\langle\pi\pi_{I=0}|K^0_{\rm L}\rangle + \sqrt{\frac{2}{3}}\langle\pi\pi_{I=2}|K^0_{\rm L}\rangle}{-\sqrt{\frac{1}{3}}\langle(\pi\pi_{I=0}|K^0_{\rm S}\rangle + \sqrt{\frac{2}{3}}\langle(\pi\pi_{I=2}|K^0_{\rm S}\rangle}$$

For η_{+-}, divide by $\sqrt{\frac{2}{3}}\langle\pi\pi_{I=0}|K^0_{\rm S}\rangle$ top and bottom gives,

$$\eta_{+-} = \frac{\frac{\langle(\pi\pi_{I=0}|K^0_{\rm L}\rangle}{\langle\pi\pi_{I=0}|K^0_{\rm S}\rangle} + \frac{1}{\sqrt{2}}\frac{\langle\pi\pi_{I=2}|K^0_{\rm L}\rangle}{\langle\pi\pi_{I=0}|K^0_{\rm S}\rangle}}{\frac{\langle\pi\pi_{I=0}|K^0_{\rm S}\rangle}{\langle\pi\pi_{I=0}|K^0_{\rm S}\rangle} + \frac{1}{\sqrt{2}}\frac{\langle\pi\pi_{I=2}|K^0_{\rm S}\rangle}{\langle\pi\pi_{I=0}|K^0_{\rm S}\rangle}} = \frac{\epsilon + \frac{1}{\sqrt{2}}\frac{\langle\pi\pi_{I=2}|K^0_{\rm L}\rangle}{\langle\pi\pi_{I=0}|K^0_{\rm S}\rangle}}{1 + \frac{\omega}{\sqrt{2}}} = \frac{\epsilon + \frac{\omega}{\sqrt{2}}\frac{\langle\pi\pi_{I=2}|K^0_{\rm L}\rangle}{\langle\pi\pi_{I=2}|K^0_{\rm S}\rangle}}{1 + \frac{\omega}{\sqrt{2}}}\,,$$

where we now specify ϵ to be the *CP* violation parameter for the $I = 0$ final state,

$$\epsilon \;=\; \frac{\langle\pi\pi_{I=0}|K^0_{\rm L}\rangle}{\langle\pi\pi_{I=0}|K^0_{\rm S}\rangle}\,, \quad \text{and} \quad \omega \;=\; \frac{\langle\pi\pi_{I=2}|K^0_{\rm S}\rangle}{\langle\pi\pi_{I=0}|K^0_{\rm S}\rangle}$$

is the proportion of the $I = 2$ to $I = 0$ in $K^0_{\rm S}$ decays. For η_{00} it is the same logic but dividing by $-\sqrt{\frac{1}{3}}\langle\pi\pi_{I=0}|K^0_{\rm S}\rangle$,

$$\eta_{00} = \frac{\epsilon - \sqrt{2}\omega\frac{\langle\pi\pi_{I=2}|K^0_{\rm L}\rangle}{\langle\pi\pi_{I=2}|K^0_{\rm S}\rangle}}{1 - \sqrt{2}\omega}\,.$$

The last step is to add and subtract terms to the numerator and identify a common expression for the difference in *CP* violation for the $I = 2$ and $I = 0$ amplitudes, which is by definition direct *CP* violation, and labelled ϵ'.

$$\eta_{+-} = \frac{\epsilon + \frac{\omega}{\sqrt{2}}\frac{\langle\pi\pi_{I=2}|K^0_{\rm L}\rangle}{\langle\pi\pi_{I=2}|K^0_{\rm S}\rangle} + \frac{\epsilon\omega}{\sqrt{2}} - \frac{\epsilon\omega}{\sqrt{2}}}{1 + \frac{\omega}{\sqrt{2}}} = \epsilon + \frac{\frac{\omega}{\sqrt{2}}\left(\frac{\langle\pi\pi_{I=2}|K^0_{\rm L}\rangle}{\langle\pi\pi_{I=2}|K^0_{\rm S}\rangle} - \epsilon\right)}{1 + \frac{\omega}{\sqrt{2}}} = \epsilon + \frac{\frac{\omega}{\sqrt{2}}\left(\frac{\langle\pi\pi_{I=2}|K^0_{\rm L}\rangle}{\langle\pi\pi_{I=2}|K^0_{\rm S}\rangle} - \frac{\langle\pi\pi_{I=0}|K^0_{\rm L}\rangle}{\langle\pi\pi_{I=0}|K^0_{\rm S}\rangle}\right)}{1 + \frac{\omega}{\sqrt{2}}} = \epsilon + \frac{\epsilon'}{1 + \frac{\omega}{\sqrt{2}}}\,.$$
$$\eta_{00} = \frac{\epsilon - \sqrt{2}\omega\frac{\langle\pi\pi_{I=2}|K^0_{\rm L}\rangle}{\langle\pi\pi_{I=2}|K^0_{\rm S}\rangle} + \sqrt{2}\epsilon\omega - \sqrt{2}\epsilon\omega}{1 - \sqrt{2}\omega} = \epsilon - \frac{\sqrt{2}\omega\left(\frac{\langle\pi\pi_{I=2}|K^0_{\rm L}\rangle}{\langle\pi\pi_{I=2}|K^0_{\rm S}\rangle} - \epsilon\right)}{1 - \sqrt{2}\omega} = \epsilon - \frac{2\frac{\omega}{\sqrt{2}}\left(\frac{\langle\pi\pi_{I=2}|K^0_{\rm L}\rangle}{\langle\pi\pi_{I=2}|K^0_{\rm S}\rangle} - \frac{\langle\pi\pi_{I=0}|K^0_{\rm L}\rangle}{\langle\pi\pi_{I=0}|K^0_{\rm S}\rangle}\right)}{1 - \sqrt{2}\omega} = \epsilon - \frac{2\epsilon'}{1 - \sqrt{2}\omega}\,.$$

Empirically, it is observed that the $\Delta I = \frac{1}{2}$ transition is favoured over the $\Delta I = \frac{3}{2}$ transition.[3] Thus $\omega \approx 0.05$ so the following approximations are commonly quoted,

$$\eta_{+-} \approx \epsilon + \epsilon' \qquad \eta_{00} \approx \epsilon - 2\epsilon'\,.$$

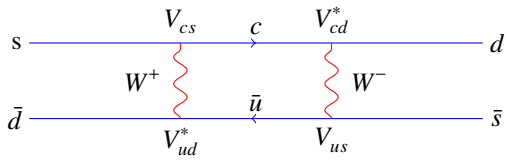
The double ratio of Eq. 25 follows using a simple binomial expansion of the ratio,

$$\frac{|\eta_{00}|^2}{|\eta_{+-}|^2} = \frac{|\,\epsilon - 2\epsilon'|^2}{|\,\epsilon + \epsilon'|^2}$$

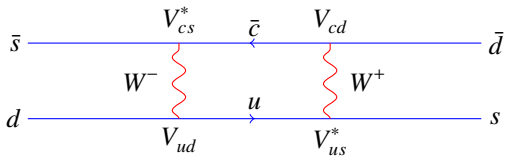
[3]The kaon lifetimes, $\tau(K^+) = 12.4$ ns, $\tau(K^0_{\rm S}) = 89$ ps, shows a noteworthy disparity because both decay to a $\pi\pi$ final state. Their total isospin must be even coming from a symmetric [flavour] wavefunction in the kaon: $I = 0, 2$ not 1. $I_3(\pi^+\pi^-) = I_3(\pi^0\pi^0) = 0$ but $I_3(\pi^+\pi^0) = 1$. Therefore the $K^0_{\rm S}$ decay can be $\Delta I = \frac{3}{2}$ or $\Delta I = \frac{1}{2}$, but the K^+ decay can only be $\Delta I = \frac{3}{2}$. The long lifetime shows that $\Delta I = \frac{3}{2}$ transitions are suppressed.

3 CKM mechanism for mixing *CP* violation

Neutral kaon mixing is a second-order weak transition which is described in the standard model by a box diagram. The vertex factors of the box diagram are proportional to the relevant CKM element. For example,



$\mathcal{M}_{fi} \propto V_{ud}^* V_{cs} V_{us} V_{cd}^*$



$\mathcal{M}_{if} \propto V_{ud} V_{cs}^* V_{us}^* V_{cd}$

$$\begin{pmatrix} u \\ c \end{pmatrix} \leftarrow W^{\pm} \rightarrow \begin{pmatrix} d' \\ s' \end{pmatrix} = \begin{pmatrix} V_{ud} & V_{us} \\ V_{cd} & V_{cs} \end{pmatrix} \begin{pmatrix} d \\ s \end{pmatrix}$$

this is just illustrative for the moment....

In the SM, ΔM_K has dependence on CKM factors and a difference of quark masses, which explains the mixing period,

$$\Delta M_K \approx \frac{G_F}{3\pi^2} V_{ud}^* V_{cs} V_{us} V_{cd}^* f_K^2 m_K \frac{(m_c^2 - m_u^2)^2}{m_c^2}$$

By comparing the $K^0 \rightarrow \overline{K}^0$ box diagram with the *CP*-conjugate $\overline{K}^0 \rightarrow K^0$ (which is also the *T*-conjugate $K^0 \leftarrow \overline{K}^0$ by the *CPT* ansantz) one sees that the rate differs if at least one of the contributing CKM elements is complex.

Most generally, a complex $N \times N$ matrix has $2N^2$ parameters but there are two important constraints. First, the matrix must be unitary; total probability needs to be respected, $V^\dagger V = 1$, this places N^2 constraints leaving N^2 free parameters. Second, the $2N$ quark fields can be arbitrarily rotated to remove $2N - 1$ unobservable relative phases,

$$\langle q_i | V_{ij} | q_j \rangle \rightarrow \langle q_i | e^{-i\phi_i} V_{ij} e^{i\phi_j} | q_j \rangle \quad : \quad V_{ij} \rightarrow e^{i(\phi_j - \phi_i)} V_{ij} \, .$$

Thus the quark mixing matrix has $N^2 - (2N - 1)$ independent physical parameters.

- N=2 gives just 1 physical parameter, a rotation between the first and second generation: the Cabibbo angle, θ_{12}.
- N=3 gives 4 physical parameters, three of which are the Euler rotations, leaving one complex phase.

$$V_{\text{CKM}} = \begin{pmatrix} 1 & 0 & 0 \\ 0 & \cos\theta_{23} & \sin\theta_{23} \\ 0 & -\sin\theta_{23} & \cos\theta_{23} \end{pmatrix} \times \begin{pmatrix} \cos\theta_{13} & 0 & \sin\theta_{13} e^{-i\delta} \\ 0 & 1 & 0 \\ -\sin\theta_{13} e^{-i\delta} & 0 & \cos\theta_{13} \end{pmatrix} \times \begin{pmatrix} \cos\theta_{12} & \sin\theta_{12} & 0 \\ -\sin\theta_{12} & \cos\theta_{12} & 0 \\ 0 & 0 & 1 \end{pmatrix}$$

The single, irreducible complex phase in V_{CKM} generates all *CP* violation phenonoma. Kobayashi and Maskawa predicted three generations of quarks after the Cronin&Fitch discovery a decade before the direct observation of the third generation.

Multiplied out, one finds the the imaginary part of V_{cs} and V_{cd} are indeed non-zero (compared to V_{ud}).

$$\begin{pmatrix} u \\ c \\ t \end{pmatrix} \leftarrow W^{\pm} \rightarrow \begin{pmatrix} \cos\theta_{12}\cos\theta_{13} & \sin\theta_{12}\cos\theta_{13} & \sin\theta_{13} e^{i\delta} \\ -\sin\theta_{12}\cos\theta_{23} - \cos\theta_{12}\sin\theta_{23}\sin\theta_{13} e^{i\delta} & \cos\theta_{12}\cos\theta_{23} - \sin\theta_{12}\sin\theta_{23}\sin\theta_{13} e^{i\delta} & \sin\theta_{23}\cos\theta_{13} \\ \sin\theta_{12}\cos\theta_{23} - \cos\theta_{12}\cos\theta_{23}\sin\theta_{13} e^{i\delta} & -\cos\theta_{12}\sin\theta_{23} - \sin\theta_{12}\cos\theta_{23}\sin\theta_{13} e^{i\delta} & \cos\theta_{23}\cos\theta_{13} \end{pmatrix} \begin{pmatrix} d \\ s \\ b \end{pmatrix}$$

But it is not immediately obvious from this parameterisation which CKM element has the largest imaginary part. There is a more convenient form, known as the Wolfenstein parameterisation expands the matrix in powers of the sine of the

Cabibbo angle, usually labelled[4] $\lambda = \sin\theta_{12}$,

$$\begin{pmatrix} V_{ud} & V_{us} & V_{ub} \\ V_{cd} & V_{cs} & V_{cb} \\ V_{td} & V_{ts} & V_{tb} \end{pmatrix} = \begin{pmatrix} \mathbf{1} - \lambda^2/2 - \lambda^4/8 & \lambda & A\lambda^3(\rho - i\eta) \\ -\lambda + \frac{\lambda^5}{2}A^2\,(1 - 2(\rho + i\eta)) & \mathbf{1} - \lambda^2/2 - \lambda^4/8(1 + 4A^2) & A\lambda^2 \\ A\lambda^3(1 - \rho - i\eta) + \frac{\lambda^5}{2}A(\rho + i\eta) & -A\lambda^2 + \frac{\lambda^4}{2}A\,(1 - 2(\rho + i\eta)) & \mathbf{1} - \lambda^4/2A^2 \end{pmatrix} + O(\lambda^6) \quad (26)$$

which makes the hierarchy in the CKM coupling transparent. Between the first and second generations the vertex factor is suppressed by $\sim \lambda \approx 0.22$. From generations one to three, the transition is suppressed by $\sim \lambda^3 \approx 0.01$ at the amplitude level. The size of the imaginary parts of V_{cs} and V_{cd} are tiny; the largest imaginary contributions are in V_{td} and V_{ub}.

The underlying origin of the hierarchy of the CKM elements is unknown and the four CKM parameters (either $\theta_{12}, \theta_{23}, \theta_{13}, \delta$, or λ, A, ρ, η) are fundamental parameters of the SM that must be measured from decays sensitive to the CKM elements. CKM element magnitudes can be deduced from comparing branching fractions of processes that differ only by the ratio of CKM factors, for example:

- $|V_{cd}| = 0.2256 \pm 0.0010$: from comparing $D^0 \to \pi^- e^+ \nu$ decays to $D^0 \to K^- e^+ \nu$ decays, assuming a known $|V_{cs}|$.
- $|V_{cb}| = 0.0393 \pm 0.0006$: from the branching fraction of $B \to D^{(*)} l\nu$ with some assumption on the hadronic model.
- $|V_{ub}| = 0.0035 \pm 0.0002$: from comparing $B \to \pi l\nu$ to $B \to D^{(*)} l\nu$, assuming a known $|V_{cb}|$.

Sensitivity to CKM phase information comes from *CP* violation. A *CP*-violating transition must have at least two contributing amplitudes, at least one of which has a non-zero imaginary part.

4 Mixing beyond kaons

Oscillatory phenomena is established on all four neutral meson systems. The mathematical model of neutral meson mixing is the same as in kaons though different simplifications are possible due to the particular lifetimes, lifetime and mass differences each case.

4.1 *B* physics

B mesons come in four varieties, differing by the flavour of the quark in the $q\bar{b}$ bound state. In increasing mass, these are,

$$B_u^+\,(5279\,\mathrm{MeV}/c^2) \quad B_d^0\,(5280\,\mathrm{MeV}/c^2) \quad B_s^0\,(5366\,\mathrm{MeV}/c^2) \quad B_c^+\,(6276\,\mathrm{MeV}/c^2)\,.$$

In contrast to kaons, *B* mesons decay to a range of final states all with considerable phase-space. This means the lifetime difference evident in kaons does not occur and we default back to labelling the mass eigenstates *Heavy* and *Light*.

B-mesons decay by a weak transition of the *b*-quark, or perhaps the *c*-quark in the case of the B_c meson. Due to the inaccessibility of its generational partner, the top, it must decay at tree-level to a charm, or occasionally an up quark ($|V_{cb}| >> |V_{ub}|$). This leads to a characteristically low transition probability, or to put it another way, a long lifetime,

$$B_u^\pm\,(1.64\,\mathrm{ps}) \qquad B_d^0\,(1.52\,\mathrm{ps}) \quad \Delta\Gamma \approx 0 \qquad B_{s,H}\,(1.62\,\mathrm{ps}) \quad B_{s,L}\,(1.42\,\mathrm{ps}) \qquad B_c^\pm\,(0.51\,\mathrm{ps})\,,$$

where the shorter lifetime of the $B_c^\pm$ is due to the additional partial width of Cabibbo-favoured *c*-quark decays. Only kaons, charged pions and muons, which also decay via the weak-force but with much smaller phase-space, live longer.

[4] There is a clash of notation but the *CP*-violating parameter $\lambda = qA/p\bar{A}$ and the Wolfenstein expansion parameter, $\lambda = \sin\theta_{\mathrm{Cabibbo}}$ are unrelated.

Over the 40 years since their discovery, B mesons have been studied by many experiments. These are of two types:

- e^+e^- beams can be tuned precisely to collide at specific energies. The $\Upsilon(4S)$ state is just above the kinematic threshold for B^+B^-,$B^0\bar{B}^0$ production. With nothing else in the event, this means a clean experimental environment although the $\Upsilon(4S)$ production cross-section is relatively low. A further advantage is that the two B mesons are produced in a quantum-entangled state. Experiments are ARGUS, CLEO, Babar, Belle and now Belle II.

- pp collisions have much larger production cross-sections than e^+e^-, especially at the TeV scales of the LHC. Backgrounds are much larger so a high granularity detector and sophisticated (albeit inefficient) selections are needed to cleanly identify signals. The principle handles for identifying a relatively heavy, relatively long-lived B meson is high transverse momentum of the decay products, and a large impact parameter with respect to the primary pp collision vertex. A big advantage of the LHC is that all types of b-hadrons are produced, B^0,B^+,B_s,B_c,Λ_b etc..., according to their hadronisation fractions. The dedicated B-physics experiment at the LHC is called LHCb.

4.2 $B_{(s)}$-meson mixing

The formalism for B mixing is almost identical to that of kaons though an important simplification is that the B mesons are heavy and there is lots of phase space available for the decay products. This means the lifetime difference between the two mass eigenstates is negligible ($\Delta\Gamma_{B^0} << \Delta M_{B^0}$) and we put $\Gamma_H = \Gamma_L = \Gamma$. This means for the probability of finding B^0 or $\bar{B}^0$ from a B^0 initial state at t=0 is,

$$\mathcal{P}_{B^0}(t) = |\langle B^0|B^0_{t=0}(t)\rangle|^2 = \frac{1}{2}e^{-\Gamma t}\left(1+\cos(\Delta M_{B^0}t)\right) \qquad \mathcal{P}_{\bar{B}^0}(t) = |\langle \bar{B}^0|B^0_{t=0}(t)\rangle|^2 = \frac{1}{2}e^{-\Gamma t}\left(1-\cos(\Delta M_{B^0}t)\right), \tag{27}$$

which is equivalent to the kaon rates in Eq. 12 with $\Gamma_H = \Gamma_L = \Gamma$.

We remember $\Delta M_K \approx 5\times10^{-3}\,\text{ps}^{-1}$ with $\tau(K^0_S) = 89\,\text{ps}$. The B^0 meson lifetime is much shorter (1.5 ps) so the potential to observe B^0 mixing depends on ΔM_{B^0} being at large 'enough' to occur within this shortened time. Let's consider the second-order $W^\pm$ box diagram, Fig. 6. The transition rate of this box process dominates the mixing probability: the larger

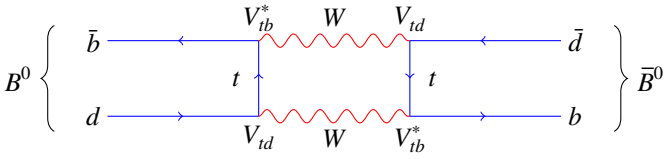


Figure 6: The second-order $W^\pm$ box diagram driving B-mixing. The asterisks denote CP-conjugation (time reversal) of the CKM coupling: $d(b) \to t$ becomes $t \to d(b)$ with an asterisk.

the mass difference, the higher the transition rate. ΔM_{B^0} received a contribution from u, c and t quark currents in the box. If all these quarks had identical mass, GIM suppression would be exact and there would be no mixing. However, as the top mass is much larger than the others, its contribution dominates ΔM_{B^0}. This is not the case for ΔM_K as the top contribution is moderated by the CKM coupling. In the SM,

$$\Delta M_{B^0} \;\approx\; 0.26\,|V_{tb}V^*_{td}|^2\left(\frac{m_t}{\text{GeV}/c^2}\right)^2\text{ps}^{-1} \;\approx\; 2.9\times10^{-5}\left(\frac{m_t}{\text{GeV}/c^2}\right)^2\text{ps}^{-1}. \tag{28}$$

For m_t in the range[5] $8-15\,\text{GeV}/c^2$, ΔM_{B^0} would be in the range $10^{-3}-10^{-2}\,\text{ps}^{-1}$, similar to ΔM^0_K.

[5] In the early 1980s, following the confirmation of the third quark generation by the observation of the Υ ($b\bar{b}$) resonances around $10\,\text{GeV}/c^2$, there was an expectation that the top mass would not be much higher. If fact, m_t is much, much higher, $172.4\pm0.5\,\text{GeV}/c^2$ (TeVatron 1995).

The Argus experiment (DESY 1987) first measured ΔM_{B^0} from $e^+e^- \to \Upsilon(4S) \to B^0\bar{B}^0$ pair production by counting the number of B^0 that oscillate after the $\bar{B}^0$ decays semileptonically. In 17% of double-semileptonic events, the two leptons were of the same charge. Same lepton charge means the same B-meson flavour, i.e. one had mixed.

The event display shows this: two $D^{*-}\mu^+\nu$ decays, $D^{*-} \to [K^+\pi^-]_{\bar{D}^0}\pi^-$ and $D^{*-} \to [K^+\pi^-\pi^-]_{\bar{D}^-}[\gamma\gamma]_{\pi^0}$ are reconstructed hence indicating the $\bar{B}^0$ ($|b\bar{d}\rangle$) has oscillated to a B^0 ($|\bar{b}d\rangle$). The analysis of the ARGUS data estimated $\Delta M_{B^0} \sim 0.5\,\text{ps}^{-1}$ and thus, from Eq. 28, $m_t \approx 130\,\text{GeV}/c^2$. This was the first indication of a very-high top quark mass and predated the direct discovery of the top quark by eight years. The B_d mass difference is now known precisely, $\Delta M_{B^0} = 0.510 \pm 0.004\ \text{ps}^{-1}$.

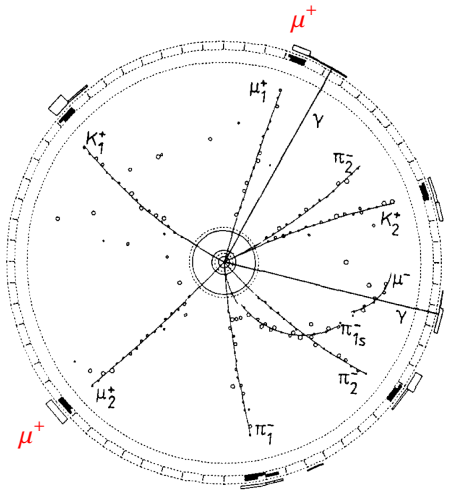


Fig. 2. Completely reconstructed event consisting of the decay $\Upsilon(4S) \to B^0\bar{B}^0$.

And what of the final neutral meson, the B_s meson? The B_s mixing diagram is identical to that of B^0 above except the spectator d quark is replaced with an s quark so $|V_{ts}|$ appears in the Δ_M formula instead of $|V_{td}|$. Inspection of the CKM matrix, indicates that these two elements differ by at least a factor $\lambda = \sin\theta_C \approx 0.22$, so expect,

$$\Delta M_{B_s} = \frac{|V_{ts}|^2}{|V_{td}|^2}\Delta M_{B^0} \geq \left(\frac{1}{0.22}\right)^2 0.51\text{ps}^{-1} \approx 11\text{ps}^{-1}\,.$$

which is so fast that it presents an experimental problem to see such rapid oscillations. The CDF experiment (TeVatron 2006) were first to detect a high B_s oscillation frequency finding $\Delta M_{B_s} \approx 18\text{ps}^{-1}$. LHCb has superior vertexing capability and could spatially resolve the small distances involved, see Fig. 7. LHCb data for the slower oscillation of the B^0 meson is also shown. The final state flavour is tagged from the decay, $B^0_{(s)} \to D^-_{(s)}\pi^+$ or $\bar{B}^0_{(s)} \to D^+_{(s)}\pi^-$. The initial flavour is tagged by "the other B" in the $pp \to BBX$ production. This is the same idea as tagging the initial kaon flavour from "the other K" in CPLear, though the tagging at LHC is not 100% accurate. Such mistagging reduces the amplitude of the flavour oscillations but does not effect the period.

4.3 D-mixing

The neutral D meson, at 1864 MeV/c^2 is much heavier than the kaons and pions that it predominantly decays into ($\sim$ 490 and $\sim$ 140 MeV/c^2 respectively) which allows a wide range of different decay modes. This large phase-space is available to both mass eigenstates and so, unlike with kaons, the difference in the lifetime is small and the mass ordering uncertain so we default back to labelling them mass eigenstates 1&2,

$$|D_1\rangle = p\,|D^0\rangle| + q\,|\bar{D}^0\rangle$$
$$|D_2\rangle = p\,|D^0\rangle| - q\,|\bar{D}^0\rangle\,,$$

and $|p|^2 + |q|^2 = 1$. Following the kaon formalism above, the time evolution is described by,

$$|D(t)\rangle = g_+\,|D^0\rangle + \frac{q}{p}g_-\,|\bar{D}^0\rangle$$
$$|\overline{D}(t)\rangle = g_+\,|\bar{D}^0\rangle + \frac{p}{q}g_-\,|D^0\rangle$$

where the time-dependent factors are again, $g_\pm(t) = \frac{1}{2}\left[e^{-iM_1t-\Gamma_1t/2} \pm e^{-iM_2t-\Gamma_2t/2}\right]$.

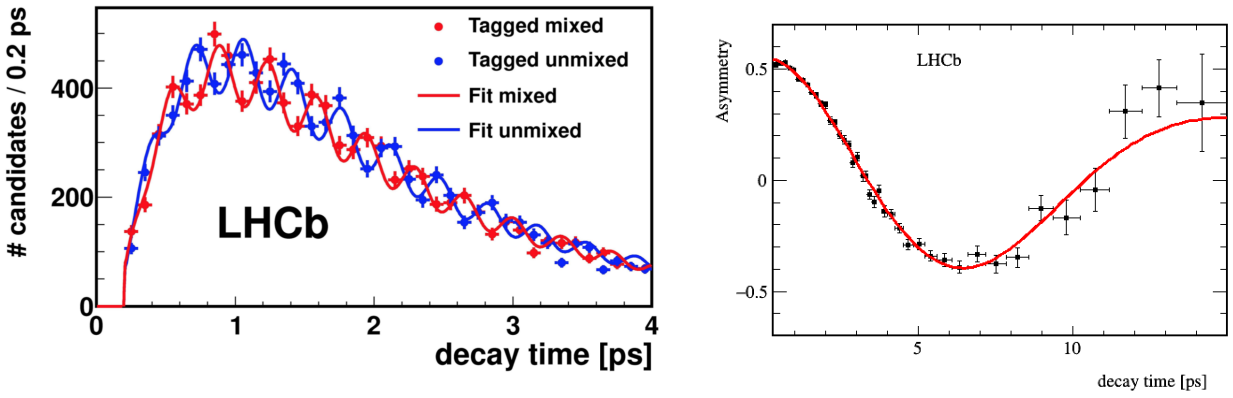


Figure 7: B_s oscillations from $D_s^{\pm}\pi^{\mp}$ data (left). Asymmetry= $\frac{N(\bar{B}^0)-N(B^0)}{N(\bar{B}^0)+N(B^0)}$ from $D^{\pm}\pi^{\mp}$ data (right). Note the differing x-scales; the B_s mesons oscillates 35 times faster than B^0 mesons. The initial flavour at $t = 0$ is know from "flavour tagging". The oscillations do not seem to fall to zero (go to asymmetries of ± 1) only because of imperfect tagging and time resolution. The plots does not start at $t = 0$ because a flight distance selection is mandatory to get a clean samples of B mesons.

As the phase space is large and charm-to-strange transitions are Cabibbo-favoured (as opposed to strange-to-up transitions in kaon decays), the lifetimes of the two D mass eigenstates are several orders or magnitude smaller than that of the kaons ($\sim 4 \times 10^{-13}$s rather than 5×10^{-8}s for the K_L^0). This is bad for observing mixing because essentially all D-mesons will decay before having a chance to oscillate[6]. The equivalent of Fig. 3 for D mesons would show both red and blue curves dropping to zero immediately (in a few picoseconds) long before one oscillation period.

The shortness and similarity of the lifetimes means that both the mass difference ΔM and lifetime difference $\Delta\Gamma$ need simultaneous consideration. This makes both the algebra and the measurement more complicated. It is useful to define,

$$M \equiv \frac{M_1 + M_2}{2} \;, \qquad \Gamma \equiv \frac{\Gamma_1 + \Gamma_2}{2} \;, \qquad \Delta M \equiv M_1 - M_2 \;, \qquad \Delta\Gamma \equiv \Gamma_1 - \Gamma_2 \;, \qquad x \equiv \frac{\Delta M}{\Gamma} \;, \qquad y \equiv \frac{\Delta\Gamma}{2\Gamma}$$

and rewrite the time-dependent factors,

$$g_+(t) = e^{-iMt-\Gamma t/2} \cos\left(\frac{1}{2}\Delta M t - \frac{i}{4}\Delta\Gamma t\right) = e^{-iMt-\Gamma t/2} \cos\left(\frac{x}{2}\Gamma t - \frac{iy}{2}\Gamma t\right) \tag{29}$$

$$g_-(t) = e^{-iMt-\Gamma t/2}\, i \sin\left(\frac{1}{2}\Delta M t - \frac{i}{4}\Delta\Gamma t\right) = e^{-iMt-\Gamma t/2}\, i \sin\left(\frac{x}{2}\Gamma t - \frac{iy}{2}\Gamma t\right). \tag{30}$$

The kaon oscillation measurement is more straightforward because the the kaon flavour is tagged at both production and decay. Here, a beam of D^0 mesons is not feasible but large numbers of $D^{*\pm}$ mesons are produced in collider experiments. The flavour of neutral D mesons (*charm* or *anticharm*) can be known by inspecting the charge on the pion from $D^{*\pm}$ decays: $D^{*+} \to D^0\pi^+$ or $D^{*-} \to \bar{D}^0\pi^-$.

The shortness of the D^0 lifetime compared to the oscillation period means the D^0 equivalent of Fig. 3 cannot be used. Instead one uses an additional interference: that between a suppressed decay and mixing. The transition $c \to s + W^+$ is preferred over $c \to d + W^+$. This means a $K^+\pi^-$ decay can come from a D^0, but is 2 orders of magnitude more likely to have come from a $\bar{D}^0$ (favoured: $\bar{c} \to \bar{s} + W^-$),

$$\frac{\langle K^+\pi^-|D^0\rangle}{\langle K^+\pi^-|\bar{D}^0\rangle} \equiv r_D e^{-i\delta_D} \;, \qquad |r_D|^2 \approx 0.003 \;.$$

[6]This statement assumes the oscillation rate is similar to that of kaons due to the mixing box-diagram being dominated by the first two generations of quarks which are somewhat similar in mass and couplings.

Thus, if the mixing effect is occurs rarely, say in $\sim 1/500$ times, one has two paths or similar magnitude, going to an identical final state, see Fig 8. This is exactly the criteria for a system to exhibit interference and we next show this new interference is a larger effect than looking for the mixing directly with semileptonic decays.

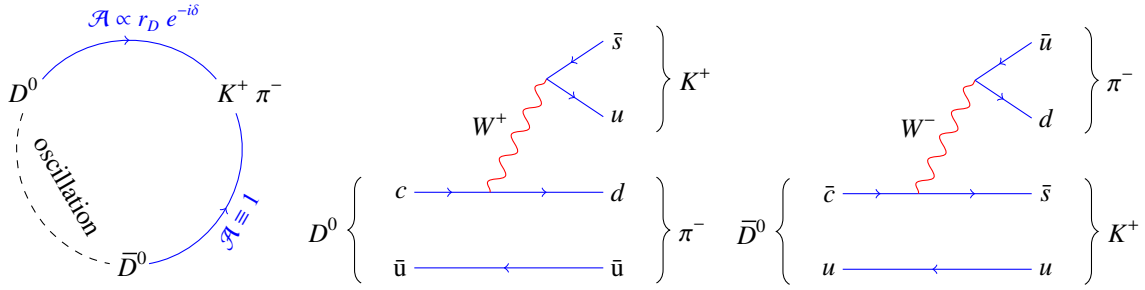


Figure 8: Illustration of the two ways in which a D^0 may transition of a $K^+\,\pi^-$ final state: (1) directly with a suppressed transition or (2) via an oscillation to a $\bar{D}^0$ and a favoured transition. Inspection of the Feynman diagrams reveal the reason for the suppression: one diagram have small CKM vertex factors, $V_{cd}V_{us}^*$ whilst the other's are of-order unity, $V_{cs}^*V_{ud}$.

As the final state is accessible to both D^0 and $\bar{D}^0$, we must consider the time-dependent rate of finding an initially-tagged D^0 in the suppressed final state $K^+\pi^-$ by either route.

$$\begin{aligned}\Gamma(D^0 \to K^+\pi^-) &= \left|\, \langle K^+\pi^-|D(t)\rangle \,\right|^2 \\ &= \left|\, g_+(t)\, \langle K^+\pi^-|D^0\rangle \;+ g_-(t)\, \langle K^+\pi^-|\bar{D}^0\rangle \,\right|^2 \\ &= \left|\, g_+(t)\, r_D e^{-i\delta_D} \;+\; g_-(t) \,\right|^2 \end{aligned} \tag{31}$$

where we reasonably neglect *CP* violation, $q/p = 1$.

Plugging Eq. 29 and 30 into Eq. 31 and expanding,

$$\begin{aligned}\Gamma(D^0 \to K^+\pi^-) &= \left| e^{-iMt-\Gamma t/2} \left[\cos\left(\frac{x}{2}\Gamma t - \frac{iy}{2}\Gamma t\right) r_D e^{-i\delta_D} + i \sin\left(\frac{x}{2}\Gamma t - \frac{iy}{2}\Gamma t\right)\right]\right|^2 \\ &= e^{-\Gamma t}\left[r_D^2 \cos^2\left(\frac{x}{2}\Gamma t - \frac{iy}{2}\Gamma t\right) + \sin^2\left(\frac{x}{2}\Gamma t - \frac{iy}{2}\Gamma t\right)\right] \\ &+ e^{-\Gamma t}\left[ir_D\left[\cos\left(\frac{x}{2}\Gamma t + \frac{iy}{2}\Gamma t\right)\sin\left(\frac{x}{2}\Gamma t - \frac{iy}{2}\Gamma t\right)e^{i\delta_D} - \cos\left(\frac{x}{2}\Gamma t - \frac{iy}{2}\Gamma t\right)\sin\left(\frac{x}{2}\Gamma t + \frac{iy}{2}\Gamma t\right)e^{-i\delta_D}\right]\right]\end{aligned}$$

Use of standard identities, remembering $\cos(i\theta) = \cosh\theta$ and $\sin(i\theta) = i\sinh\theta$ gives,

$$\begin{aligned}\Gamma(D^0 \to K^+\pi^-) &= e^{-\Gamma t}\left[\frac{1}{2}r_D^2\left(\cosh(y\Gamma t) + \cos(x\Gamma t)\right) + \frac{1}{2}\left(\cosh(y\Gamma t) - \cos(x\Gamma t)\right) + r_D\left(\cos\delta_D \sinh(y\Gamma t) - \sin\delta_D \sin(x\Gamma t)\right)\right] \\ &\simeq e^{-\Gamma t}\left[r_D^2\left(1 + \frac{y^2-x^2}{4}(\Gamma t)^2\right) + r_D\left(y\cos\delta_D - x\sin\delta_D\right)\Gamma t + \frac{y^2+x^2}{4}(\Gamma t)^2\right]\end{aligned}$$

Where the last step uses a small-angle approximation for the trigonometric and hyperbolic functions:

$$\cos x \approx 1 - \tfrac{x^2}{2}\,; \quad \cosh x \approx 1 + \tfrac{x^2}{2}\,; \quad \sinh x \approx \sin x \approx x\,.$$

The derivation for the favoured events initially tagged $\bar{D}^0$, for which a tiny fraction also oscillate before decay, is almost identical except one must take the complex conjugate of the decay amplitude which propagates to one sign-flip in the interference term. However in this case, the interference term is orders of magnitude smaller than the direct rate (which is no longer moderated by r_D^2) and can thus be safely neglected.

$$\begin{aligned}\Gamma(\bar{D}^0 \to K^+\pi^-) &\simeq e^{-\Gamma t}\left[\left(1 + \frac{y^2-x^2}{4}(\Gamma t)^2\right) + r_D\left(y\cos\delta_D + x\sin\delta_D\right)\Gamma t + r_D^2\frac{y^2+x^2}{4}(\Gamma t)^2\right] \\ &\approx e^{-\Gamma t}\end{aligned}$$

Taking the the ratio of rates, remembering the total width is just the inverse lifetime, $\Gamma = 1/\tau$ and further neglecting the quadruply-suppressed $r_D^2(x^2 + y^2)/4$ term one arrives at a quadratic in multiples of the D^0 lifetime,

$$R = \frac{D^0 \to K^+\pi^-}{\overline{D}^0 \to K^+\pi^-} \simeq r_D^2 + r_D\,(y\cos\delta_D - x\sin\delta_D)\left(\frac{t}{\tau}\right) + \frac{y^2 + x^2}{4}\left(\frac{t}{\tau}\right)^2 . \tag{32}$$

This function is fitted to the data in Fig. 9.

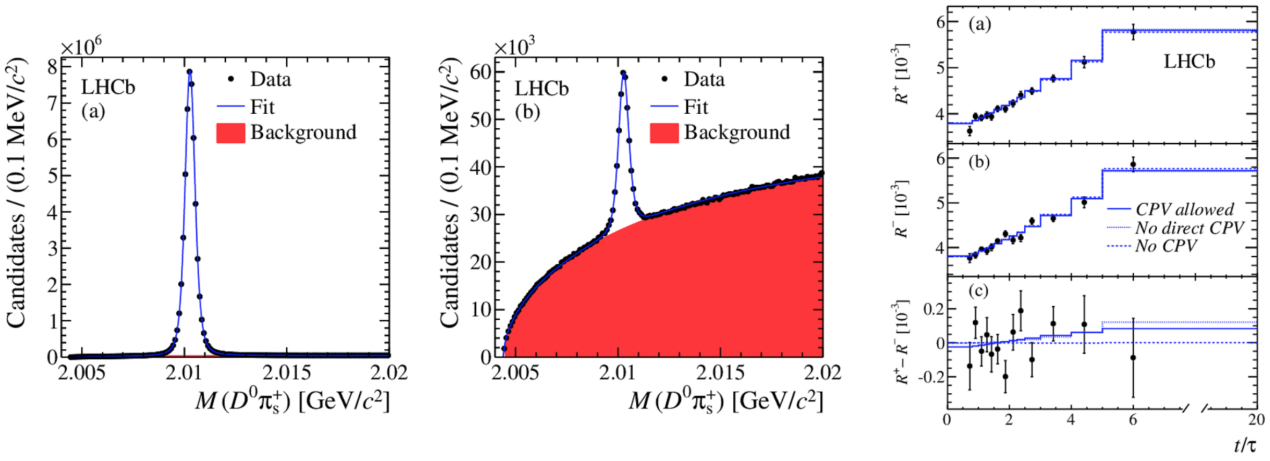


Figure 9: (a) Histogram of "right-sign" $D^{*-} \to [K^+\pi^-]_D\pi^-$ events. (b) Histogram of "wrong-sign" $D^{*+} \to [K^+\pi^-]_D\pi^+$ events. (c) The ratio of R in bins of $D^0/\overline{D}^0$ lifetime with a best-fit curve of Eq. 32.

One sees the dominant feature of the data is the approximately linear rise in number of "wrong-sign" $D^{*+} \to [K^+\pi^-]_D\pi^+$ events as a function of time. The slight curving of the fit is the quadratic term - to which the semileptonic decays have sensitivity - which we see yields comparatively little information.[7] This justifies the use of $D \to K\pi$ decays rather than semileptonic decays (as done with kaons) for which the linear term, proportional to $x\&y$, is not present.

From the fit values of the mixing parameters and the phase can be extracted; the world average (Moriond 2019) is,

$$x = 0.0039 \pm 0.0012 \qquad y = 0.0065 \pm 0.0007\,, \qquad \text{and} \quad \delta_D = (12 \pm 9)^\circ$$

which are small quantities. For the purpose of comparison to kaon oscillations, one can calculate from x the mass-difference, ΔM as the D^0 lifetime is 0.41 ps,

$$\begin{aligned}\Delta M\ [\text{eV}] = x\Gamma = \frac{x}{\tau} &= \frac{0.0037}{0.41\times10^{-12}} &&\approx 9.5\times10^{-3}\ [\text{ps}^{-1}]\\ &= \frac{x}{\tau}\cdot\frac{\hbar}{e} = 9.5\times10^{-3}\cdot\frac{1.05\times10^{-34}}{1.6\times10^{-19}} &&\approx 6.2\times10^{-6}\ [\text{eV}]\,.\end{aligned}$$

Which is close (less than a factor 2) to the same quantity in kaons, as expected from the CKM picture. Thus we understand that it is only the exceptionally long $K^0_{\rm L}$ lifetime that permits kaon oscillations to be seen rather easily. Neutral B mesons also have short lifetimes but their mixing rate is much higher so mixing effects are readily seen.

CP violation in charm

[7] to further persuade that semileptonic decays can only access the quadratic term, look again at Eq. 12 and notice the mixing dependence on $\cos\Delta Mt$ which for small $\Delta Mt = xt/\Gamma$ in the case of D mesons, is $\approx 1 + \frac{x^2}{2}(\Gamma t)^2$...

In 2019, LHCb announced the observation of *CP*-violation in charm after an analysis of ∼ 70M decays. Specifically, the analysis chose to measure a difference in two charge asymmetries as many systematic errors cancel in the subtraction,

$$\Delta A_{CP} = A_{CP}\left(D^0 \to K^+K^-\right) - A_{CP}\left(D^0 \to \pi^+\pi^-\right) \;=\; (-0.15 \pm 0.03)\%\,,$$
$$\text{where,}\;\; A_{CP}(D^0 \to f) = \frac{N(D^0 \to f) - N(\bar{D}^0 \to f)}{N(D^0 \to f) + N(\bar{D}^0 \to f)}\,,$$

and the initial flavour of the neutral charm meson is known by also reconstructing its parent particle,

$$\bar{B}^0 \to D^0\mu^-\bar{\nu} \;\text{ vs. }\; B^0 \to \bar{D}^0\mu^+\nu \quad \text{or} \quad D^{*-} \to D^0\pi^- \;\text{ vs. }\; D^{*+} \to \bar{D}^0\pi^+\,.$$

Because these are neutral mesons, it is not clear is the *CP* violation is direct *CP* violation or a time-dependent phenomenon. The LHCb dataset will increase by a factor 7 in the 2020s to resolve this question.

5 CP-violation in B mesons

If the CKM matrix describes all possible quark coupling via the weak force then total probability must be conserved, the matrix must be unitary. This, in turn, requires the matrix to satisfy unitarity relations, for example that the dot product of any two rows, or any two columns must equal 1 and thus the dot product of two different columns must be 0.

1. $V_{us}^*V_{ud}+V_{cs}^*V_{cd}+V_{ts}^*V_{td} = 0$ — *first and second columns*
2. $V_{ub}^*V_{ud}+V_{cb}^*V_{cd}+V_{tb}^*V_{td} = 0$ — *first and third columns*
3. $V_{ub}^*V_{us}+V_{cb}^*V_{cs}+V_{tb}^*V_{ts} = 0$ — *second and third columns*

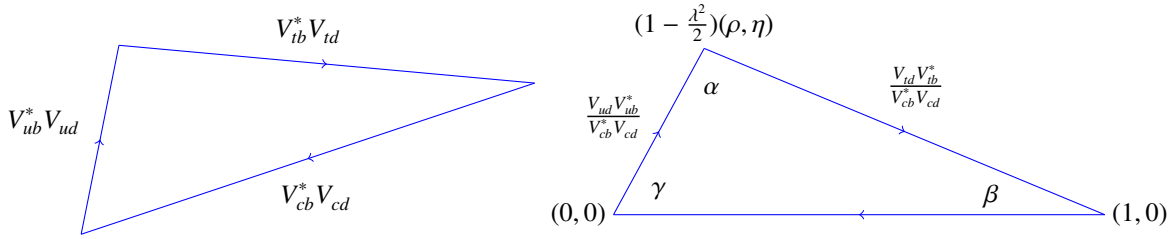
The sum of three complex numbers equalling zero are triangles in the complex plane. Consulting the CKM matrix in the Wolfenstein parameterisation neglecting terms smaller than $O(\lambda^4)$,

$$\begin{pmatrix} V_{ud} & V_{us} & V_{ub} \\ V_{cd} & V_{cs} & V_{cb} \\ V_{td} & V_{ts} & V_{tb} \end{pmatrix} = \begin{pmatrix} 1-\lambda^2/2-\lambda^4/8 & \lambda & A\lambda^3(\rho-i\eta) \\ -\lambda & 1-\lambda^2/2-\lambda^4/8(1+4A^2) & A\lambda^2 \\ A\lambda^3(1-\rho-i\eta) & -A\lambda^2+\frac{\lambda^4}{2}A\,(1-2(\rho+i\eta)) & 1-\lambda^4/2A^2 \end{pmatrix} + O(\lambda^5) \tag{33}$$

it is informative to notice the size of the triangles,

1. $O(\lambda) + O(\lambda) + O(\lambda^5)$ — $s-d$ *triangle :* K^0 *decays*
2. $O(\lambda^3) + O(\lambda^3) + O(\lambda^3)$ — $b-d$ *triangle :* B^0 *decays*
3. $O(\lambda^4) + O(\lambda^2) + O(\lambda^2)$ — $b-s$ *triangle :* B_s *decays*

The relative height of these triangles give an indication of the magnitude of the *CP* violation effect involved. The first triangle relates to the neutral kaon system and its modest height reflect the size of the observed *CP* violation, $(0.22)^{(5-1)} = 0.0023$ and $|\epsilon| = 2.3 \times 10^{-3}$. The second triangle suggests large *CP* asymmetries $O(1)$ seem possible. Graphically, it is,



where we "rotate and scale" in the second diagram, i.e. choose a convention where one side is unity. The three internal angles are *CP*-violating quantities that can be studied in many *B*-decay modes.

$$\alpha = \arg\left(-\frac{V_{tb}^*V_{td}}{V_{ub}^*V_{ud}}\right) \qquad \beta = \arg\left(-\frac{V_{cb}^*V_{cd}}{V_{tb}^*V_{td}}\right) \qquad \gamma = \arg\left(-\frac{V_{ub}^*V_{ud}}{V_{cb}^*V_{cd}}\right)$$

The Wolfenstein parameterisation places the *CP* violation only in the off-diagonal corners of the CKM matrix: in V_{td} and V_{ub} (to $O(\lambda^3)$). Thus, and noticing the minus sign of V_{cd}, these Unitarity Triangle angles simplify to,

$$V_{td} = |V_{td}|e^{-i\beta} \qquad V_{ub} = |V_{ub}|e^{-i\gamma} \qquad \alpha = \pi - \beta - \gamma\,. \tag{34}$$

To measure phases we two amplitude to interfere. For γ, at least one of the interfering processes must involve $b \to u$ quark transitions in B-meson decay. For β, at least one of the interfering processes must involve $d \to t$ quark transitions. As we shall see next, this is also achieved with B-mesons.

5.1 Formalism of *CP* violation with neutral *B* mesons

The derivations of Eqs. 16&17 imagined kaons but they are equally applicable to B mesons decaying to final state f,

$$\begin{aligned}\mathcal{A}_{B^0 \text{ at } t=0}(t) &= A_f g_+(t) + \bar{A}_f \frac{q}{p} g_-(t) \\ &= A_f \left(g_+(t) + \lambda\ g_-(t)\right)\end{aligned} \qquad \begin{aligned}\bar{\mathcal{A}}_{\bar{B}^0 \text{ at } t=0}(t) &= \bar{A}_f g_+(t) + A_f \frac{p}{q} g_-(t) \\ &= \bar{A}_f \left(g_+(t) + \lambda^{-1} g_-(t)\right)\end{aligned}$$

$$\Gamma(B^0_{t=0} \to f) = |A_f|^2 \left[|g_+(t)|^2 + |\lambda|^2\ |g_-(t)|^2 + \quad 2\,\Re\left[\lambda^* g_+(t)\, g_-^*(t)\ \right]\right] \tag{35}$$

$$\Gamma(\bar{B}^0_{t=0} \to f) = |\bar{A}_f|^2 \left[|g_+(t)|^2 + |\lambda|^{-2}|g_-(t)|^2 + |\lambda|^{-2} 2\,\Re\left[\lambda\, g_+(t)\, g_-^*(t)\ \right]\right], \tag{36}$$

and again, use some shorthand symbol (a, b) in the expansion of the time-dependent factors for the *Light* and *Heavy* mass eigenstates. An important property of B^0 mesons, simplifying the algebra, is that the difference in the lifetimes of the two mass eigenstate is negligibly small due to the large available phase space: $\Delta\Gamma = 0, \Gamma_H = \Gamma_L = \Gamma$.

$$g_\pm = \tfrac{1}{2}[\underbrace{e^{-i\,M_L t - \Gamma t/2}}_{a} \pm \underbrace{e^{-i\,M_H t - \Gamma t/2}}_{b}] \qquad \begin{aligned} a^2 &= e^{-\Gamma t} \\ b^2 &= e^{-\Gamma t}\end{aligned} \qquad \begin{aligned} ab^* &= e^{i\Delta M t} e^{-\Gamma t} \\ ab^* - ba^* &= 2\,i \sin(\Delta M t)\, e^{-\Gamma t}\end{aligned} \qquad \Delta M = M_H - M_L$$

Thus developing Eq. 35,

$$\begin{aligned}\Gamma(B^0_{t=0} \to f) &= |A_f|^2\ \tfrac{1}{4}\Big(\ a^2\ +\ b^2\ +2\ \ \Re\left[ab^*\right] \quad\ + |\lambda|^2\Big(\ a^2\ +\ b^2\ -2\,\Re\left[ab^*\right]\ \Big)\ +\ 2\Re\left[\lambda^*(a+b)(a^*-b^*)\right]\Big) \\ &= |A_f|^2\ \tfrac{1}{4}\left(e^{-\Gamma t} + e^{-\Gamma t} + 2e^{-\Gamma t}\Re\left[e^{i\Delta M t}\right] + |\lambda|^2\left(e^{-\Gamma t} + e^{-\Gamma t} - 2e^{-\Gamma t}\Re\left[e^{i\Delta M t}\right]\right)\ -\ e^{-\Gamma t} 2\Re\left[\lambda^* 2i\sin(\Delta M t)\right]\right) \\ &= |A_f|^2\ \tfrac{1}{2}e^{-\Gamma t}\Big(\quad 1\quad +\quad \cos(\Delta M t)\quad + |\lambda|^2\,(\quad 1\quad -\ \cos(\Delta M t)\ )\ -\quad 2\Im\left[\lambda\right]\ \sin(\Delta M t)\quad\Big) \\ &= |A_f|^2\ \tfrac{1}{2}e^{-\Gamma t}\quad (1+|\lambda|^2)\,(1 + C\cos(\Delta M t) - S\,\sin(\Delta M t))\ ,\end{aligned} \tag{37}$$

$$\text{where}\quad C = \frac{1-|\lambda|^2}{1+|\lambda|^2} \qquad S = \frac{2\Im\left[\lambda\right]}{1+|\lambda|^2} \qquad \lambda = \frac{q\bar{A}_f}{pA_f}\,.$$

Similarly for Eq. 36,

$$\begin{aligned}\Gamma(\bar{B}^0_{t=0} \to f) &= |\bar{A}_f|^2\ \tfrac{1}{4}\Big(\ a^2\ +\ b^2\ +2\ \ \Re\left[ab^*\right] \quad\ + |\lambda|^{-2}\Big(\ a^2\ +\ b^2\ -2\,\Re\left[ab^*\right]\ \Big)\ +\quad |\lambda|^{-2} 2\Re\left[\lambda(a+b)(a^*-b^*)\right]\Big) \\ &= |\bar{A}_f|^2\ \tfrac{1}{4}\left(e^{-\Gamma t} + e^{-\Gamma t} + 2e^{-\Gamma t}\Re\left[e^{i\Delta M t}\right] + |\lambda|^{-2}\left(e^{-\Gamma t} + e^{-\Gamma t} - 2e^{-\Gamma t}\Re\left[e^{i\Delta M t}\right]\right)\ -\ e^{-\Gamma t}|\lambda|^{-2}\, 2\Re\left[\lambda 2i\sin(\Delta M t)\right]\right) \\ &= |\bar{A}_f|^2\ \tfrac{1}{2}e^{-\Gamma t}\Big(\quad 1\quad +\quad \cos(\Delta M t)\quad + |\lambda|^{-2}\,(\quad 1\quad -\ \cos(\Delta M t)\ )\ +\quad |\lambda|^{-2} 2\Im\left[\lambda\right]\ \sin(\Delta M t)\quad\Big) \\ &= |\bar{A}_f|^2\ \tfrac{1}{2}e^{-\Gamma t}|\lambda|^{-2}\left(|\lambda|^2 + |\lambda|^2\cos(\Delta M t)\ +\quad 1\ -\ \cos(\Delta M t)\ +\quad 2\Im\left[\lambda\right]\ \sin(\Delta M t)\quad\right) \\ &= |A_f|^2\ \tfrac{1}{2}e^{-\Gamma t}\left|\tfrac{p}{q}\right|^2 (1+|\lambda|^2)\,(1 - C\cos(\Delta M t) + S\,\sin(\Delta M t))\ .\end{aligned} \tag{38}$$

For the derivation of the *CP* violation in kaons in the context of CPLear, we considered a final state $f = \pi\pi$, which is manifestly self conjugate. To be more general The *CP* conjugate equations of Eq. 37 and Eq. 38 should also be considered,

$$\Gamma(\bar{B}^0_{t=0} \to \bar{f}) = |\bar{A}_{\bar{f}}|^2\ \tfrac{1}{2}e^{-\Gamma t} \quad (1+|\bar{\lambda}|^2)\left(1 + \bar{C}\cos(\Delta M t) - \bar{S}\,\sin(\Delta M t)\right), \tag{39}$$

$$\Gamma(B^0_{t=0} \to \bar{f}) = |\bar{A}_{\bar{f}}|^2\ \tfrac{1}{2}e^{-\Gamma t}\left|\tfrac{q}{p}\right|^2 (1+|\bar{\lambda}|^2)\left(1 - \bar{C}\cos(\Delta M t) + \bar{S}\,\sin(\Delta M t)\right), \tag{40}$$

$$\text{where} \quad \bar{C} = \frac{1-|\bar{\lambda}|^2}{1+|\bar{\lambda}|^2} \qquad S_{\bar{f}} = \frac{2\Im\left[\bar{\lambda}\right]}{1+|\bar{\lambda}|^2} \qquad \bar{\lambda} = \frac{pA_{\bar{f}}}{q\bar{A}_{\bar{f}}}\,.$$

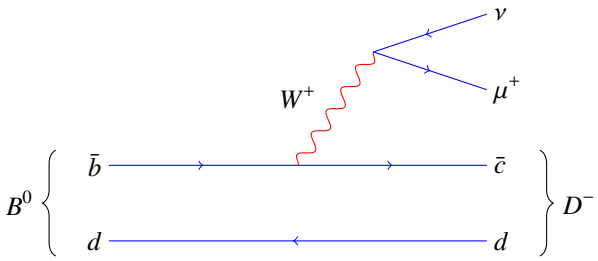
If f is a self-conjugate final state (e.g. $\pi^+\pi^-$), then $\bar{\lambda} = \lambda^{-1}$. Eqs. 39&40 become identical to Eqs. 38&37.

In the limit of *CP* conservation, $q = p$ and $A_{\bar{f}}/\bar{A}_{\bar{f}} = \bar{A}_f/A_f$. Thus $\bar{\lambda} = \lambda$, $\bar{C} = C$ and $\bar{S} = S = 0$. Inspection of Eqs. 37-39 with these substitutions gives $\Gamma(\bar{B}^0_{t=0} \to \bar{f}) = \Gamma(B^0_{t=0} \to f)$ and $\Gamma(B^0_{t=0} \to \bar{f}) = \Gamma(\bar{B}^0_{t=0} \to f)$, as would be expected.

5.2 *CP* violation in *B* mixing

As with kaons, *CP* violation in B^0-$\bar{B}^0$ mixing can be isolated with semileptonic decays. In this case, the charge of the muon in $B^0 \to D\mu\nu$ decays uniquely identifies the flavour of the decaying B meson: μ^+ identifies a B^0 decay, μ^- means a $\bar{B}^0$ decay. In the formalism of the previous section with $f = D^-\mu^+\nu$,

$$\bar{A}_f = 0\,, \quad A_{\bar{f}} = 0\,. \quad \text{Thus } \lambda = \bar{\lambda} = 0\,.$$



In addition, each semileptonic decays has just one contributing process so there is no direct *CP* violation: $\bar{A}_{\bar{f}} = A_f$.

CP violation in mixing is parameterised by $p \neq q$, or equivalently, by a non-zero semileptonic decay asymmetry,

$$a_{sl} = 1 - \left|\frac{q}{p}\right|^2 \neq 0\,.$$

This is measured by counting the number of $B \to D^-\mu^+\nu$ decays as well as the number of $B \to D^+\mu^-\nu$ decays where B is an untagged sample of B^0 and $\bar{B}^0$ mesons. It is assumed the B mesons are produced in equal number.

$$A^B_{sl} = \frac{N(B \to f) - N(B \to \bar{f})}{N(B \to f) + N(B \to \bar{f})} = \frac{\Gamma(B^0 \to f) + \Gamma(\bar{B}^0 \to f) - \Gamma(\bar{B}^0 \to \bar{f}) + \Gamma(B^0 \to \bar{f})}{\Gamma(B^0 \to f) + \Gamma(\bar{B}^0 \to f) + \Gamma(\bar{B}^0 \to \bar{f}) + \Gamma(B^0 \to \bar{f})}\,,$$

then substitute in Eqs. 37-39 with $\lambda = \bar{\lambda} = 0$, $|\bar{A}_{\bar{f}}|^2 = |A_f|^2$ and $|q/p|^2 = (1 - a_{sl})$,

$$\begin{aligned} A^B_{sl} &= \frac{1 + \cos(\Delta Mt) + (1-a_{sl})^{-1}(1 - \cos(\Delta Mt)) - \left[1 + \cos(\Delta Mt) + (1-a_{sl})(1 - \cos(\Delta Mt))\right]}{1 + \cos(\Delta Mt) + (1-a_{sl})^{-1}(1 - \cos(\Delta Mt)) \;+\; 1 + \cos(\Delta Mt) + (1-a_{sl})(1 - \cos(\Delta Mt))} \\ &= \frac{(1 + a_{sl} + \ldots)(1 - \cos(\Delta Mt)) - (1-a_{sl})(1 - \cos(\Delta Mt))}{2(1 + \cos(\Delta Mt)) + (1 + a_{sl} + \ldots)(1 - \cos(\Delta Mt)) + (1-a_{sl})(1 - \cos(\Delta Mt))} \\ &= \frac{a_{sl}}{2}\,(1 - \cos(\Delta Mt))\,. \end{aligned} \tag{41}$$

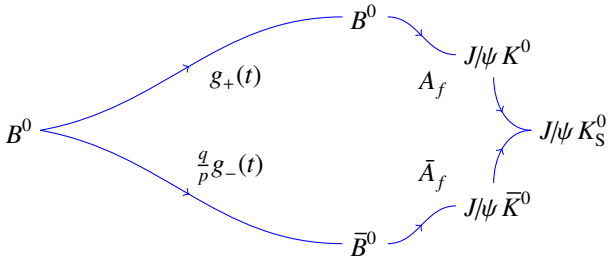
This is a measurement that does not require tagging of the initial flavour. This is experimentally useful because tagging is never perfect; typical correct tagging efficiencies are $\sim 5\%$ in hadron collider experiments and $\sim 30\%$ at e^+e^- B-factories.

The assumption that B^0 and $\bar{B}^0$ are produced in equal numbers is appropriate for colliders with a symmetric initial state like the e^+e^- B-factories or the $p\bar{p}$ collisions of the TeVatron. The pp collisions at the LHC are matter-antimatter asymmetric. A $\sim 0.5\%$ production asymmetry is expected and must be taken into account in a measurement of A^B_{sl}.

With kaons, the semileptonic asymmetry $\delta_{sl} = \frac{1-|q/p|^2}{1+|q/p|^2}$, Eq. 20. This is equivalent to A^B_{sl} in the case that $1 + |q/p|^2 \approx 2$, and $\Delta M << t$ such that $\langle \cos \Delta Mt \rangle \to 0$. Thus for kaons $a^K_{sl} \approx 2\delta_{sl} = 6.6 \times 10^{-3}$. With B^0 mesons, a smaller *CP*-violating effect in mixing is expected in the SM: $a^B_{sl}(\text{SM}) = -4 \times 10^{-4}$. Current data does not have statistical sensitivity at this level. Results for a^B_{sl} are consistent with zero with errors around the 2×10^{-3}.

5.3 *CP* violation in the interference of mixing and decay: the Unitarity Triangle angle β

The decay $B^0 \to J/\psi\, K^0_S$ offers an excellent example of *CP* violation in interference between mixing and decay amplitudes. This type of *CP* violation is that which occurs when λ has a non-zero imaginary part even though the its modulus is unity. The two paths to the same final state are mixed and unmixed B^0 mesons followed by *CP*-conjugate decays, $B \to J/\psi\, K^0_S$ is chosen because it is a *CP* eigenstate with high branching fraction, clean signature and good reconstruction efficency.[8]



The unmeasured *CP* violation in B-mixing tells us that $|M_{12}| \gg |\Gamma_{12}|$ so the short-range 'box' diagram drives B-mixing. We also remember that M_{12} is the off-diagonal element that describes how much of a pure-B^0 wavefunction at $t = 0$ has transformed to $\bar{B}^0$, via the box diagram shown in Fig. 6. Thus, following Eq. 10,

$$\frac{q}{p} = \sqrt{\frac{M_{12} - \frac{i}{2}\Gamma_{12}}{M^*_{12} - \frac{i}{2}\Gamma^*_{12}}} \Rightarrow \sqrt{\frac{M_{12}}{M^*_{12}}} = \sqrt{\frac{V_{td}V^*_{tb}V_{td}V^*_{tb}}{V^*_{td}V_{tb}V^*_{td}V_{tb}}} = \frac{|V_{td}|\, e^{-i\beta}}{|V_{td}|\, e^{+i\beta}} = e^{-i2\beta}\,.$$

using the definition of β from Eq. 34, and taking $V_{tb} = 1$.

The decay amplitudes are almost identical and involve only real CKM elements,

$$\frac{\overline{A}_f}{A_f} = \frac{A\left(\bar{B}^0 \to J/\psi\, \bar{K}^0\right)}{A\left(B^0 \to J/\psi\, K^0\right)} = \frac{V_{cb}V^*_{cs}}{V^*_{cb}V_{cs}} = 1 \qquad \left(\text{i.e. no contribution to the phase down to } O(\lambda^5).\right)$$

Finally, the neutral kaon propagates as one of two mass eigenstates, which have opposing *CP* quantum numbers,

$$CP|J/\psi\rangle = -1|J/\psi\rangle,\quad CP|K^0_S\rangle \simeq +|K^0_S\rangle \quad \text{hence} \quad CP|J/\psi\, K^0_S\rangle = -|J/\psi\, K^0_S\rangle. \quad CP \text{ eigenvalue, } \eta = -1 \text{ for } f_{CP} = J/\psi\, K^0_S\,.$$
$$\text{Similarly, } CP|K^0_L\rangle \simeq -|K^0_L\rangle \quad \text{hence} \quad CP|J/\psi\, K^0_L\rangle = +|J/\psi\, K^0_L\rangle. \quad CP \text{ eigenvalue, } \eta = +1 \text{ for } f_{CP} = J/\psi\, K^0_L.$$

Altogether, for $J/\psi\, K^0_S$ and $J/\psi\, K^0_L$,

$$\lambda = \frac{q}{p}\frac{\overline{A}_f}{A_f} = \eta e^{-2i\beta} = \mp\cos 2\beta \pm i \sin 2\beta\,.$$

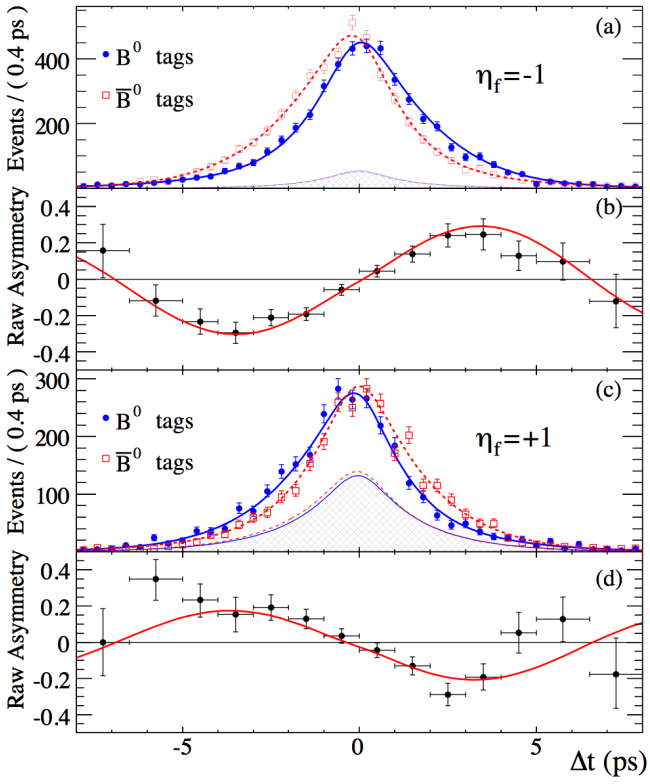
Finally, we form a time-dependent asymmetry from the rates defined in Eq. 37&38 knowing that $|q/p| = 1$ is established,

$$A_{CP}(t) = \frac{\Gamma(\bar{B}^0 \to f_{CP}) - \Gamma(B^0 \to f_{CP})}{\Gamma(\bar{B}^0 \to f_{CP}) + \Gamma(B^0 \to f_{CP})} = -\,C\cos\Delta M t + S\,\sin\Delta M t\,.$$

And furthermore, as $|\lambda|^2 = 1$, so $C = 0$ and $S = \Im(\lambda) = \pm\sin 2\beta$,

$$\begin{aligned} A_{CP}(t) &= \Im(\lambda)\sin\Delta M t \\ &= +\sin 2\beta \sin\Delta M t \qquad \text{for } J/\psi\, K^0_S\,, \\ &= -\sin 2\beta \sin\Delta M t \qquad \text{for } J/\psi\, K^0_L\,. \end{aligned}$$

[8] $\mathcal{B}(B^0 \to J/\psi\, K^0_S) = 4.35 \times 10^{-4}$, $\mathcal{B}(J/\psi \to \mu\mu) = 5.9\%$, $\mathcal{B}(K^0_S \to \pi^+\pi^-) = 69\%$. Total $\sim 2 \times 10^{-5}$ so need 10^8 B^0 to record $O(1000)$ of these decays.



These data come from the B-factories, KEKB and PEP2 (1999-2008) operated with an asymmetric e^+e^- collision energy of $\sqrt{s} = 10.58\,\mathrm{GeV}/c^2$ (9.0 vs. $3.1\,\mathrm{GeV}/c^2$). This is the same CoM energy as used by ARGUS, to produce $B\bar{B}$ pairs at the $\Upsilon(4S)$ resonance.

This measurement relies on quantum coherence. Only when one B decays is the 'clock' started. Hence the time-dependent CP study is conducted in both positive and negative time (expressed as Δt in the plot). The sign of the time depends on when the 'flavour tagging' associated decay ('of the other B') occurred before or after the signal $J/\psi\ K^0_S$ (or $J/\psi\ K^0_L$) decay.

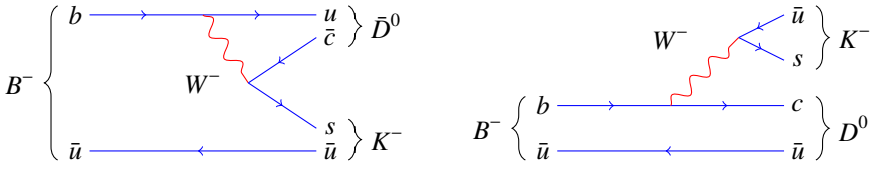
The period of the time-dependent CP asymmetry is defined by ΔM but the amplitude is $\sin 2\beta$. The amplitude is diluted by the imperfect tagging and the final measurement of $\sin 2\beta$ requires a measurement of the tagging efficiency. This is achieved by applying the tagging algorithms to samples of charged $B^\pm$ decays, as their b-flavour is known.

The result of these data and and all others gives,

$$\sin(2\beta) = 0.699 \pm 0.017 \qquad \Rightarrow \qquad \beta = (22.2 \pm 0.7)^\circ$$

5.4 Direct *CP* violation: the Unitarity Triangle angle γ

Of the three Unitarity angles, γ is the only one that is not dependent on a virtual coupling to the top quark in a box diagram. This means mixing is not needed and we can look for direct CP violation. Charged $B^\pm \to DK^\pm$ decays do not mix and so can be effected by direct CP violation in the decay amplitudes only.



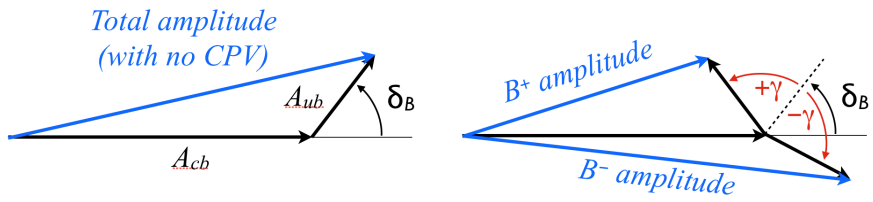
Because the the left and right processes produce a $\bar{D}^0$ and D^0 respectively, it is necessary to reconstruct them in a decay that is accessible to both; for example $D \to K^+K^-$. Also, the γ sensitivity aries because these two diagrams interference and one of them has a dependency on V_{ub} (the second has a negligible weak phase). We write that the amplitude of the right-hand [most abundant] process as A_{fav} and the left-hand suppressed process as,

$$A_{\mathrm{sup}} = A_{\mathrm{fav}} \cdot r_B e^{i\delta_B} e^{-i\gamma} \qquad \leftarrow\ CP\ \rightarrow \qquad \overline{A}_{sup} = \overline{A}_{\mathrm{fav}} r_B e^{i\delta_B} e^{+i\gamma}\,.$$

The symbol r_B is the relative magnitude, $r_B = \frac{|\overline{A}_{sup}|}{|\overline{A}_{fav}|}$ and δ_B is a *CP*-conserving "strong" phase difference between the two diagrams. The manner in which the complex amplitudes sum is shown in the cartoon for $\gamma = 0$ as well as a [large] finite value. By definition in this derivation, $\overline{A}_{\rm fav} = A_{\rm fav}$ so the partial rate equations are,

$$\begin{aligned}\Gamma(B^- \to [K^+K^-]_D K^-) &= |A_{\rm fav} + A_{\rm sup}|^2 = |A_{\rm fav}|^2 \left|1 + r_B e^{i\delta_B} e^{-i\gamma}\right|^2 \\ &= |A_{\rm fav}|^2 \left[1 + r_B^2 + 2r_B \cos(\delta_B - \gamma)\right] \\ \Gamma(B^+ \to [K^+K^-]_D K^+) &= |A_{\rm fav} + \overline{A}_{\rm sup}|^2 = |A_{\rm fav}|^2 \left[1 + r_B^2 + 2r_B \cos(\delta_B + \gamma)\right] .\end{aligned}$$

As charged B mesons cannot mix, this is an example of direct *CP* violation where the difference between matter and



antimatter originates in the decay amplitude only. The following data (LHCb 2011) exemplifies the large, $O(10^{-1})$, *CP*-violation effects in B-decays. One remembers that the direct *CP*-violation seen with kaons is small, $\left|\frac{\epsilon'}{\omega}\right| \approx O(10^{-4})$. The

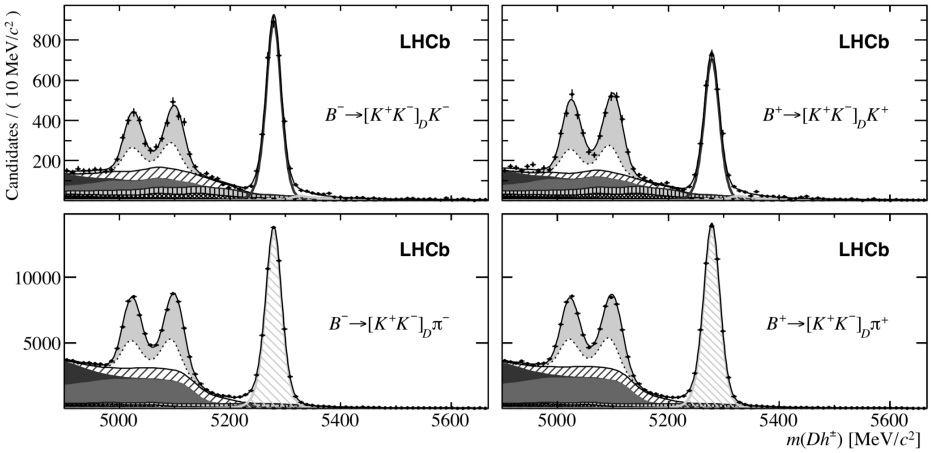


Figure 10: LHCb data (2011-2016) showing $B^\pm \to DK^\pm$ data (top) which has a large value of r_B and thus shows good sensitivity to γ. The bottom row shows $B^\pm \to D\pi^\pm$ data, which has a value or r_B which is $\sim{}^1/_{20}$ that of $B^\pm \to DK^\pm$ decays. The measurement of the asymmetry in the top row is, $A_{CP}^{DK} = (12.6 \pm 1.4)\%$.

result of these data and and all others gives,

$$\gamma = (67.0 \pm 4.0)^\circ .$$

Together the measurements of γ and β and the length of top side of the Unitarity Triangle that apex can be constrained experimentally to test the unitarity of quark couplings. The length of the top side, R_t is proportional to the magnitude of $V_{td}V_{tb}^*$, which depends of the measurements of the mixing frequency, ΔM_{B^0} described earlier. Global fits to all CKM-related data show reasonable consistency with unitarity, as expected in the SM.

In 1914, Chadwick[9] showed that the energy spectrum of the electron in nuclear β^- decay was continuous. It had been expected the emitted electron be monochromatic, and equal to the energy lost by the nucleus, as had been observed in α and γ decay. A number of confirmations followed in the 1920s. In1930, Pauli wrote a letter to a conference of experimentalists gathered in Türbingen regarding,

> *"the possibility that in the nuclei there could exist electrically neutral particles, which I will call neutrons* [later renamed neutrino]*, that have spin 1/2 and obey the exclusion principle and that further differ from light quanta in that they do not travel with the velocity of light. The mass of the neutrons should be of the same order of magnitude as the electron mass and in any event not larger than 0.01 proton mass. - The continuous beta spectrum would then make sense with the assumption that in beta decay, in addition to the electron, a neutron is emitted such that the sum of the energies of neutron and electron is constant."*

Twenty years later, in 1934, Fermi published his theory of β decay describing the contact interaction of four fermions. He imagined a vector current, like electromagnetism, but with weaker strength. His conclusion from the data was that the neutrino mass was small. 1934: Joliot-Curie produce an isotope of phosphorus, ${}^{30}_{15}P$ that emitted a positive particle, β^+

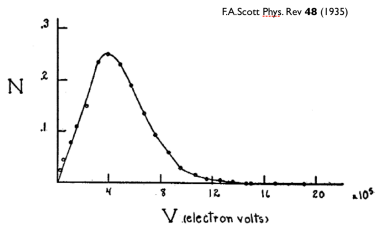


FIG. 5. Energy distribution curve of the beta-rays.

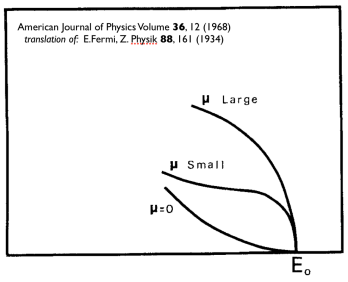


FIG. 1. The end of the distribution curve for $\mu=0$ and for large and small values of μ.

with the same m/e as the positron found two years earlier in cosmic rays (Anderson). It exhibited a continuous energy spectrum suggesting an antineutrino.

Two decades later, Cowan&Reines (1956) positively detected the neutrino by observing the coincidence of detection of a neutron and a positron from $\nu + p \rightarrow n + e^+$ in a water tank placed next to a nuclear reactor. A short while after, Lederman/Schwartz/Steinberger (1962) identified a second flavour of neutrino associated with muon production. Direct confirmation of a third type of neutrino waited until 2000 when the DONUT experiment (Fermilab) found a neutrino associated with τ lepton production. The ν_τ source was $D_s^+ \rightarrow \tau^+\nu_\tau$ decays from a fixed target.

Limits on the neutrino masses

A direct measure of the electron neutrino mass comes from the electron energy spectrum in beta decay. The maximum electron energy is equal to the change in mass the transmuting nuclei, E_0, minus the [at-rest] neutrino mass. It is possible

[9] Chadwick is most famous for detecting the the neutron by identifying (1932) a highly penetrating neutral emission when beryllium is bombarded with α particles. The high mass of this particle precluded it being the neutral particle associated with β decay.

to form the "Kurie" variable which is proportional to the electron energy in the absence of neutrino mass,

$$K(E) \propto \left[(E_0 - E)\left[(E_0 - E)^2 - m_\nu^2\right]^{\frac{1}{2}}\right]^{\frac{1}{2}} \quad \text{(not derived)}$$

Deviations from linearity at the end point the Kurie spectrum (see Fig. 11) would be evidence for neutrino mass. The distributions seems linear and an upper limit on the ν_e mass is < 0.8 eV (2021). Upper limits on muon and tau neutrinos

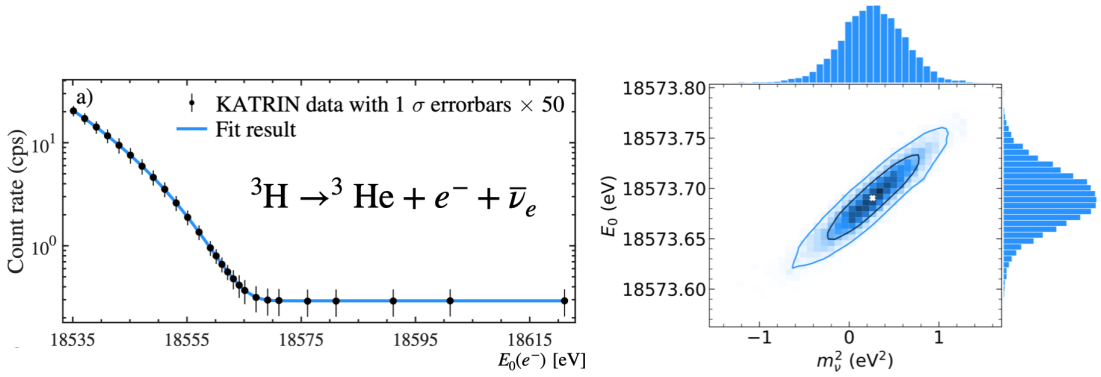
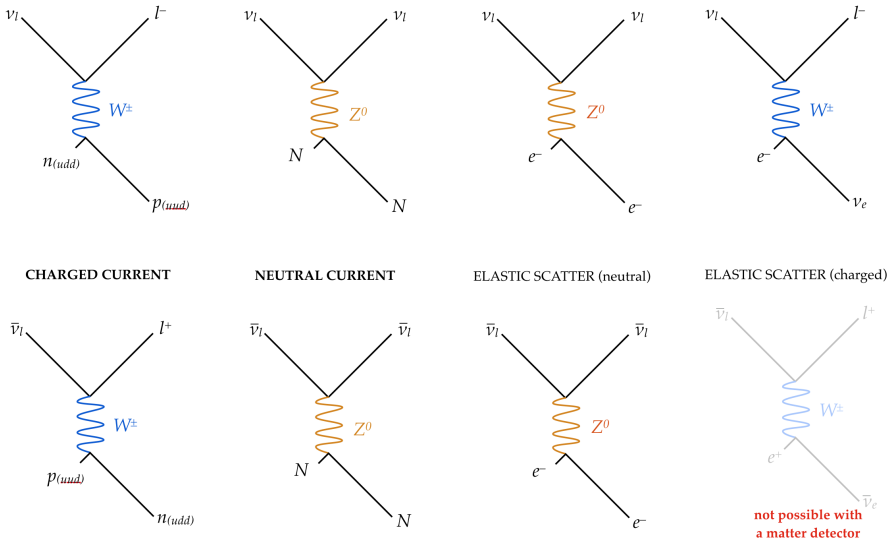


Figure 11: Kurie plot from KATRIN (2021), which makes precision measurements of tritium decays .

come from particle decay: $m(\mu_\mu) < 170$keV comes from a momentum analysis of stopped-pion decay; a kinematic analysis of a few thousand $\tau \rightarrow \pi\pi\pi\nu_\tau$ decays from $e^+e^- \rightarrow \tau^+\tau^-$ (LEP) yields the limit on $m(\mu_\tau) < 19$MeV. The most stringent limits on the sum of all three neutrino masses come from the power spectrum of the cosmic microwave background: $\sum_{i=1,2,3} m_i = 0.11 - 0.26\,\mathrm{eV}$ depending on the cosmological model considered (Planck 2018).

Direct neutrino detection

Neutrinos only feel the weak force so their detection can only proceed by the exchange of the massive weak-force boson, $W^\pm$ or Z^0. $W^\pm$ exchange precipitates a change of lepton flavour. A Z^0 exchange leaves the flavour unchanged.



Neutrino flavour is inferred by the production of their associated lepton in the charged current process. An electron neutrino will interact via the charged weak interaction with the electron only, and so forth. For an interaction to occur, the CoM energy must be sufficient to produce the lepton. Consider three cases:

- **Charged current scattering off a nucleon (CC)**, where the nucleon changes flavour, $\nu_l + n \to l + p$:

$$\begin{aligned} s &= (P_\nu + m_n)^2 > (m_l + m_p)^2 \\ \cancel{m_\nu^2} + 2E_\nu m_N + m_N^2 &> m_l^2 + 2m_l m_N + m_N^2 \qquad m_n \approx m_p = m_N \\ E_\nu &\gtrsim \frac{m_l^2}{2m_N} + m_l \end{aligned} \tag{42}$$

  which give the production thresholds for electrons, muons and taus as: 511keV, 112MeV and 3.45GeV respectively. The muon threshold is still high compared to nuclear processes though reasonable for cosmic rays or accelerators.

- **Neutral current scattering off a nucleon (NC)**, where the nucleon does not change its flavour, $\nu_l + N \to \nu_l + N$. This process has no energy threshold and is equally sensitive to all neutrino flavours.

- **Scattering off an atomic electron (ES)**: $\nu_l + e^- \to \nu_e + l^-$

$$\begin{aligned} s &= (P_\nu + P_e)^2 > m_l^2 \\ \cancel{m_\nu^2} + 2E_\nu P_e + m_e^2 &> m_l^2 \qquad P_e = m_e \text{ as initially at rest.} \\ E_\nu &> \frac{m_l^2 - m_e^2}{2m_e} \end{aligned} \tag{43}$$

  which requires energies greater than zero, 11GeV and 3.1TeV for e^-, μ^- and τ^- production respectively. This means that in practice, scattering off atomic electrons in neutrino experiments is sensitive to electron neutrinos only.

6 Solar Neutrinos

The Sun's core produces $2 \times 10^{38} \nu_e\, s^{-1}$ radiating out in 4π, giving a flux at Earth's orbit of $6.3 \times 10^{10} cm^{-2} s^{-1}$. 91% of these come from proton-proton fusion, $p + p \to {}^2_1D + e^+ \nu_e$, with neutrino energy up to ~ 0.4 MeV, which are difficult to detect. The next-most abundant process (8.1%) is electron capture by beryllium ${}^7_4\text{Be} + e^- \to {}^7_3Li + \nu_e$ that releases a monochromatic 0.9 MeV neutrino. The largest source of detected solar neutrinos is the ^{8}B ("Boron-8") process by which $\sim 0.01\%$ of the total neutrino flux are in the 1-12 MeV range.

The energies of ${}^7_4$Be neutrinos and most ^{8}B neutrinos are above threshold for charged-current capture, $\nu_e + n \to p + e^-$, by Chlorine ($E^{th} > 0.81$ MeV). The cross section for the charged-current interaction varies considerably from 2×10^{-46} cm^2 at 0.85 MeV to $< 10^{-41}$ cm^2 at 14 MeV. This means that though the ${}^7_4$Be neutrinos is orders of magnitude larger, most interactions with Chlorine atoms come from the higher-energy ^{8}B neutrinos.

The Homestake mine neutrino experiment (1968-1994) what constructed to verify the nuclear fusion energy generation mechanism in the Sun. 2.2×10^{30} chlorine atoms were placed 1478m underground in the form of 613 ton of dry-cleaning fluid (C_2Cl_4). For example, the expected number of interactions from the mono-energetic ${}^7_4$Be neutrinos is,

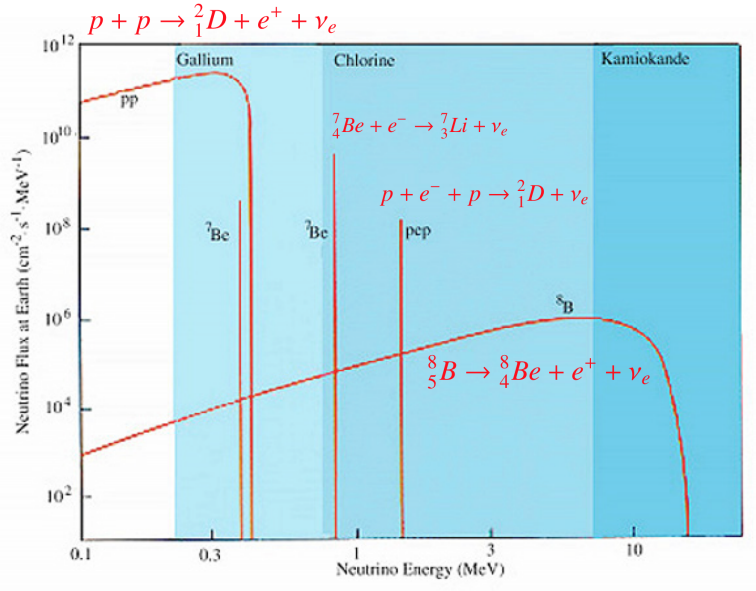
$$6.3 \times 10^{10} cm^{-2} s^{-1} \cdot 8.1\% \cdot 2 \times 10^{-46} cm^2 \cdot 10^{36} \approx 1.0 \text{ SNU (interactions per } 10^{36} \text{atoms per second)},$$

Six times this number of interactions is expected from the higher-energy ^{8}B neutrinos giving a total expectation of $R^{SSM}({}^{37}Cl) = (7.6 \pm 1.2)$ SNU. The principle experimental challenge is filtering out the few radioactive atoms of ^{37}Ar (solar neutrino interaction rate $O(1)\,day^{-1}$).

The first publication of a discrepancy between the measured neutrino flux (R. Davis Jr.) and a calculation using the emerging Standard Solar Model (J. Bahcall) occurred in 1968 and reported the observed flux to be 2.5 times lower than expectation. Following this initial work, Davis Jr. built, improved and maintained the Homestake mine experiment until 1994. The Standard Solar Model also developed over this time and in by the late 1990s a strong statement was made.

$$R^{\rm exp}(^{37}{\rm Cl}) = 2.56 \pm 0.23 {\rm SNU\ (interactions\ per\ } 10^{36} {\rm atoms\ per\ second}),$$

which is around one third that expected according to the Standard Solar Model (SSM).



Detection by radio-chemical capture:

$$\nu_e + {}^{72}_{31}{\rm Ga} \rightarrow {}^{72}_{32}{\rm Ge} + e^{-}$$
$$\nu_e + {}^{37}_{17}{\rm Cl} \rightarrow {}^{37}_{18}{\rm Ar} + e^{-}$$

Final state isotopes must be separated out and counted. Sensitive to rate only.

Or by Cherenkov detection in water:

$$\nu_e + e^{-} \rightarrow e^{-} + \nu_e$$

Useful for $E_\nu > 7$ MeV. Measures the direction of incoming neutrino.

The GALLEX (1991 –1997, Gran Sasso, Italy) and SAGE (1989 –2007, Baskan, Russia) experiments performed a similar measurements but with gallium- rather than chlorine-capture. Importantly, the $\nu_e + {}^{72}{\rm Ga} \rightarrow {}^{72}{\rm Ge} + e^{-}$ reaction has a lower threshold of 0.233 MeV giving sensitivity to the higher flux of pp fusion neutrinos, which have a maximum energy of 0.42 MeV. These experiments detected a ν_e flux that was 55% that expected from the SSM.

Further evidence of a diminished neutrino flux came from the SuperKamiokande experiment in Japan which, from 1995 until 2000, collected data from ES neutrinos by detecting the Cherenkov light from the recoiling electron in water. As the electron must recoil at relativistic speeds to generate Cherenkov, and to keep backgrounds from geo-radioactivity, the threshold is set higher than the calculation of Eq. 43. Over the lifetime of the experiment, techniques improved and the threshold was varied from 10 down to 7 MeV. The cross section for electrons from ES neutrino interactions is heavily peaked towards the the direction of the incoming neutrino ($\theta \sim 0$). The electron direction in ES interaction thus "points back" to the neutrino source. The flux of neutrinos in this energy region is observed to be under half that expected for the ^{8}B process in the SSM. The annual flux varied however, by about 7% from summer to winter as expected from the known eccentricity of Earth's orbit.

6.1 SNO

The Sudbury Neutrino Observatory, located 2km underground in Ontario, Canada was built to measure the flux of all neutrino flavours and thus measure the total neutrino flux from the Sun. It held 1000 tonnes of heavy water, D_2O which make a neutron-enriched target for performing neutrino astronomy. The fiducial spherical volume was contained within an outer water jacket which served as a shield, and veto counter for geo-radioactive backgrounds. SNO detect the flux of neutrinos from the Sun by all three reactions discussed above:

−− **Charged current:** reactions are detected by a cone of Cherenkov light from the fast-recoiling electron.

This component is sensitive to the the electron flux only as it requires the production of a lepton and only the electron is energetically accessible. Expect ~ 30 CC reactions per day.

$$\nu_e + D \rightarrow p + p + e^-$$
$$\text{charged current rate} \propto \phi(\nu_e)$$

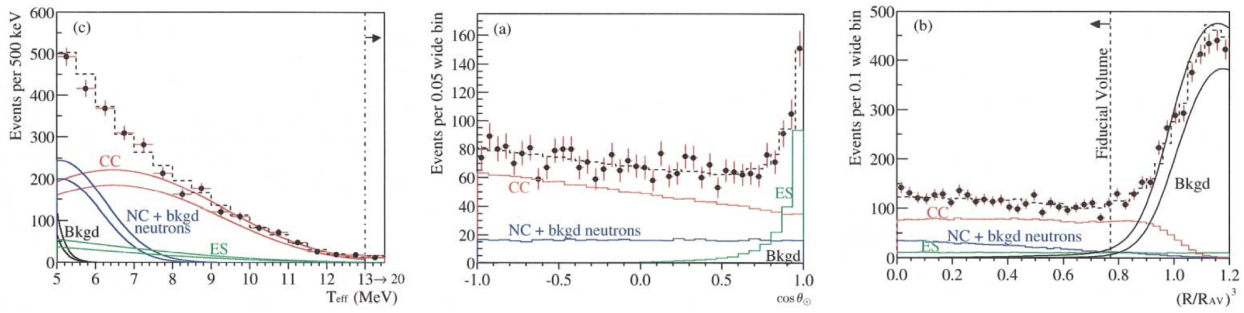
−− **Neutral current:** reaction causes the neutron to fly off and is eventually captured by another deuterium nuclei with an associated cascade of gamma-rays, which in turn scatter electrons to give a "haze" of Cherenkov light. Expect ~ 30 NC per day though the neutron capture by deuterium is only ~ 30% efficient.
This component is sensitive to all neutrino species equally.

$$\nu_x + D \rightarrow p + n + \nu_x$$
$$\text{neutral current rate} \propto \phi(\nu_e) + \phi(\nu_\mu) + \phi(\nu_\tau)$$

−− **Elastic scatter:** off atomic electrons can occur via both $W^\pm$ and Z^0 exchange. This scattering has enhanced sensitivity to the election flux because only the CC is sensitive only to the ν_e flux whereas the NC process sees all three flavours. The neutrino cross section for electron CC scattering is a factor ten smaller than that of the nucleon CC reactions and the out-going electron is strongly peaked in the forward direction (low scattering angle).

$$\text{elastic scattering rate} \propto \phi(\nu_e) + \tfrac{1}{6}\left(\phi(\nu_\mu) + \phi(\nu_\tau)\right)$$

In the analysis, these three components are distinguished by their visible energy, their direction of any produced light with respect to the Sun and distance from the edge of the reservoir (distinguishes geo-radioactive backgrounds). Using



calculable interaction cross sections and efficiencies the flux were found:

$$\phi_{CC} = (1.76 \pm 0.12) \times 10^6\,\text{cm}^{-2}\,\text{s}^{-1}$$
$$\phi_{NC} = (5.09 \pm 0.63) \times 10^6\,\text{cm}^{-2}\,\text{s}^{-1}$$
$$\phi_{ES} = (2.39 \pm 0.27) \times 10^6\,\text{cm}^{-2}\,\text{s}^{-1}\,.$$

The neutral current result compares well to the expectation from the SSM, $(5.05 \pm 0.95) \times 10^6\,\text{cm}^{-2}\,\text{s}^{-1}$. Is is trivial to deduce the individual components and so confirm the Homestake result: neutrinos change flavour en-route from the Sun.

$$\phi_{\nu_e} = (1.76 \pm 0.12) \times 10^6\,\text{cm}^{-2}\,\text{s}^{-1}$$
$$\phi_\mu + \phi_\tau = (3.41 \pm 0.64) \times 10^6\,\text{cm}^{-2}\,\text{s}^{-1}\,.$$

6.2 Two species mixing

With neutral mesons we saw that flavour oscillation occur if the eigenstates of the Hamiltonian, i.e. the mass eigenstates that propagate in space, are not identical to the [weak] interaction eigenstates. Here, we apply a similar idea to neutrinos, though unlike the meson formalism which is done in the meson rest frame, we work in the laboratory frame.

The flavour eigenstates are labelled $|\nu_e\rangle$ and $|\nu_\mu\rangle$, the mass eigenstates are $|\nu_1\rangle$ and $|\nu_2\rangle$. A mixing angle θ is defined:

$$\begin{pmatrix} |\nu_1\rangle \\ |\nu_2\rangle \end{pmatrix} = \begin{pmatrix} \cos\theta & \sin\theta \\ -\sin\theta & \cos\theta \end{pmatrix} \begin{pmatrix} |\nu_e\rangle \\ |\nu_\mu\rangle \end{pmatrix}$$

The mass eigenstates of energy E propagate in time as plane waves,

$$|\nu_1(t)\rangle = \exp\left(i(\underline{p}_1 \cdot \underline{x} - Et)/\hbar\right)\,|\nu_1\rangle \qquad\qquad |\nu_2(t)\rangle = \exp\left(i(\underline{p}_2 \cdot \underline{x} - Et)/\hbar\right)|\nu_2\rangle$$

The neutrino has zero mass ($\ll 1\mathrm{eV}/c^2$) so $mc^2 \ll E$ and

$$|\underline{p}|c \;=\; \sqrt{E^2 - m^2c^4} \;=\; E\left(1 - \tfrac{1}{2}\tfrac{m^2c^4}{E^2} + \ldots\right) \;\simeq\; E - \frac{m^2c^4}{2E}\,.$$

$\underline{p}\cdot\underline{x} - Et$ is recast as $t(|\underline{p}|c - E)$ given the neutrino travels at, or essentially at, the speed of light.

$$\begin{aligned} i\frac{t}{\hbar}\left(|\underline{p}_1|c - E\right) = \;& i\frac{t}{\hbar}\left(\cancel{E} - \frac{m_1^2c^4}{2E} - \cancel{E}\right) \\ =\; & -i\frac{m_1^2c^4}{2\,E}\frac{t}{\hbar} \;= -i\chi_1 t\,. \end{aligned}$$

The wavefunction in the mass basis is,

$$\psi_{\rm mass}(t) \;=\; \begin{pmatrix} \psi_1(t) \\ \psi_2(t) \end{pmatrix} = \begin{pmatrix} e^{-i\chi_1 t} & 0 \\ 0 & e^{-i\chi_2 t} \end{pmatrix} \begin{pmatrix} |\nu_1\rangle \\ |\nu_2\rangle \end{pmatrix},$$

so that the TDSE returns χ_i as the eigenvalues of the Hamiltonian,

$$i\frac{d\psi_{\rm mass}(t)}{dt} = H\psi_{\rm mass}(t) \;=\; \begin{pmatrix} \chi_1 & 0 \\ 0 & \chi_2 \end{pmatrix} \psi_{\rm mass}(t)\,.$$

Using the similarity transform, $\Sigma = UDU^{-1}$ where U is the two-particle mixing matrix, the flavour wavefunction is

$$\begin{aligned} \psi_{\rm flav}(t) \;=\; \begin{pmatrix} \psi_e(t) \\ \psi_\mu(t) \end{pmatrix} &= \begin{pmatrix} \cos\theta & -\sin\theta \\ \sin\theta & \cos\theta \end{pmatrix} \begin{pmatrix} e^{-i\chi_1 t} & 0 \\ 0 & e^{-i\chi_2 t} \end{pmatrix} \begin{pmatrix} \cos\theta & \sin\theta \\ -\sin\theta & \cos\theta \end{pmatrix} \begin{pmatrix} |\nu_e\rangle \\ |\nu_\mu\rangle \end{pmatrix} \\ &= \begin{pmatrix} \cos^2\theta\, e^{-i\chi_1 t} + \sin^2\theta\, e^{-i\chi_2 t} & -\sin\theta\cos\theta\left(e^{-i\chi_2 t} - e^{-i\chi_1 t}\right) \\ -\sin\theta\cos\theta\left(e^{-i\chi_2 t} - e^{-i\chi_1 t}\right) & \sin^2\theta\, e^{-i\chi_1 t} + \cos^2\theta\, e^{-i\chi_2 t} \end{pmatrix} \begin{pmatrix} |\nu_e\rangle \\ |\nu_\mu\rangle \end{pmatrix} \\ &= \begin{pmatrix} \frac{1}{2}\left(e^{-i\chi_2 t} + e^{-i\chi_1 t}\right) - \frac{1}{2}\cos 2\theta\left(e^{-i\chi_2 t} - e^{-i\chi_1 t}\right) & -\frac{1}{2}\sin 2\theta\left(e^{-i\chi_2 t} - e^{-i\chi_1 t}\right) \\ -\frac{1}{2}\sin 2\theta\left(e^{-i\chi_2 t} - e^{-i\chi_1 t}\right) & \frac{1}{2}\left(e^{-i\chi_2 t} + e^{-i\chi_1 t}\right) + \frac{1}{2}\cos 2\theta\left(e^{-i\chi_2 t} - e^{-i\chi_1 t}\right) \end{pmatrix} \begin{pmatrix} |\nu_e\rangle \\ |\nu_\mu\rangle \end{pmatrix} \end{aligned} \tag{44}$$

(using double-angle formula). The Hamiltonian in the flavour basis, H', is thus,

$$i\frac{d\psi_{\rm flav}(t)}{dt} \;=\; H'\psi_{\rm flav}(t) = \begin{pmatrix} \frac{\chi_2+\chi_1}{2} - \frac{\chi_2-\chi_1}{2}\cos 2\theta & -\frac{\chi_2-\chi_1}{2}\sin 2\theta \\ -\frac{\chi_2-\chi_1}{2}\sin 2\theta & \frac{\chi_2+\chi_1}{2} + \frac{\chi_2-\chi_1}{2}\cos 2\theta \end{pmatrix} \psi_{\rm flav}(t)\,. \tag{45}$$

Now consider a neutrino produced in the Sun. It is of definite electron flavour at $t = 0$: $\psi_{\rm flav}(0) = \begin{pmatrix} \psi_e(0) \\ 0 \end{pmatrix}$. From the top line of Eq. 44, the probability of detecting either a muon neutrino, or electron neutrino at time t later is,

$$\begin{aligned} \left|\langle\nu_e|\psi_e(t)\rangle\right|^2 &= \left|\tfrac{1}{2}(e^{-i\chi_2 t} + e^{-i\chi_1 t}) - \tfrac{1}{2}\cos 2\theta\,(e^{-i\chi_2 t} - e^{-i\chi_1 t})\right|^2 \\ \left|\langle\nu_\mu|\psi_e(t)\rangle\right|^2 &= \left|-\tfrac{1}{2}\sin 2\theta\,(e^{-i\chi_2 t} - e^{-i\chi_1 t})\right|^2 \end{aligned}$$

A little more trigonometry give the oscillation probability,

$$\begin{aligned} P(\nu_e \to \nu_\mu) = \left|\langle\nu_\mu \mid \psi_e(t)\rangle\right|^2 &= \tfrac{1}{4}\sin^2 2\theta\left(e^{-i\chi_2 t} - e^{-i\chi_1 t}\right)^2 \\ &= \quad'' \qquad 1 - e^{i(\chi_2-\chi_1)t} - e^{-i(\chi_2-\chi_1)t} + 1 \\ &= \quad'' \qquad 2 - \left(e^{i\chi_{21}t} + e^{-i\chi_{21}t}\right) \qquad\qquad \chi_{21} = \chi_2 - \chi_1 \\ &= \quad'' \qquad 2 - 2\cos(\chi_{21}t) \\ &= \sin^2 2\theta\,\sin^2\left(\tfrac{1}{2}\chi_{21}t\right) \end{aligned}$$

using: $\cos(2x) = 2\cos^2 x - 1 = 1 - 2\sin^2 x$.

A similar piece of trigonometry give the no-oscillation "survival" probability,

$$P(\nu_e \to \nu_e) = |\langle \nu_e | \psi_e(L) \rangle|^2 = \cos^2 2\theta \; + \sin^2 2\theta \; \cos^2\left(\tfrac{1}{2}\chi_{21} t\right) \quad \text{or indeed,} \quad 1 - \sin^2 2\theta \; \sin^2\left(\tfrac{1}{2}\chi_{21} t\right).$$

The last step is to resolve the time-dependent factor using practical units of GeV and kilometres given that the neutrino travels a large distance $L = tc$ at the speed of light.

$$\begin{aligned}
\tfrac{1}{2}\chi_{21} t &= \tfrac{1}{2}\left(\chi_2 t - \chi_1 t\right) \\
&= \frac{1}{2}\left(\frac{m_2^2 c^4}{2\,E}\frac{t}{\hbar} - \frac{m_1^2 c^4}{2\,E}\frac{t}{\hbar}\right) \\
&= \left(\underbrace{\left(m_2^2 c^4 - m_1^2 c^4\right)}\frac{tc}{4E\,\hbar c}\right) \quad \text{where } \hbar c = 197\,\text{MeV fm} \\
&= \Delta m^2_{21}[\text{eV}^2]\,\frac{L[\text{km}]}{E[\text{GeV}]} \cdot \frac{10^{18}_{(\text{km}\to\text{fm})}}{10^{9}_{(\text{GeV}\to\text{eV})}} \cdot \frac{1}{4 \times \cdot 197 \times 10^6 \text{eV fm}} \\
&= \Delta m^2_{21}[\text{eV}^2]\,\frac{L[\text{km}]}{E[\text{GeV}]} \cdot \frac{10^3}{4 \times 197} \\
&= 1.27\;\Delta m^2_{21}[\text{eV}^2]\,\frac{L[\text{km}]}{E[\text{GeV}]}
\end{aligned}$$

Thus the widely-used survival probability in the two-flavour model is,

$$P(\nu_e \to \nu_e) = 1 - \sin^2 2\theta \sin^2\left(1.27\;\Delta m^2_{21}[\text{eV}^2]\frac{L[\text{km}]}{E[\text{GeV}]}\right) \tag{46}$$

For a monochromatic neutrino, a regular oscillation with distance is expected, see Fig. 12. For a fixed distance, the resolvability of the oscillations depends on the energy resolution of the detector. Due the large distance to the Sun, these plots show solar neutrino oscillations with $\sim 10^{-11}\text{eV}^2$. However, energy measurements at fractions of a MeV would be

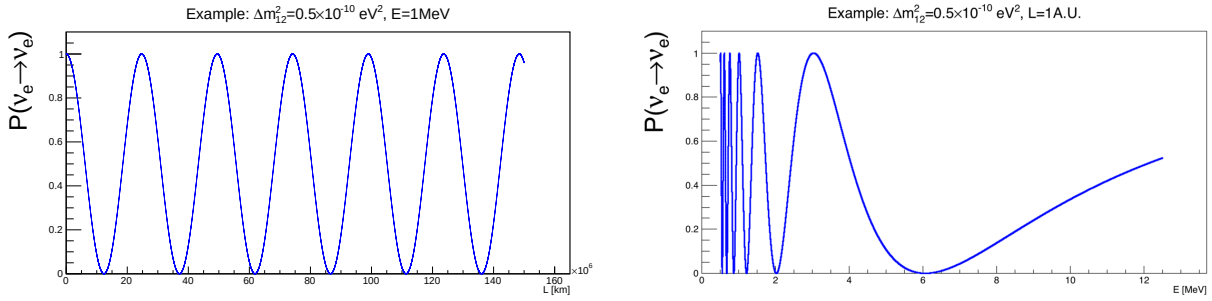


Figure 12: Neutrino survival probability plotted against distance (left) and neutrino energy (right) imagining $\Delta m^2_{12} = 5 \times 10^{-11}\,\text{eV}^2$. The amplitude of the oscillation is defined by the mixing angle which is assumed maximal (45°) in these plots.

extremely challenging. By 2005, fits to SNO data measured $\Delta m^2_{12} = 6.5^{+4.4}_{-2.3} \times 10^{-5}\text{eV}^2$, $\theta = (42 \pm 6)^\circ$. which gives oscillations a million times more rapid than those shown in Fig. 12. The realistic survival probability is $1 - \sin 2\theta \langle \sin^2(x) \rangle = 1 - \frac{1}{2}\sin 2\theta$; i.e. between 0.5 and 1.0 depending on the value of θ.

In designing an experimental baseline, it can be useful to know the distance to the first minimum (at $\pi/2$ for a $\sin^2$ function). For a given neutrino energy,

$$L_{\frac{\pi}{2}}[\text{km}] = 1.24\frac{E\;[\text{GeV}]}{\Delta m^2[\text{eV}^2]}. \tag{47}$$

Deducing the rotation angle

For a symmetric $n \times n$ matrix A, there exists a diagonal matrix D and orthonormal matrices U that are related by the similarity transform,

$$A = UDU^{-1} \quad \text{or equivalently,} \quad AU = UD\,.$$

where A has n eigenvalues λ_i. A real 2×2 U is a rotation matrix, parameterised by an angle x,

$$\begin{aligned}\begin{pmatrix} A_{11} & A_{12} \\ A_{12} & A_{22} \end{pmatrix} &= \begin{pmatrix} \cos x & -\sin x \\ \sin x & \cos x \end{pmatrix}\begin{pmatrix} \lambda_1 & 0 \\ 0 & \lambda_2 \end{pmatrix}\begin{pmatrix} \cos x & \sin x \\ -\sin x & \cos x \end{pmatrix} \\ &= \begin{pmatrix} \frac{1}{2}(\lambda_2+\lambda_1) - \frac{1}{2}(\lambda_2-\lambda_1)\cos 2x & -\frac{1}{2}(\lambda_2-\lambda_1)\sin 2x \\ -\frac{1}{2}(\lambda_2-\lambda_1)\sin 2x & \frac{1}{2}(\lambda_2+\lambda_1) + \frac{1}{2}(\lambda_2-\lambda_1)\cos 2x \end{pmatrix}\end{aligned}$$

The rotation angle x that is required to diagonalise A can be simply calculated,

$$\tan 2x = \frac{2A_{12}}{A_{11} - A_{22}}$$

6.3 MSW-effect

Though each have different energy ranges, the experiments discussed so far (Homestake, GALLEX, SuperKamiokande, SNO) have poor, or no, intrinsic energy resolution. They count the average rate with little sensitivity to the periodicity of the "L/E" term of Eq. 46. If the oscillations are not resolved, the average value of the $\sin^2$ term is $\frac{1}{2}$ so the survival probability should be $P_e = 1 - \frac{1}{2}\sin^2 2\theta$, which lies in the range $0.5 < P(\nu_e \to \nu_e) < 1$. However, except for the gallium experiments, all the experimental data indicates that the survival probability for electron neutrinos is closer to a third.

This discrepancy arises because the standard two-neutrino derivation is for transmission through vacuum. MSW (L. Wolfenstein (1978) and S. P. Mikheyev, A. Yu Smirnov (1986)) predicted an electron neutrino perturbation by charge current weak interactions in the dense solar matter. An MSW potential is introduced into the Hamiltonian for electron neutrinos only, $V = \sqrt{2}G_F N_e(r)$, where $G_F = 1.17\text{eV}^2(\hbar c)^3$ is the Fermi coupling constant and $N_e(r)$ is the number density of electrons which varies as a function of radius from the Sun's core.

$$H' = \begin{pmatrix} H'_{e\to e} & H'_{e\to\mu} \\ H'_{\mu\to e} & H'_{\mu\to\mu} \end{pmatrix} = \begin{pmatrix} \frac{\chi_2+\chi_1}{2} - \frac{\chi_2-\chi_1}{2}\cos 2\theta + \frac{\sqrt{2}}{\hbar}G_F N_e(r) & \frac{\chi_2-\chi_1}{2}\sin 2\theta \\ \frac{\chi_2-\chi_1}{2}\sin 2\theta & \frac{\chi_2+\chi_1}{2} + \frac{\chi_2-\chi_1}{2}\cos 2\theta \end{pmatrix}.$$

Conceptually, the additional scattering can be thought of raise the potential energy of the electron neutrino eigenstate such that he heavier mass eigenstate not only rises in mass but takes a greater proportion of that weak eigenstate. Mathematically the MSW effect modifies effective mixing from the intrinsic neutrino mixing in vacuum. To calculate the "matter-mixing" angle, θ_m the Hamiltonian is rediagonalised,

$$\begin{aligned}\tan 2\theta_m(r) &= \frac{-2\frac{\chi_2-\chi_1}{2}\sin 2\theta}{-\frac{\chi_2-\chi_1}{2}\cos 2\theta + \frac{\sqrt{2}}{\hbar}G_F N_e(r) - \frac{\chi_2-\chi_1}{2}} \\ &= \frac{\sin 2\theta}{\cos 2\theta - \frac{\sqrt{2}G_F N_e(r)}{(\chi_2-\chi_1)\hbar}}\end{aligned} \tag{48}$$

Three regimes are considered:

- Least dense outer regions of the Sun: $N_e(r) \to 0$, $\tan 2\theta_m \to \tan 2\theta$, $\theta_m \to \theta$. Intrinsic mixing, no matter effect.
- MSW resonant density: $\sqrt{2}G_F N_e(r) = (\chi_2 - \chi_1)\hbar \cos 2\theta$. This gives $\tan 2\theta_m \to \infty$, $\theta_m \to \pi/4$.
- The dense core of the Sun: $N_e(r) \to \infty$, $\tan 2\theta_m \to -0$, $\theta_m \to \pi/2$. Mixing suppressed by matter effects.

The MSW resonant density depends on the neutrino energy. The threshold for water cherenkov experiments (SNO and Kamiokande) is ~ 7 MeV. For neutrinos of this energy, and assuming $\theta = 33^\circ$, the MSW resonant density is,

$$\begin{aligned} N_e(r) = \frac{(\chi_2 - \chi_1)\hbar \cos 2\theta}{\sqrt{2}G_F} &= \frac{\Delta m^2_{21} \hbar \cos 2\theta}{2E\hbar\sqrt{2}G_F} \\ &= \frac{8 \times 10^{-5}[\,\mathrm{eV}^2] \cos 2\theta}{2\sqrt{2} \cdot 7 \times 10^6[\,\mathrm{eV}] \cdot 1.17 \times 10^{-23}[\,\mathrm{eV}^{-2}(\hbar c)^3]} \\ &= 1.4 \times 10^{11}\,\mathrm{eV}^3(\hbar c)^{-3} \\ &= 1.8 \times 10^{31}\mathrm{m}^{-3}\,, \end{aligned}$$

given $\hbar c = 197 \times 10^{-9}[\,\mathrm{eV\,m}]$. This electron number density, assuming a neutral hydrogen plasma ($m(N_{\mathrm{Av}}(H)) = 1\mathrm{g}$)

$$\frac{1.8 \times 10^{31}}{6.02 \times 10^{23}} = 30 \times 10^6 \mathrm{mol/m}^3\,, \quad \text{which is } \rho = 30\,\mathrm{gcm}^{-3}\,.$$

The core density of the sun is $\sim 160\,\mathrm{gcm}^{-3}$, far above the MSW resonant density for a 7 MeV neutrino.

As the density of matter is much above the MSW resonant density then electron neutrinos (produced in the fusion process) will align with the heavier mass eigenstate,

$$\begin{pmatrix} \nu_1 \\ \nu_2 \end{pmatrix} = \begin{pmatrix} \cos\theta_m & -\sin\theta_m \\ \sin\theta_m & \cos\theta_m \end{pmatrix} \begin{pmatrix} \nu_e \\ \nu_\mu \end{pmatrix} \quad \Rightarrow \quad \begin{pmatrix} 0 & -1 \\ 1 & 0 \end{pmatrix} \begin{pmatrix} \nu_e \\ \nu_\mu \end{pmatrix} \quad \text{as} \quad \theta_m \to \frac{\pi}{2}\,.$$

Thus is is predominantly the heavier mass eigenstate, $|\nu_2\rangle$ that is produced from the Sun and propagates to Earth where is its detected as an electron neutrino with probability,

$$P_e = \sin^2\theta \;\text{ from }\; |\nu_2\rangle = \sin\theta|\nu_e\rangle + \cos\theta|\nu_\mu\rangle\,.$$

This is always lower than the energy-averaged survival probability when matter effects are negligible, $P_e = 1 - \frac{1}{2}\sin^2 2\theta$.

If the number density calculation is redone in the context of the GALLEX experiment, which has a lower neutrino energy threshold and whose dataset contains a high proportion of the low energy pp neutrinos with $E \sim 0.35$MeV, the resonant electron density becomes 20 times larger: $\sim 600\,\mathrm{gcm}^{-3}$! The density of the Sun's core is not large enough to suppress mixing through the MSW effect in this low energy range. The Gallium-capture experiments (SAGE/GALLEX) measure a higher survival probability because the MSW matter effect is much diminished in their dataset. This an estimation of $\sin^2 2\theta_{12}$ can be made.

$$\theta_{12} = \tfrac{1}{2}\sin^{-1}\left(2(1 - P_{\mathrm{surv}}(\nu_e \to \nu_e)\right) \approx 33^\circ\,,$$

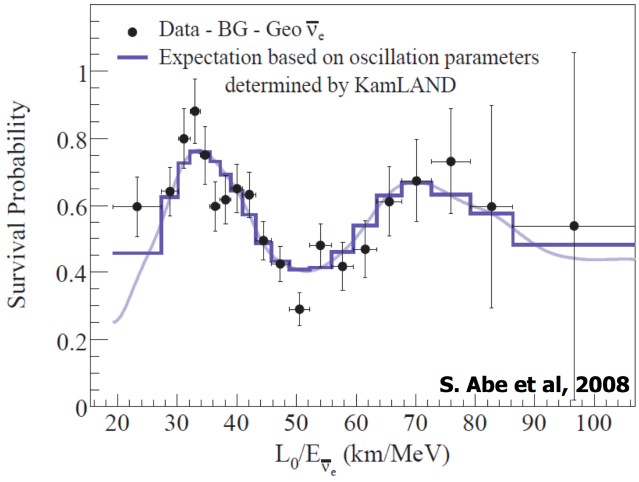
somewhat larger than Cabibbo mixing ($\lambda = 0.22,\ \theta_{\mathrm{C}} = 12.7^\circ$).

6.4 Reactor experiment at the same L/E

Upon inspection of Eq. 46 we notice that the probability depends on the ratio of L/E on the experiment, not their absolute values. Therefore one can probe the same phenomena at different places in the oscillation probability if one chooses the L and E correctly. The case in point is that the maximal oscillation criteria for $\Delta m^2 \sim \times 10^{-4}$ can be accessed by using MeV antineutrinos from a reactor over a distance of $O(10^2)$ km. In 2002 Kamland reactor experiment has made such

a complementary, and precise measurement of Δm^2_{12} at much shorter distance, free on the MSW effect that complicates solar-based measurements. The antineutrino are produced from β decay, $n \to p + e^- + \bar{\nu}_e$, in the fission reactor 180km away. They are detected via inverse β decay, $p + \bar{\nu}_e \to n + e^+$ in a liquid scintillator where an energy measurement with a 1.8 MeV threshold. The figure plots number of events vs. L/E and shows a period of 33km/MeV. Remembering the period of a $\sin^2 x$ function is π (not 2π),

$$\Delta m^2_{12} = \frac{\pi}{1270 \frac{L[\text{km}]}{E[\text{MeV}]}} = \frac{\pi}{1270 \cdot 33} \approx 7.5 \times 10^{-5}\,\text{eV}^2\,.$$



The combination of reactor and solar measurements provide a precise measure of both mixing angle and mass-difference-squared of the first two neutrino mass eigenstates. Furthermore, the MSW effect identifies the **hierarchy** of the two mass eigenstates: the derivation of MSW resonant condition defined in Eq. 48 show it to be sensitive to the sign of $(\chi_2 - \chi_1)$. $|\nu_2\rangle$ is heavier eigenstate. $|\nu_1\rangle$ is the lighter mass eigenstate that is otherwise most aligned with the $|\nu_e\rangle$ flavour eigenstate.

7 Atmospheric neutrinos

A large flux of high energy neutrinos is incident on Earth from cosmic ray showers in the upper atmosphere. These hadronic showers contain many pions, which decay through the chain, $\pi^+ \to \mu^+ \nu_\mu$, with $\mu^+ \to e^+ \nu_e \bar{\nu}_\mu$. The expected ratio or fluxes is,

$$\frac{\phi(\nu_\mu + \bar{\nu}_\mu)}{\phi(\nu_e + \bar{\nu}_e)} = 2\,.$$

Experiments in the 1990s reported evidence that this ratio was less than expected. Could this "atmospheric neutrino anomaly" be caused by the same mechanism as the "solar neutrino problem"? No.

7.1 Super-K

To investigate this "atmospheric" neutrino deficiency, Superkamiokande, the 50 kiloton water Cherenkov detector was built under Mt Ikenoyama in Japan. The water volume is surrounded on all sides by photon detectors with electronics primed to see coincident light signal across many devices. Of primary interest is neutrinos from charged-current interactions that produce a relativistic lepton that, in turn, produces Cherenkov light. The typical energies (> 10 GeV) are well above muon threshold from the charged-current interaction so two lepton species are observable. Electron and muons are distinguished by the shape of the Cherenkov ring, elections scatter more easily so the Cherenkov ring is "fuzzier".

Importantly, the incoming neutrinos are of large energy and the kinematics of the scattering off the fixed nuclear matter target (the water) means the direction of the incoming neutrino and the scattered lepton are highly correlated. This allows the analysis to know the distance that he neutrino has passed through since creation: between 50km (zenith angle = 0°) and 12400km (zenith angle = 180°).

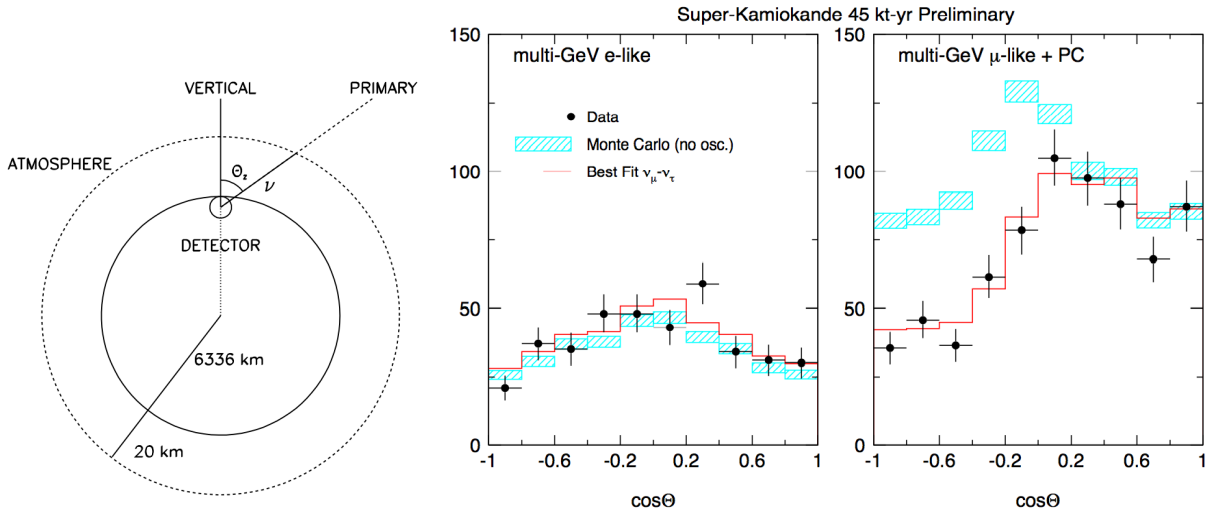


Figure 13: Superkamiokande data.

The data shows the muonic flux exhibits a clear dependence on zenith angle: where the neutrino has travelled farthest, there are fewer than expected. This implies ν_μ disappearance, but not to ν_e as the election flux is seen to be as expected. The "solar" neutrino oscillations have $\Delta m^2_{12} \approx 8 \times 10^{-5}$. A deficit of ν_μ could not be due to an oscillation to ν_e because of the distances involved. The typical energy of atmospheric neutrinos is $O(10\ \text{GeV})$. The two-neutrino mixing,

$$P(\nu_\mu \to \nu_x) \propto \sin^2\left(1.27\Delta m^2 \frac{L[\text{km}]}{E[\text{GeV}]}\right),$$

shows that ν_μ would need a distance $\sim 10^5$ km (10 times the Earth diameter) to have "enough time" to oscillate to ν_e. The oscillation of the ν_μ must be predominantly to a third mass eigenstate ν_3 most closely aligned to a third flavour (ν_τ). This oscillation is driven by a second mass-difference, $\Delta m^2_{23} \sim 10^{-3} - 10^{-2}\text{ev}^2$. What is striking about the Kamiokande data is that at azimuthal angle $\cos\theta = -1$ is the close-to maximal discrepancy from expectation. From the earlier discussion, the minimum $P_{\text{surv}}(\nu_e \to \nu_e)$ in the absence of matter effects, is 0.5. This is what is seen for the upward flux of neutrinos coming through the Earth, so we conclude maximal mixing

$$\sin^2 2\theta_{23} \approx 1.0 \qquad \Rightarrow \qquad \theta_{23} \approx 45^\circ.$$

Though not as well determined, Δm^2_{23} is clearly much larger Δm^2_{12} which precipitates solar oscillations.

7.2 MINOS: accelerator-based study of "atmospheric" oscillations

Just as the KamLand experiment chose a suitable L and E for "solar" oscillations, the MINOS experiment was designed to target maximal "atmospheric" oscillations. With $\Delta m^2_{32} \approx 3 \times 10^{-3}$ we need hundreds of kilometres per GeV; GeV neutrinos from an accelerator benefits from low natural background. The distances involved and the difficulty of perfectly collimating a neutrino source means a high intensity initial beam of decaying pions is needed, $\pi^+ \to \mu^+\nu_\mu$.

Fermilab points the focussed pion beam towards MINOS, which first passes though a "near" hall detector which measures the initial muon neutrino spectrum, then a larger, but otherwise identical detector is in the "far" hall, 735km away in

Minnesota. At the far detector, the beam is spread over kilometres so a large detector volume is needed. The MINOS experiment uses cheap scintillator layers interspersed with magnitised iron plates. The scintillator measures the energy of the recoiling nucleon whereas the bending of the resultant muon in the magnetised material measures its momentum. The energy spectra are shown below for both neutrinos and antineutrinos and are compared with the expected flux, assuming no oscillation (i.e. just from solid angle). The data confirms the atmospheric disappearance. Note that the charge of the pion beam is reversed and antineutrinos can be studied. This is first step towards probing *CP* violation in neutrinos.

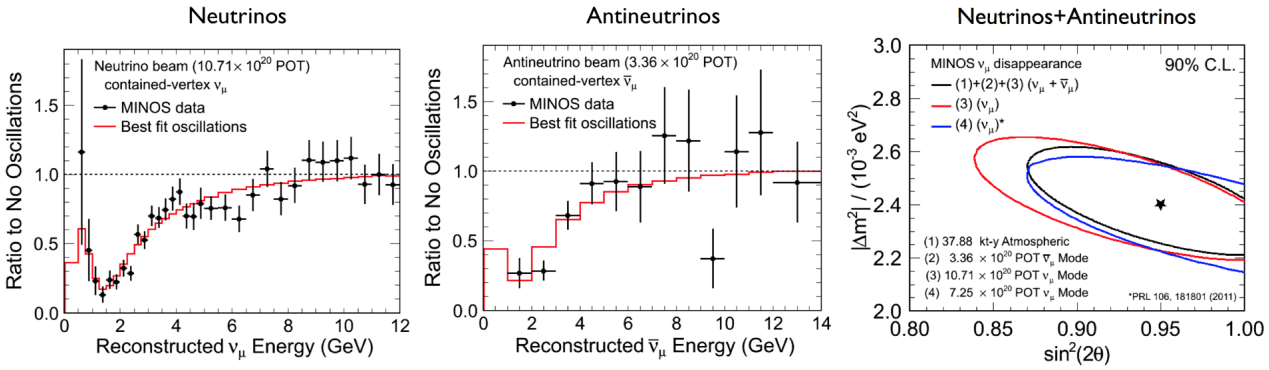


Figure 14: Minos data.

8 Three generations: the PMNS matrix

Normal vs. Inverted hierarchy

With two distinct oscillation phenomena, visible at different L/E, one understands that there must be a neutrino mass hierarchy with the a third generation neutrino somewhat difference in mass compared to the first two: Δm^2_{12} is small, Δm^2_{23} is large, thus Δm^2_{13} is similarly large. Because this involves squared quantities, it is not known if the $m_3 > m_1, m_2$ or $m_3 < m_1, m_2$, these scenarios are known as the normal and inverted hierarchies. As $\Delta m^2_{13} \approx \Delta m^2_{23}$, one can postulate that it should be possible to detect mixing between electron and tau neutrinos at "atmospheric" L/E. At this stage, the full 3 generation mixing needs consideration.

Pontecorvo-Maka-Nakagawa-Sakata (PMNS) matrix

Inspired by the CKM mechanism we write the PMNS matrix as a starting point to describing mixing between three neutrino species,

$$\begin{pmatrix} \nu_e \\ \nu_\mu \\ \nu_\tau \end{pmatrix} = \begin{pmatrix} U_{e1} & U_{e2} & U_{e3} \\ U_{\mu 1} & U_{\mu 2} & U_{\mu 3} \\ U_{\tau 1} & U_{\tau 2} & U_{\tau 3} \end{pmatrix} \begin{pmatrix} \nu_1 \\ \nu_2 \\ \nu_3 \end{pmatrix} \tag{49}$$

Unitarity is imposed and inverse defined: $U^{-1} = U^\dagger = (U^*)^T$.

$$\begin{pmatrix} \nu_1 \\ \nu_2 \\ \nu_3 \end{pmatrix} = \begin{pmatrix} U^*_{e1} & U^*_{\mu 1} & U^*_{\tau 1} \\ U^*_{e2} & U^*_{\mu 2} & U^*_{\tau 2} \\ U^*_{e3} & U^*_{\mu 3} & U^*_{\tau 3} \end{pmatrix} \begin{pmatrix} \nu_e \\ \nu_\mu \\ \nu_\tau \end{pmatrix}. \tag{50}$$

We know from CKM that a three-generation mixing implies three mixing angles and the presence of an irreducible

complex phase that can give rise to *CP* violation. In a decomposition identical to that of the CKM matrix,

$$U = \begin{pmatrix} 1 & 0 & 0 \\ 0 & \cos\theta_{23} & \sin\theta_{23} \\ 0 & -\sin\theta_{23} & \cos\theta_{23} \end{pmatrix} \times \begin{pmatrix} \cos\theta_{13} & 0 & \sin\theta_{13}e^{-i\delta} \\ 0 & 1 & 0 \\ -\sin\theta_{13}e^{-i\delta} & 0 & \cos\theta_{13} \end{pmatrix} \times \begin{pmatrix} \cos\theta_{12} & \sin\theta_{12} & 0 \\ -\sin\theta_{12} & \cos\theta_{12} & 0 \\ 0 & 0 & 1 \end{pmatrix}$$

we can see how the "regimes" factorise:

- the first rotation describes the rotation between the 2nd and 3rd generations whilst preserving the first. This dominates "ν_μ disappearance" in Atmospheric neutrino physics.
- the third rotation describes the rotation between the 1st and 2nd generations. This dominates "ν_e disappearance" in traditional Solar neutrino physics.
- θ_{13}, the smallest rotation angle, describes the mixing between the 1st and 3rd generations.

The three rotation angles, the *CP* violating phase parameter, plus two of the three mass differences (the 3rd is derivable) are the six fundamental parameters that can be measured in neutrino oscillation experiments,

$$U = \begin{pmatrix} \cos\theta_{12}\cos\theta_{13} & \sin\theta_{12}\cos\theta_{13} & \sin\theta_{13}e^{i\delta} \\ -\sin\theta_{12}\cos\theta_{23} - \cos\theta_{12}\sin\theta_{23}\sin\theta_{13}e^{i\delta} & \cos\theta_{12}\cos\theta_{23} - \sin\theta_{12}\sin\theta_{23}\sin\theta_{13}e^{i\delta} & \sin\theta_{23}\cos\theta_{13} \\ \sin\theta_{12}\cos\theta_{23} - \cos\theta_{12}\cos\theta_{23}\sin\theta_{13}e^{i\delta} & -\cos\theta_{12}\sin\theta_{23} - \sin\theta_{12}\cos\theta_{23}\sin\theta_{13}e^{i\delta} & \cos\theta_{23}\cos\theta_{13} \end{pmatrix} \quad (51)$$

The magnitudes of the PMNS matrix elements can be numerically summarised below. The off diagonal elements of the PMNS matrix are much larger than those in the CKM matrix.

$$U^{\text{NuFit 2020}}_{\text{PMNS}} = \begin{pmatrix} U_{e1} & U_{e2} & U_{e3} \\ U_{\mu 1} & U_{\mu 2} & U_{\mu 3} \\ U_{\tau 1} & U_{\tau 2} & U_{\tau 3} \end{pmatrix} \approx \begin{pmatrix} 0.80-0.85 & 0.51-0.58 & 0.14-0.16 \\ 0.23-0.50 & 0.47-0.69 & 0.64-0.78 \\ 0.27-0.53 & 0.48-0.69 & 0.61-0.76 \end{pmatrix}. \qquad \text{c.f. } V_{\text{CKM}} = \begin{pmatrix} \sim 1 & 0.22 & 0.01 \\ 0.22 & \sim 1 & 0.05 \\ 0.01 & 0.05 & \sim 1 \end{pmatrix}$$

Most recently, the third mixing angle, θ_{13} was measured using both reactor and accelerator sources. Measurement of this angle is an important precursor to the understanding of the final PMNS parameter: the *CP*-violating phase, δ.

8.1 θ_{13} from ν_e disappearance

Consider the production of an electron neutrino at $t = 0$ in the weak interaction (flavour) eigenstate, which is a mixture of mass eigenstates according to the PMNS matrix,

$$\psi_e(0) = |\nu_e\rangle = U_{e1}|\nu_1\rangle + U_{e2}|\nu_2\rangle + U_{e3}|\nu_3\rangle\,.$$

The evolution over time and space is:

$$\psi_e(t) = U_{e1}|\nu_1\rangle e^{i(\underline{p}_1\cdot\underline{x}-E_1t)/\hbar} + U_{e2}|\nu_2\rangle e^{i(\underline{p}_2\cdot\underline{x}-E_2t)/\hbar} + U_{e3}|\nu_3\rangle e^{i(\underline{p}_3\cdot\underline{x}-E_3t)/\hbar}$$

with which we make the same simplification as in the two-neutrino derivation,

$$\psi_e(t) = U_{e1}|\nu_1\rangle e^{-i\chi_1 t} + U_{e2}|\nu_2\rangle e^{-i\chi_2 t} + U_{e3}|\nu_3\rangle e^{-i\chi_3 t} \qquad \text{where } \chi_i = \frac{m_i^2c^4}{2\,E\hbar}$$

and use the inverse PMNS matrix, Eq. 50 to definition the mass eigenstates in terms of the flavour eigenstates,

$$\begin{aligned} \psi_e(t) = &(U_{e1}U^*_{e1}e^{-i\chi_1 t} + U_{e2}U^*_{e2}e^{-i\chi_2 t} + U_{e3}U^*_{e3}e^{-i\chi_3 t})\,|\nu_e\rangle \\ &(U_{e1}U^*_{\mu 1}e^{-i\chi_1 t} + U_{e2}U^*_{\mu 2}e^{-i\chi_2 t} + U_{e3}U^*_{\mu 3}e^{-i\chi_3 t})\,|\nu_\mu\rangle \\ &(U_{e1}U^*_{\tau 1}e^{-i\chi_1 t} + U_{e2}U^*_{\tau 2}e^{-i\chi_2 t} + U_{e3}U^*_{\tau 3}e^{-i\chi_3 t})\,|\nu_\tau\rangle \end{aligned}$$

Let's develop the probability of electron survival, $\nu_e \to \nu_e$, From the first line we have,

$$P(\nu_e \to \nu_e) \;=\; \left|\langle \nu_e \mid \psi_e(t)\rangle\right|^2 = \left|\; U_{e1}U_{e1}^* e^{-i\chi_1 t} + U_{e2}U_{e2}^* e^{-i\chi_2 t} + U_{e3}U_{e3}^* e^{-i\chi_3 t}\;\right|^2$$

Then using the complex number identity,

$$|z_1 + z_2 + z_3|^2 = |z_1|^2 + |z_2|^2 + |z_3|^2 + 2\,\Re(z_1 z_2^* + z_1 z_3^* + z_2 z_3^*) \tag{52}$$

$$\begin{aligned} P(\nu_e \to \nu_e) = {} & |U_{e1}U_{e1}^*|^2 + |U_{e2}U_{e2}^*|^2 + |U_{e3}U_{e3}^*|^2 \\ & + 2\,\Re\left[U_{e1}U_{e1}^* U_{e2}^* U_{e2} e^{i(\chi_2-\chi_1)t} + U_{e1}U_{e1}^* U_{e3}^* U_{e3} e^{i(\chi_3-\chi_1)t} + U_{e2}U_{e2}^* U_{e3}^* U_{e3} e^{i(\chi_3-\chi_2)t}\right]. \end{aligned} \tag{53}$$

The unitarity of the PMNS matrix requires the dot-product of rows (or columns) i and j to be δ_{ij}. Thus,

$$U_{e1}U_{e1}^* + U_{e2}U_{e2}^* + U_{e3}U_{e3}^* \;=1\,.$$

Using the Eq. 52 again, we can relate the PMNS elements:

$$\begin{aligned} |U_{e1}U_{e1}^* + U_{e2}U_{e2}^* + U_{e3}U_{e3}^*\,|^2 &= 1 \\ |U_{e1}U_{e1}^*|^2 + |U_{e2}U_{e2}^*|^2 + |U_{e3}U_{e3}^*|^2 &= 1 - 2\,\Re\left(U_{e1}U_{e1}^* U_{e2}^* U_{e2} + U_{e1}U_{e1}^* U_{e3}^* U_{e3} + U_{e2}U_{e2}^* U_{e3}^* U_{e3}\right) \end{aligned} \tag{54}$$

The right hand side of Eq. 54 replaces the first three terms of Eq. 53. Unifying, one gets,

$$\begin{aligned} P(\nu_e \to \nu_e) = {} & 1 + 2\,\Re\left[U_{e1}U_{e1}^* U_{e2}^* U_{e2}(e^{i(\chi_2-\chi_1)t} - 1)\right] \\ & + 2\,\Re\left[U_{e1}U_{e1}^* U_{e3}^* U_{e3}(e^{i(\chi_3-\chi_1)t} - 1)\right] \\ & + 2\,\Re\left[U_{e2}U_{e2}^* U_{e3}^* U_{e3}(e^{i(\chi_3-\chi_2)t} - 1)\right] \end{aligned} \tag{55}$$

$$\begin{aligned} = {} & 1 + 2\,|U_{e1}|^2|U_{e2}|^2\,\Re\left[e^{i(\chi_2-\chi_1)t} - 1\right] \\ & + 2\,|U_{e1}|^2|U_{e3}|^2\,\Re\left[e^{i(\chi_3-\chi_1)t} - 1\right] \\ & + 2\,|U_{e2}|^2|U_{e3}|^2\,\Re\left[e^{i(\chi_3-\chi_2)t} - 1\right] \end{aligned} \tag{56}$$

Note that the survival probability carries no sensitivity to the complex phase of the PMNS matrix and is not sensitivity to *CP* violation. The exponential contains the time dependence becomes,

$$\begin{aligned} \Re\left[e^{i(\chi_j-\chi_i)t} - 1\right] &= \cos(\chi_j - \chi_i)t - 1 \\ &= -2\sin^2\left(\frac{\chi_j - \chi_i}{2}t\right) \\ &= -2\sin^2\Delta_{ji} \qquad \text{where } \Delta_{ji} = \frac{(m_j^2 - m_i^2)c^4}{4E}\frac{tc}{\hbar c}\ \text{(natural units)} \quad = \quad 1.27\Delta m_{ji}^2[\text{eV}^2]\frac{L[\text{km}]}{E[\text{GeV}]} \end{aligned}$$

Continuing from Eq. 56,

$$P(\nu_e \to \nu_e) = 1 - 4|U_{e1}|^2|U_{e2}|^2\sin^2\Delta_{21} - 4|U_{e1}|^2|U_{e3}|^2\sin^2\Delta_{31} - 4|U_{e2}|^2|U_{e3}|^2\sin^2\Delta_{32}$$

Which can be simplified a little with reasonable assumptions.

$$\begin{aligned} P(\nu_e \to \nu_e) &\approx 1 - 4|U_{e1}|^2|U_{e2}|^2\sin^2\Delta_{21} - 4\left(|U_{e1}|^2 + |U_{e2}|^2\right)|U_{e3}|^2\sin^2\Delta_{32} && \text{hierarchy: } \Delta_{32} \approx \Delta_{31} \\ &\approx 1 - 4|U_{e1}|^2|U_{e2}|^2\sin^2\Delta_{21} - 4\left(1 - |U_{e3}|^2\right)|U_{e3}|^2\sin^2\Delta_{32} && \text{unitarity: } |U_{e1}|^2 + |U_{e2}|^2 + |U_{e3}|^2 = 1 \end{aligned}$$

Next we substitute in the mixing angles (and use trigonometry, $2\sin x\cos x = \sin 2x$),

$$\begin{aligned} P(\nu_e \to \nu_e) &= 1 - 4(\cos\theta_{12}\cos\theta_{13})^2(\sin\theta_{12}\cos\theta_{13})^2\sin^2\Delta_{21} - 4(1 - \sin^2\theta_{13})\sin^2\theta_{13}\sin^2\Delta_{32} \\ &= 1 - \cos^4\theta_{13}\sin^2 2\theta_{12}\sin^2\Delta_{21} - \sin^2 2\theta_{13}\sin^2\Delta_{32} \end{aligned}$$

We see that the electron neutrino survival probability has two terms; a dominant part that has large mixing angle but depends on Δm_{21}^2 and so needs long distances to occur. The second part is "subdominant" but dependent on Δm_{32}^2 giving faster oscillations.

θ_{13} at Daya Bay

In 2012, the Daya Bay experiment in southern China measured θ_{13} by looking at electron neutrino disappearance in the flux of $\bar{\nu}_e$ from a set of nuclear power stations. The detection technique is inverse β decay, $\bar{\nu}_e + p \to e^+ + n$ in liquid scintillator. The coincidence of the prompt scintillation from the e^+ and the haze of light from the delayed neutron capture provides a distinctive signature.

A "near and far" detector setup is used. Detectors were placed 363 m / 500 m from each of two reactors and one far detector, located 1615m and 1985m from the two reactors, to measure the neutrino flux at distance. At least two identical detectors (to reduced systematic errors) are bathed in a fiducial water bath to protect them from geological radioactivity backgrounds.

From the baseline calculation, Eq. 47, we see that the oscillations involving Δm^2_{21} are insignificant over the Daya Bay baseline distance, $\lambda_{12} = 30$km whereas $\lambda_{32} = 0.8$km. So the electron survival probability, Eq. 57, simplifies to,

$$P(\nu_e \to \nu_e) \approx 1 - \sin^2 2\theta_{13} \sin^2 \Delta_{32}$$

By placing the near and far detectors a little over a km apart, the deficit of $\bar{\nu}_e$ in the far hall compared to the near hall, should be near-maximal. The deficit is shown below and the Daya Bay collaboration's measurement is,

$$\sin^2 2\theta_{13} = 0.092 \pm 0.016(\text{stat}) \pm 0.005(\text{syst}) .$$

or, $\theta_{13} \approx 8.5^\circ$, assuming a 1$^{\text{st}}$ quadrant solution.

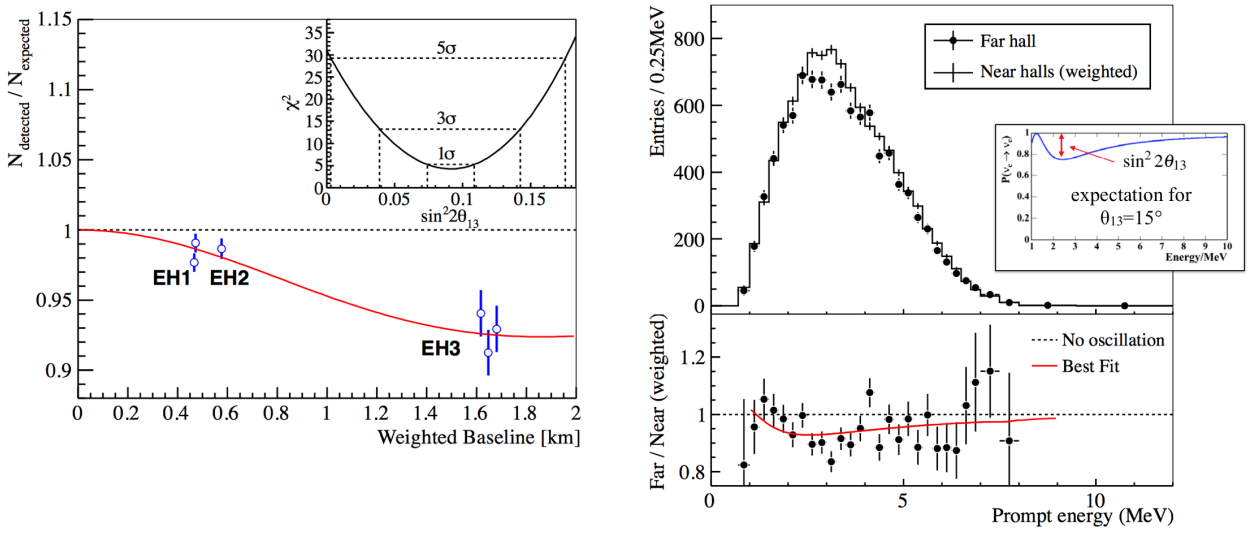


Figure 15: Daya Bay 2012 result.

8.2 θ_{13} from $\nu_\mu \to \nu_e$ appearance

We consider the ν_e appearance in an initially ν_μ beam from an accelerator neutrino source,

$$P(\nu_\mu \to \nu_e) = |\langle \nu_e | \psi_\mu(t) \rangle|^2 = \left| U_{\mu 1} U^*_{e1} e^{-i\chi_1 t} + U_{\mu 2} U^*_{e2} e^{-i\chi_2 t} + U_{\mu 3} U^*_{e3} e^{-i\chi_3 t} \right|^2 .$$

The derivation is the same as far as Eq. 55 though the relevant PMNS unitarity condition is not equal to one, but zero:

$U_{\mu1}U^*_{e1} + U_{\mu2}U^*_{e2} + U_{\mu3}U^*_{e3} = 0$. So,

$$\begin{aligned} P(\nu_\mu \to \nu_e) = \; & 2\,\Re\left[U_{\mu1}U^*_{e1}U^*_{\mu2}U_{e2}\left(e^{i(\chi_2-\chi_1)t}-1\right)\right] \\ & +2\,\Re\left[U_{\mu1}U^*_{e1}U^*_{\mu3}U_{e3}\left(e^{i(\chi_3-\chi_1)t}-1\right)\right] \\ & +2\,\Re\left[U_{\mu2}U^*_{e2}U^*_{\mu3}U_{e3}\left(e^{i(\chi_3-\chi_2)t}-1\right)\right]. \end{aligned} \tag{57}$$

The simplification at Eq. 56 does not apply when the creation and detection species differ. Sensitivity to the imaginary part of the PMNS matrix, and hence sensitivity to the *CP*-violating PMNS matrix phase, arises. The general form of each line is

$$\begin{aligned} 2\,\Re\left[U(e^{ix}-1)\right] = \; & 2\Re\left[U(\cos x - 1 + i\sin x)\right], & (58)\\ = \; & -4\Re\left[U\right]\sin^2\tfrac{x}{2} - 2\Im\left[U\right]\sin x, & (59) \end{aligned}$$

where we note the oscillation is twice as frequent for the imaginary part. So with

$$\Delta^C_{ji} = C\frac{\Delta m^2_{ji} L[\,\mathrm{km}]}{E[\,\mathrm{GeV}]},$$

Eq. 57 is rewritten,

$$\begin{aligned} P(\nu_\mu \to \nu_e) = & -4\,\Re\left[U_{\mu1}U^*_{e1}U^*_{\mu2}U_{e2}\right]\sin^2\Delta^{1.27}_{21} - 2\,\Im\left[U_{\mu1}U^*_{e1}U^*_{\mu2}U_{e2}\right]\sin\Delta^{2.54}_{21} \\ & -4\,\Re\left[U_{\mu1}U^*_{e1}U^*_{\mu3}U_{e3}\right]\sin^2\Delta^{1.27}_{31} - 2\,\Im\left[U_{\mu1}U^*_{e1}U^*_{\mu3}U_{e3}\right]\sin\Delta^{2.54}_{31} \\ & -4\,\Re\left[U_{\mu2}U^*_{e2}U^*_{\mu3}U_{e3}\right]\sin^2\Delta^{1.27}_{32} - 2\,\Im\left[U_{\mu2}U^*_{e2}U^*_{\mu3}U_{e3}\right]\sin\Delta^{2.54}_{32}. \end{aligned} \tag{60}$$

This expression shows the rate of this oscillation is sensitive to the imaginary part of the PMNS matrix and can be used to probe *CP* violation with neutrinos.

θ_{13} and δ_{CP} at T2K

In 2013, the Tokai-to-Kamioka (T2K) experiment accelerator-neutrino experiment release a result using an "off-axis" technique[10] to tune the average ν_μ energy to $\sim$ 600 MeV to maximise the oscillation. To see how this measurement can be made, four terms of Eq.60 are removed by neglecting *CP* violation ($\delta = 0$, $\Im[U] = 0$) and approximating $\Delta_{12} = 0$ (negligible slow "solar regime" effect) and thus, $\Delta_{13} \simeq \Delta_{23}$,

$$\begin{aligned} P(\nu_\mu \to \nu_e) \; & \approx -4\,\Re\left[U_{\mu1}U^*_{e1}U^*_{\mu3}U_{e3}\right]\sin^2\Delta^{1.27}_{31} \; - \; 4\,\Re\left[U_{\mu2}U^*_{e2}U^*_{\mu3}U_{e3}\right]\sin^2\Delta^{1.27}_{32} \\ & \approx -4\,(U_{\mu1}U_{e1} + U_{\mu2}U_{e2})U_{\mu3}U_{e3}\sin^2\Delta^{1.27}_{32} \\ & \approx \; 4\,|U_{\mu3}|^2|U_{e3}|^2\sin^2\Delta^{1.27}_{32}, \end{aligned} \tag{61}$$

where the last step uses a PMNS unitarity condition, $U_{\mu1}U^*_{e1} + U_{\mu2}U^*_{e2} + U_{\mu3}U^*_{e3} = 0$.

$P(\nu_\mu \to \nu_e)$ appearance to measure θ_{13} by looking for the "fuzzy" electron rings in the SuperKamiokande water Cherenkov detector in neutrino events from a ν_μ beam produced at J-PARC, 245km away in Tokai. Populating Eq. 61 with the PMNS elements, Eq. 51, gives the electron appearance probability,

$$\begin{aligned} P(\nu_\mu \to \nu_e) & \approx 4\,|\sin\theta_{23}\cos\theta_{13}|^2|\sin\theta_{13}e^{i\delta}|^2\sin^2\Delta_{31} \\ & \approx \sin^2\theta_{23}|4\cos\theta_{13}\sin\theta_{13}|^2\sin^2\Delta_{31} \\ & \approx \sin^2\theta_{23}\sin^2 2\theta_{13}\sin^2\Delta_{31} \end{aligned}$$

The 2013 result reported, $\sin^2 2\theta_{13} = 0.140^{+0.038}_{-0.032}$, which is compatible with the Daya Bay result.

This measurement was superseded in 2019 by a T2K comparative measurement of $P(\nu_\mu \to \nu_e)$ and $P(\bar{\nu}_\mu \to \bar{\nu}_e)$. Using the full development of Eq.60 a measurement of $\sin\delta_{CP}$ is made as well as an update of θ_{13}. The data is shown in Fig 16

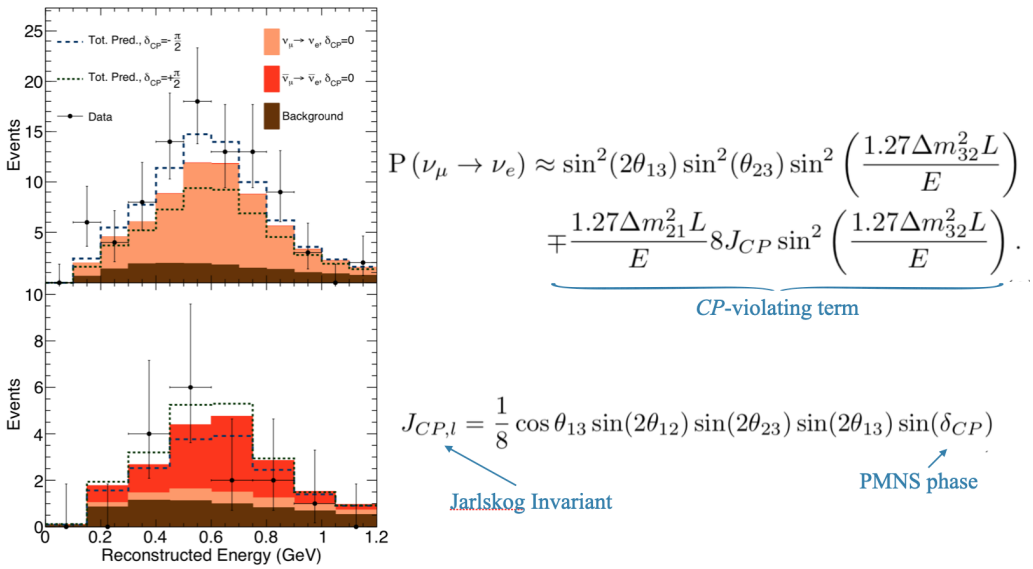


Figure 16: T2K - 2019 publication. The full expression including *CP* violation is shown.

for both neutrino and antineutrino beams as well as the CPV-allowed version of Eq. 61. The central value for the PMNS phase is preferred by the data, $\delta_{CP} \approx -\frac{\pi}{2}$.

The importance of neutrino *CP* violation measurements is emphasised by the Jarlskog Invariant, J_{CP} (Cecelia Jarkskog, 1973), which is a non-unique, but nevertheless useful contruct which quantifies the 'amount' of *CP* violation in a given system. The key characteristic of J_{CP} is that it combines all the parameters of the complex, unitary mixing matrices such that it falls to zero if any of the mixing angle or phases are zero, and the matrix can be rotated to be fully real.

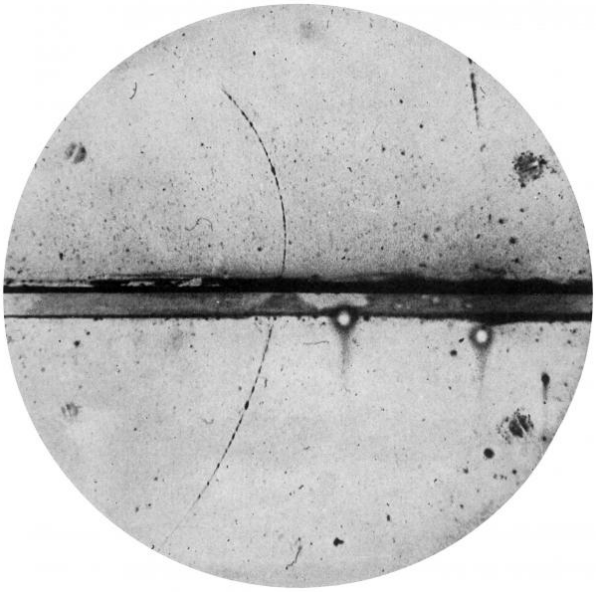
$$J_{CP} = \frac{1}{8}\cos\theta_{13}\sin(2\theta_{12})\sin(2\theta_{23})\sin(2\theta_{13})\sin(\delta_{CP})$$

For quarks, from the CKM matrix, $|J_{CP,q}| = 2.9 \times 10^{-5}$ ($\theta_{12} \approx 13^\circ$, $\theta_{23} \approx 2.4^\circ$, $\theta_{13} \approx 0.2^\circ$, $\delta_{CP} = 65^\circ$). In contrast the T2K indicates the same quantity for neutrinos is perhaps, up to three orders of magnitude larger, $|J_{CP,l}| < 3.3 \times 10^{-2}$! ($\theta_{12} \approx 33^\circ$, $\theta_{23} \approx 45^\circ$, $\theta_{13} \approx 8.4^\circ$, $\delta_{CP} \approx -\frac{\pi}{2}$). Given that the cosmological matter-antimatter asymmetry is known to be far too large for the CKM mechanism to be the only source of *CP* violation in the early Universe (Sakharov conditions), neutrinos clearly have huge potential to play a role in explaining the matter-dominated Universe.

8.3 Comment on neutrino masses

The formalism developed in this chapter demonstrates that oscillations phenomena can be explained by neutrinos having mass. It does not explain how neutrinos obtain mass, nor how neutrino oscillation is compatible with the Standard Model, which has $m(\nu) = 0$ built-in via maximal parity violation. This is a subject of theoretical conjecture and cutting-edge experimentation to prove, or disprove, the mechanism involved. The neutrino masses can be generated through the Higgs mechanism but, in addition to the three, *active*, left-handed neutrinos, existence of a right-handed neutrino current is required. This RH fermion would be a singlet of the weak force, only interacting gravitationally and thereby it is given the label *sterile* neutrino. The mass of the sterile neutrino is unconstrained and could be large, even be a candidate for cold dark matter. The future experimental sensitivity to such an object is through studies of unitarity violations amongst the mixing and *CP* violation of the PMNS matrix.

[10]The central axis of the beam is contains the most collomated, highest energy neutrinos. The average energy of the beam decreases away from the axis. Pointing the J-PARC beam $\sim 10^\circ$ off axis achieves the optimal $\frac{L}{E}$.



The Oxford MPhys Course

C4: Particle Physics

Problem Set Seven

1. For each of the following transitions, discuss the extent to which they are suppressed or forbidden.

(a) $e^+e^- \to \eta_c$ $[\eta_c$ is the 0^- state of $c\bar{c}]$

(b) $D^+ \to K^+\pi^+\pi^-$

(c) $B^+ \to \overline{D^0}\pi^+$

(d) $\tau^+ \to K^+\bar{\nu}_\tau$

(e) $K_L^0 \to \pi^+\pi^-$

(f) $K^+ \to \pi^+\bar{\nu}\nu$

(g) $\pi^0 \to \gamma\gamma\gamma$

(h) $\eta \to \pi^+\pi^-$

(i) $t \to W^+b$

©University of Oxford 2021

2. The K^0 is a neutral meson and if we assume that *CP* is conserved in the decays of the neutral kaons, show that the neutral kaon states with definite lifetimes are given by

$$\begin{aligned} |K_1^0\rangle &= \frac{1}{\sqrt{2}}\left\{|K^0\rangle + |\bar{K}^0\rangle\right\} \\ |K_2^0\rangle &= \frac{1}{\sqrt{2}}\left\{|K^0\rangle - |\bar{K}^0\rangle\right\}, \end{aligned}$$

where $|K^0\rangle$ and $|\bar{K^0}\rangle$ are the eigenstates of the strong interaction.

(a) Explain why the lifetimes of the two neutral kaons are very different. Would you expect the lifetimes of the equivalent neutral B mesons to be different?
Discuss the experimental evidence for *CP* violation in the decays of neutral kaons.

(b) Data for some of the decay modes of K_S^0 and K_L^0 mesons are given in the table:

	Branching fractions	
Decay mode	K_S^0	K_L^0
$\pi^+\pi^-$	0·6920	$1{\cdot}966\ 10^{-3}$
$\pi^- e^+ \nu_e$		0·19463
$\pi^+ e^- \bar{\nu}_e$		0·19337
Mean lifetime	$\tau_\mathrm{S} = 0{\cdot}896\ 10^{-10}$s	$\tau_\mathrm{L} = 5{\cdot}116\ 10^{-8}$ s

Mixing of the pure $CP = +1$ and $CP = -1$ states in $|K_\mathrm{S}\rangle$ and $|K_\mathrm{L}\rangle$ can be written as follows:

$$\begin{aligned} |K_\mathrm{S}^0\rangle &= A[(1+\epsilon)|K^0\rangle + (1-\epsilon)|\bar{K^0}\rangle] \\ |K_\mathrm{L}^0\rangle &= A[(1+\epsilon)|K^0\rangle - (1-\epsilon)|\bar{K^0}\rangle]. \end{aligned}$$

Constant A is the appropriate normalisation and $\epsilon = |\epsilon|e^{i\phi}$. It is a good approximation to assume that ϵ is the only parameter needed to account for *CP* violation in K decays. Estimate $|\epsilon|$ from the data in the table.

(c) Show that the charge asymmetry δ defined by

$$\delta = \frac{\Gamma(K_\mathrm{L}^0 \to \pi^- e^+ \nu_e) - \Gamma(K_\mathrm{L}^0 \to \pi^+ e^- \bar{\nu}_e)}{\Gamma(K_\mathrm{L}^0 \to \pi^- e^+ \nu_e) + \Gamma(K_\mathrm{L}^0 \to \pi^+ e^- \bar{\nu}_e)}$$

is equal to $2\,\mathrm{Re}\,\epsilon$ if one neglects quantities of the order $|\epsilon|^2$. Given that $\phi = 0{\cdot}759$, calculate δ and compare your result with the data given in the table.

(d) In which other system has CP violation been observed, and in which other system might it occur? Comment briefly on the implications of CP violation in cosmology. [Quark flow diagrams allow decays $K^0 \to \pi^- e^+ \nu_e$ and $\bar{K^0} \to \pi^+ e^- \bar{\nu}_e$, but forbid $K^0 \to \pi^+ e^- \bar{\nu}_e$ and $\bar{K^0} \to \pi^- e^+ \nu_e$.]

(e) How do you make a beam of K_L^0? Discuss a possible source of background from K_S^0.

©University of Oxford 2021

3. The CPLEAR experiment has studied $K^0 \leftrightarrow \bar{K}^0$ oscillations using $\bar{p}p$ annihilations at rest to produce K^0 and $\bar{K}^0$ by the reactions

$$\begin{aligned} \bar{p}p &\rightarrow K^0 K^- \pi^+ \\ \bar{p}p &\rightarrow \bar{K}^0 K^+ \pi^-. \end{aligned}$$

(a) How can the initial flavour of the neutral kaon and the flavour of the decaying neutral kaon be determined experimentally? What are the advantages of using $\bar{p}p$ annihilations at rest?

(b) The mass eigenstates of the K^0 system can be written in terms of the strangeness eigenstates as

$$\begin{aligned} |\mathrm{K}_S\rangle &= p|\mathrm{K}^0\rangle + q|\bar{\mathrm{K}}^0\rangle \\ |\mathrm{K}_L\rangle &= p|\mathrm{K}^0\rangle - q|\bar{\mathrm{K}}^0\rangle. \end{aligned}$$

A pure $|\bar{\mathrm{K}}^0\rangle$ state is produced at $t = 0$. Find the K^0 amplitude at a later time t and show that the asymmetry in the $\bar{\mathrm{K}}^0 \leftrightarrow \mathrm{K}^0$ transition rates,

$$A = \frac{\Gamma(\bar{\mathrm{K}}^0 \rightarrow \mathrm{K}^0) - \Gamma(\mathrm{K}^0 \rightarrow \bar{\mathrm{K}}^0)}{\Gamma(\bar{\mathrm{K}}^0 \rightarrow \mathrm{K}^0) + \Gamma(\mathrm{K}^0 \rightarrow \bar{\mathrm{K}}^0)}$$

is independent of t. Express A in terms of p and q.

(c) A charge asymmetry

$$\delta_l = \frac{\Gamma(\mathrm{K}_L \rightarrow l^+ X) - \Gamma(\mathrm{K}_L \rightarrow l^- \bar{X})}{\Gamma(\mathrm{K}_L \rightarrow l^+ X) + \Gamma(\mathrm{K}_L \rightarrow l^- \bar{X})} = 3{\cdot}23 \times 10^{-3}$$

is observed in the semi-leptonic decays of K_L. Deduce a value for A.

The measured value A is $(6{\cdot}6 \pm 1{\cdot}3) \times 10^{-3}$. Compare this measured value with the expected value. See Physics at CPLEAR, CPLEAR Collaboration, Physics Reports 374 (2003) 165, https://core.ac.uk/reader/19122975

(d) Explain why the regeneration process can create a background of 2π decays from a K^0_L beam.

4. Neutral B-meson oscillations.

(a) With the aid of quark diagrams explain how mixing arises in systems of the neutral B^0 mesons. How does this mixing result in different mass eigenstates with a mass difference of ΔM, between states with definite masses and lifetimes?

©University of Oxford 2021

(b) In the B^0 system the mass eigenstates are known as $B_{\rm H}$ and $B_{\rm L}$ and have almost identical lifetimes of $\tau = 1{\cdot}54\,\text{ps}$. A B^0 is produced at $t = 0$. Assuming no CP violation, show that the probability of observing a $\bar{B}^0$ decay at a proper time t later is

$$P(B^0 \to \bar{B}^0) \;=\; \frac{e^{-t/\tau}}{2}\left[1 - \cos(\Delta M t)\right],$$

where $\Delta M = 3{\cdot}3\,10^{-10}$ MeV/c^2 is the $B_{\rm H}$ – $B_{\rm L}$ mass difference.

(c) The PEP-II B factory is an e^+e^- collider operating at the $\Upsilon(4S)$ resonance (10.58 GeV) to produce copious pairs of B^0_d and $\bar{B_d}^0$ mesons. The energy of the electron beam is 9.1 GeV.

What is the energy of the positron beam and why are asymmetric beam energies used? Estimate the resolution of a vertex detector necessary to observe $B^0 \leftrightarrow \bar{B}^0$ oscillations and suggest a suitable type of detector.

(d) Suggest how $B^0 \leftrightarrow \bar{B}^0$ oscillations could be observed when the B^0 and $\bar{B}^0$ originate from the decay of the $\Upsilon(4S)$. Why must t in the expression you derived be replaced by $|t_1 - t_2|$ where t_1 and t_2 are the decay times of the two mesons?

5. past paper question.

The Wolfenstein parameterisation of the CKM matrix up to $\mathcal{O}(\lambda^3)$ is,

$$\begin{pmatrix} V_{ud} & V_{us} & V_{ub} \\ V_{cd} & V_{cs} & V_{cb} \\ V_{td} & V_{ts} & V_{tb} \end{pmatrix} \;=\; \begin{pmatrix} 1-\lambda^2/2 & \lambda & A\lambda^3(\rho - i\eta) \\ -\lambda & 1-\lambda^2/2 & A\lambda^2 \\ A\lambda^3(1-\rho-i\eta) & -A\lambda^2 & 1 \end{pmatrix},$$

where λ is the sine of the Cabibbo angle and A is real.

(a) State the function of this matrix and comment on the relative magnitude of the nine elements. Explain why the CKM matrix is unitary and explain the importance of the phase in $\rho - i\eta$. [4]

(b) Use columns one and three of the Wolfenstein parameterisation to demonstrate the unitarity of the CKM matrix. Hence draw a "unitarity triangle" (UT) on the argand plane stating the coordinates of the three vertices. Define the three internal angles (α, β, γ) of the triangle in terms of the CKM elements (V_{ub} etc.). [8]

(c) The UT angle, β depends on V_{td} but not on V_{ub}. Suggest a B-meson process that can be exploited to measure this angle even though a top quark is far too heavy to be produced in a B decay; use a Feynman diagram to illustrate. State, with an example, the properties of a final state required to access the phase information. [7]

(d) The LHC collides protons at $\sqrt{s} = 13$ TeV. Large quantities of B-mesons are produced with average energy ≈ 47 GeV/c. Calculate the average distance that the B-meson flies before decaying. Explain why this distance is vital for measuring β. In this context, briefly explain flavour tagging. [6]

©University of Oxford 2021

6. In the two flavour approximation, the flavour eigenstates are connected to the mass eigenstates by a mixing matrix with one parameter, θ:

$$\begin{pmatrix} \nu_\alpha \\ \nu_\beta \end{pmatrix} = \begin{pmatrix} \cos\theta & \sin\theta \\ -\sin\theta & \cos\theta \end{pmatrix} \begin{pmatrix} \nu_1 \\ \nu_2 \end{pmatrix}.$$

Such that at time $t = 0$ the neutrino state is a pure flavour state:

$$|\nu(0)\rangle = |\nu_\alpha\rangle = \cos\theta\,|\nu_1\rangle + \sin\theta\,|\nu_2\rangle\,.$$

(a) Show that the survival probability for a neutrino born with flavour α travelling a distance L in free space is

$$P(\nu_\alpha \to \nu_\alpha) = 1 - \sin^2 2\theta \sin^2\left(\frac{1{\cdot}27\Delta m^2(\mathrm{eV}^2)L(\mathrm{km})}{E(\mathrm{GeV})}\right),$$

where E is the energy of the neutrino and $\Delta m^2 = |m^2(\nu_1) - m^2(\nu_2)|$ is the mass difference between the two mass eigenstates and θ is the mixing angle.

(b) What is the evidence that the oscillations of atmospheric neutrinos are predominantly $\nu_\mu \to \nu_\tau$ and not $\nu_\mu \to \nu_e$?

(c) How do you create a beam of ν_μ or $n\bar{u}_\mu$? Consider a ν_μ beam made from decays of pions with an energy (momentum) E_π ($\mathbf{p}$). Show that the energy of a neutrino travelling at an angle θ with respect to the incident pion is given by

$$E_\nu = \frac{m_\pi^2 - m_\mu^2}{2(E_\pi - p_\pi\cos\theta)}.$$

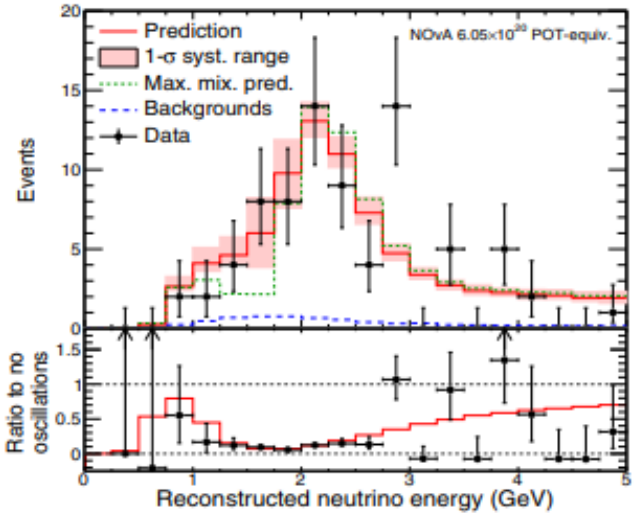
Assuming $\theta = 0^\circ$ and $E_\pi \gg m_\pi$ show that the neutrino energy is proportional to the incident pion momentum.

(d) Now consider a neutrino beam at a fixed non-zero angle θ_0 ("off-axis"). Show that the maximum neutrino energy corresponds to pions of energy $E_\pi^{max} = m_\pi/\sin\theta_0$. What is the advantage of an off-axis beam for a neutrino oscillation experiment?

(e) The NOVa experiment used such an off-axis beam with $\theta_0 = 14$mrad and a 810 km baseline to measure the ν_μ disappearance rate (PRL 118, 151802,2017). How is the neutrino flux at the far detector predicted?

The figure below shows the NOVa data. The top panel shows the number of events versus the reconstructed energy and the bottom panel shows the ratio of the number of measured events divided by the expectation for the no-oscillation hypothesis. Estimate values of Δm^2 and $\sin^2 2\theta$ from the disappearance data in the figure.

©University of Oxford 2021



7. SNO (the Sudbury Neutrino Observatory) consists of a spherical volume with a mass of 10^6 kg of heavy water (D_2O) viewed by photomultipliers. It is designed to study solar neutrinos and is sensitive to three types of neutrino interaction: charged (CC) and neutral current (NC) $\nu + \mathrm{D}$ scattering, and elastic $\nu + e$ scattering from atomic electrons.

(a) Which of these interactions has been important in allowing SNO to resolve the long-standing 'solar neutrino problem'?

(b) Calculate the neutrino threshold energy for each reaction, assuming that all neutrino masses are negligible. How can the reactions be identified experimentally and why is it necessary to require a minimum recoil electron energy of about 5 MeV in practice?
The binding energy of Deuterium is 2·25 MeV.

(c) The time dependent Schruodinger equation in the mass basis is,

$$i\frac{d\psi}{dt} = H\begin{pmatrix}|\nu_1\rangle\\|\nu_2\rangle\end{pmatrix} \text{ where } H = \begin{pmatrix}\chi_1 & 0\\0 & \chi_2\end{pmatrix}.$$

where χ_1, χ_2 are eigenvalues proportional to the neutrino masses. Use the similarity transform, $H' = U^{-1}HU$, to derive the Hamiltonian in the interaction basis in terms of $\cos 2\theta$ and $\sin 2\theta$. By inspection of H', identify which elements describes a change of neutrino flavour in time and list the requirements for this to occur.

(d) The first element of H' corresponds to an electron neutrino produced at $t = 0$ being detected as an electron neutrino some time later. By taking the modulus-squared, a survival probability is defined,

$$P_{\text{survival}} = |\langle \nu_e | \psi \rangle|^2 = \cos^2 2\theta + \sin^2 2\theta \cos^2 \left(0{\cdot}1 \frac{L[\text{km}]}{E[\text{MeV}]} \right) .$$

Assuming $\theta = 22{\cdot}5^\circ$ and an Earth-bound detector 79km from a reactor source, calculate all maxima and minima in the range $1\,\text{MeV} < E < 10\,\text{MeV}$ and draw the graph of this probability. Without further calculation, sketch P_{survival} for solar neutrinos over the same energy range. Given that the a detector like SNO has typical energy resolution around 1MeV, what survival probability is expected with the solar neutrinos?

(e) Where electron neutrinos are produced in dense matter, the Hamiltonian receives an additional potential from their interaction with atomic electrons. This alters the effective mixing angle ($\theta \to \theta_m$) which is defined with respect to the vacuum mixing angle (θ) by,

$$\tan 2\theta_m = \frac{\sin 2\theta}{\cos 2\theta - K\rho} ,$$

where ρ is the electron number density and K is a constant. In the core of the Sun, where $K\rho \gg \cos 2\theta$, what is θ_m? Thus, into which mass eigenstate are electron neutrinos most likely to be produced? Hence recalculate the probability for detecting electron neutrinos on Earth and compare the result with the previous section.

8. The PMNS matrix is th 3×3 complex matrix written in terms of just three mixing angles θ_{ij} and one phase δ,

$$\begin{pmatrix} U_{e1} & U_{e2} & U_{e3} \\ U_{\mu 1} & U_{\mu 2} & U_{\mu 3} \\ U_{\tau 1} & U_{\tau 2} & U_{\tau 3} \end{pmatrix} = \begin{pmatrix} c_{12}c_{13} & s_{12}c_{13} & s_{13}e^{-i\delta} \\ -s_{12}c_{23} - c_{12}s_{23}s_{13}e^{-i\delta} & c_{12}c_{23} - s_{12}s_{23}s_{13}e^{-i\delta} & s_{23}c_{13} \\ s_{12}s_{23} - c_{12}c_{23}s_{13}e^{-i\delta} & -c_{12}s_{23} - s_{12}c_{23}s_{13}e^{-i\delta} & c_{23}c_{13} \end{pmatrix} ,$$

where the abbreviations $c_{ij} = \cos\theta_{ij}$ and $s_{ij} = \sin\theta_{ij}$ are used.

(a) Explain the function and form of this PMNS matrix.

(b) The electron neutrino survival probability at a distance L from the source is

$$\begin{aligned} P(\nu_e \to \nu_e) = 1 \;&+\; 2|U_{e1}|^2|U_{e2}|^2\, \mathcal{R}e\left[e^{i(\phi_1-\phi_2)} - 1\right] \\ &+\; 2|U_{e1}|^2|U_{e3}|^2\, \mathcal{R}e\left[e^{i(\phi_1-\phi_3)} - 1\right] \\ &+\; 2|U_{e2}|^2|U_{e3}|^2\, \mathcal{R}e\left[e^{i(\phi_2-\phi_3)} - 1\right] , \end{aligned}$$

where $\phi_j = \frac{m_j^2 L}{2E}$ for neutrino energy E and mass m_j. Rewrite this in terms of the mixing angles and mass-difference factors $\Delta_{ij} = 2k(\phi_i - \phi_j)$, where $k = 1/4$ is a constant of proportionality. As Δ_{12} is small, you can take $\Delta_{13} = \Delta_{23}$.

(c) The value of k is $1/4$ in natural units. Calculate the value of k for the following units: L[km], E[MeV] and m[eV].

(d) Sketch the $P(\nu_e \to \nu_e)$ for L in the range 0-150km assuming the neutrinos originate from a reactor source with $E = 3$MeV.

(e) Suggest the principle design features of an experiment to measure θ_{13} from a reactor source.

[$\theta_{12} = 30^\circ$, $\theta_{23} = 45^\circ$, $\theta_{13} \approx 10^\circ$, $\Delta m_{12} = 8 \times 10^{-5}$ eV^2, $\Delta m_{23} = \Delta m_{13} = 3 \times 10^{-3}$ eV^2]

9. past paper question.

When cosmic ray protons strike the Earth's atmosphere, showers of particles are produced including neutrinos.

(a) Identify the main processes responsible and deduce an approximate value for the flavour ratio:

$$R = \frac{\nu_\mu + \bar{\nu}_\mu}{\nu_e + \bar{\nu}_e}.$$

[7]

(b) Such neutrinos, with energy $E_\nu \approx 1\,\text{GeV}$, interact primarily through quasi-elastic scattering: $\nu_\mu + n \to \mu^- + p$, $\nu_e + n \to e^- + p$ and $\bar{\nu}_\mu + p \to \mu^+ + n$, $\bar{\nu}_e + p \to e^+ + n$.

How can ν_μ and ν_e interactions in a large volume of water be detected and distinguished? [8]

(c) In a simple two-generation model, in which the mixing of the flavour eigenstates ν_α and ν_β is maximal, the probability of a produced neutrino ν_α oscillating into a neutrino flavour ν_β is given by,

$$P(\nu_\alpha \to \nu_\beta) = \sin^2\left(\frac{1{\cdot}27\Delta m^2 L}{E}\right),$$

where $\Delta m^2 = |m_1^2 - m_2^2|$ (in eV^2), m_1 and m_2 refer to the mass eigenstates, L is the distance the neutrinos have travelled (in km) and E is the neutrino energy (in GeV).

In the data below, the dashed lines show the predicted numbers of events in the absence of oscillations and the solid points are the observations. Neutrinos with $\cos\theta = 1$ have travelled a distance of $\sim 20\,\text{km}$ and those with $\cos\theta = -1$ a distance of $\sim 13\,000\,\text{km}$. Given a neutrino energy $\sim 1\,\text{GeV}$, suggest a possible interpretation of the observations and make reasoned estimates of upper and lower bounds on Δm^2. [10]

